The role of the cGAS-STING pathway in mammalian brain physiology and ageing

Thesis
for the degree of

doctor rerum naturalium (Dr. rer. nat.)

approved by the Faculty of Natural Sciences of Otto von Guericke University Magdeburg

by **MSc. Sergio Passarella**
born on 22.11.1993 in Bolzano/Bozen

Examiners:
Prof. Dr. Daniela Christiane Dieterich
Prof. Dr. Manuel Friese

submitted on: 26.08.2022
defended on: 22.06.2023

Abstract

Ageing is a phenomenon which comprises different life spheres: social, economic, and biological. In recent years, research has made big steps to decipher, how cells and tissues age. However, the study of healthy ageing remains pivotal for a better understanding of the physiological cell senescence mechanisms. Thus, it might help to establish connections to neurodegenerative pathology's development as Alzheimer and Parkinson disease. Hence, this study started with the characterization of physiological ageing using an *in vitro* model of primary neural cells of mouse. To mimic adult, middle age and old neurons, the cell cultures were maintained for 21, 40, and 60 days *in vitro* (DIV). The related experiments are based on the study of neuronal cell morphology, proteosomes, autophagy, and innate immunity-related aspects, and are conducted to focus, how these factors influence neuronal ageing *in vitro*.

Compared to younger experimental groups, the results showed a reduction of the dendritic morphology and a decrease of protein synthesis rates in neurons at DIV 60, associated with autophagic impairment, visualized via the accumulation of p62 protein.

The role of innate immunity during ageing is part of intensive research, however comparable less is known specifically about the role of the cGAS-STING pathway in brain ageing. Therefore, after first studies *in vitro*, our research focused on experiments *in vivo*, based on 8-, 24- and 107-week-old C57BL/6 mice. The level of essential proteins of the cGAS-STING pathway were analyzed on cortical tissues *via* quantitative Western blots. In summary, the results revealed a disbalance of the cGAS-STING pathway in cortex regions of elderly mice, in comparison with 8-, 24-week-old groups. Moreover, using immunohistochemical analysis, the presence of STING protein in both neurons and astrocytes could be demonstrated. Therefore, the study deepened the understanding of the cGAS-STING pathway in neuronal and brain homeostasis. Using STING$^{-/-}$ mice, primary neural cell cultures were established. Morphological studies on STING$^{-/-}$ neurons showed a different shape with shorter dendrites in comparison with the wild type. Furthermore, an autophagic and proteasomal impairment of STING-deficient neurons could be demonstrated, either by a lower accumulation of p62 following chloroquine treatment or a statistically significant higher FUNCAT signal compared to C57BL/6 cells. The immunocytochemistry data revealed a decrease of presynaptic puncta and larger areas in the STING$^{-/-}$ neurons in contrast to the wild type cells. The results reported in this

thesis contribute to a better understanding of the role of the cGAS-STING pathway in neuronal homeostasis and brain ageing.

Zusammenfassung

Altern ist ein Phänomen, das verschiedene Lebensbereiche umfasst: soziale, wirtschaftliche und biologische. In den letzten Jahren hat die Forschung große Fortschritte gemacht, um zu entschlüsseln, wie Zellen und Gewebe altern. Die Untersuchung des gesunden Alterns bleibt jedoch entscheidend für ein besseres Verständnis der physiologischen Mechanismen der Zellalterung. Daher könnte es helfen, Verbindungen zur Entwicklung neurodegenerativer Erkrankungen wie der Alzheimer- und Parkinson-Krankheit herzustellen. Daher begannen unsere Untersuchungen mit der Charakterisierung des physiologischen Alterns unter Verwendung eines *in vitro*-Modells, bestehend aus neuralen Primärzellen der Maus. Um erwachsene, mittlere und alte Neuronen zu imitieren, wurden die Zellkulturen für 21, 40 und 60 Tage *in vitro* (DIV) kultiviert. Die zugehörigen Experimente basieren auf der Untersuchung der neuronalen Zellmorphologie, Proteasomen, Autophagie und Aspekten der angeborenen Immunität und sind auf die Frage fokussiert, wie diese Faktoren die neuronale Alterung *in vitro* beeinflussen.

Im Vergleich zu jüngeren experimentellen Gruppen zeigten die Ergebnisse eine Verringerung der dendritischen Morphologie und eine Abnahme der Proteinsyntheseraten in Neuronen bei DIV 60, verbunden mit einer Beeinträchtigung autophagischer Prozesse, evident durch die Akkumulation des p62-Protein.

Die Rolle der angeborenen Immunität während des Alterns ist Teil intensiver Forschung, jedoch ist vergleichsweise wenige über die Rolle des cGAS-STING-Signalwegs bei der Gehirnalterung bekannt. Daher konzentrierte sich unsere Forschung nach ersten Studien *in vitro* auf Experimente in vivo, basierend auf 8-, 24- und 107 Wochen alten C57BL/6-Mäusen. Die Konzentration essentielle Proteine des cGAS-STING-Signalwegs wurde unter Verwendung von kortikalen Geweben mittels quantitativer Western Blots analysiert. Zusammenfassend zeigten die Ergebnisse ein Ungleichgewicht des cGAS-STING-Signalwegs im Kortex älterer Mäuse im Vergleich zu 8-, 24-Wochen-alten Gruppen. Darüber hinaus konnte durch immunhistochemische Analysen das Vorhandensein von STING sowohl in Neuronen als auch in Astrozyten nachgewiesen werden. Daher vertieft die Studie das Verständnis des cGAS-STING-Signalwegs bezüglich der neuronalen Homöostase.

Unter Verwendung von STING-/- Mäusen wurden primäre neurale Zellkulturen etabliert. Morphologische Untersuchungen an STING-/- Neuronen zeigten im Vergleich zum Wildtyp

eine veränderte Morphologie mit verkürzten Dendriten. Darüber hinaus konnte sowohl eine autophagische als auch eine proteasomale Beeinträchtigung von STING-defizienten Neuronen nachgewiesen werden, entweder durch eine geringere Akkumulation von p62 nach Chloroquin-Behandlung oder ein statistisch signifikant höheres FUNCAT-Signal im Vergleich zu den untersuchten WT-Zellen. Die immunzytochemischen Daten zeigten eine Abnahme der präsynaptischen Strukturen, aber auffallend größer Präsynapsen in den STING-/- Neuronen, im Gegensatz zu den Neuronen des Wildtyps. Die in dieser Arbeit berichteten Ergebnisse sollen damit zu einem besseren Verständnis der Rolle des cGAS-STING-Signalwegs bei der neuronalen Homöostase und der Gehirnalterung beitragen.

Table of Contents

List of figures

Abbreviations

2,3-cGAMP	2',3'-cyclic-GMP-AMP
AD	alzheimer’s disease
AHA	L-azidohomoalanine
ALS	amyotrophic lateral sclerosis
ASDs	autism spectrum disorders
ATGs	autophagy-related proteins
ATP	adenosine triphosphate
BDNF	brain-derived neurotrophic factor
BFA	bafilomycin A1
CA1	cornu ammonis 1
cGAS	cyclic GMP-AMP synthase
CMA	chaperone-mediated autophagy
CNS	central nervous system
COP	coat protein complex
CQ	chloroquine
DDR	DNA damage response
DG	dentate gyrus
DMSO	dimethyl sulfoxide
DNA	deoxyribonucleic acid
dsDNA	double stranded DNA
CQ	chloroquine
e.g.	exempli gratia
ER	endoplasmic reticulum
ETC	electron transport chain
$FADH_2$	flavin adenine dinucleotide
GABA	γ-aminobutyric acid
GST	glutathione S-transferase
GTP	guanosine-5'-triphosphate
HSV-1	herpes simplex virus 1
i.e.	id est – that is
IF	immunofluorescence
IFNs	interferons
IHC	immunohistochemistry

Abbreviations

IL	interleukins
i.p.	intraperitoneally
IRF	interferon regulatory factor
ISG	Interferon-stimulated gene
KO or -/-	knock-out
LAMP	lysosomal-associated membrane protein
LC3	light chain 3
LTP	long term potentiation
mtDNA	mitochondrial DNA
mTOR	mammalian target of rapamycin
NAD	nicotinamide adenine dinucleotide
NF-κB	nuclear factor kappa-light-chain-enhancer of activated B cells
NMDA	N-methyl-D-aspartate
O_2	oxygen
p62	sequestosome-1
PAS	pre-autophagosomal structure
PD	Parkinson disease
PE	phosphatidylethanolamine
PFC	prefrontal cortex
PI3P	phosphatidylinositol-3-phosphate
PRR	pattern recognition receptor
RNA	ribonucleic acid
ROS	reactive oxygen species
SCX	somatosensory cortex
STING	Stimulator of interferon genes
TBK1	TANK-binding kinase 1
TFEB	Transcription Factor EB
ULK1	UNC51-like kinase1
UPS	ubiquitin proteasome system
WB	western blot
WHO	World Health Organization’s

List of tables

1 Introduction

1.1 The ageing

The term aging is a complex definition which includes different life spheres: scientific, social, and economic. Although, these areas seem to be far apart, they are well interconnected. Thanks to the scientific contribution, it may be possible to improve the life quality enabling a larger number of elderly people (Population Ageing - A Threat to the Welfare State? 2010).

The concept of ageing, how logical and obvious it seems to be, hides characteristics that are still completely unknown for us today (Tinker 2002). The average life expectancy has increased considerably over the course of the 20th century passing in western countries from about 50 to over 80 years (Clegg et al. 2013). The global population aged 60 years or more reached 962 million in 2017, more than twice as large as in 1980, when there were 382 million older persons worldwide (Nichols et al. 2022).

As shown in figure 1, over the last few centuries, despite all the pandemics that have occurred, such as Spanish flu, polio, HIV and the recent Sars-Cov-2, the world's population continues to increase in age (Ng and Gui 2020; Torres Acosta and Singer 2020).

The number of older persons is expected to double again by 2050, when it is projected to reach 2.1 billion. These recent data show that the continuously growing number of elderly people within our society leads to a series of new challenges, including the long-term maintenance of health and cognitive function. Furthermore, the increase in the number of elderly people must be seen as a medical success story, but at the same time it confronts humanity with new problems such as the increase in age-related diseases such as cataracts, osteoarthritis, or dementia (Bengtsson and Scott 2010). Therefore, it is important that global programs as “The Decade of Healthy Ageing (2021–2030)” be set up to warrant equal access to health long term care and good life quality.

Due to the multiple variables which influences aging, it is not easy to find one single classification. The United Nations have tried to determinate the elderly, as people aged 65 years or over, nevertheless the sub-grouping definitions are distinguishing also young old (60 to 69), middle old (70 to 79), and the very old (80+) (Zhang et al. 2021).

Global data confirm that a demographic change is taking place in a way that the elderly population is growing, whereas simultaneously the young one is decreasing.

Therefore, on one hand steps forward have been made in postponing the aging, on the other hand the economic and social well-being, have led to a shift to older populations with fewer children.

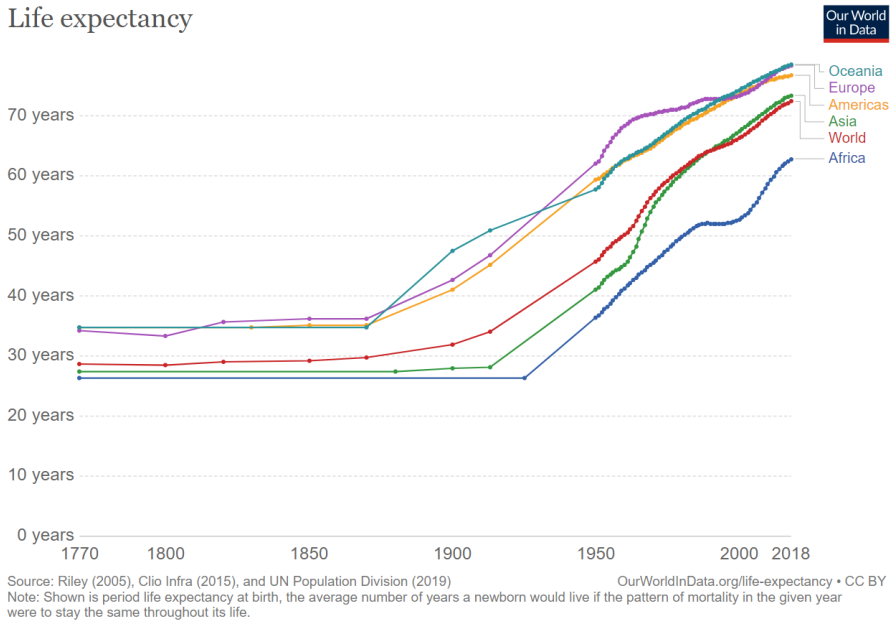

Figure 1: Life expectancy between 1770 and today
The graph shows the exponential increase of life expectancy over the last centuries. Source: Statista.com 2021

The ageing process cannot be considered exclusively from a chronological point of view, in terms of years passed from the birth; but also from a biological perspective (Radkiewicz et al. 2022). This latter indeed defines ageing as physiological process of the decline of biological functions. Moreover, scientific research has been able to discover several cellular markers which vary significantly over age as for example genetics/epigenetics or metabolites (Zhou et al. 2021). These factors are paramount for aging and age-related diseases as also inflammatory cell states or alterations in stress balances and adaptation (Rossiello et al. 2022). Furthermore, by highlighting putative ageing markers it was possible to discover new molecular pathways involved in senescence and potential targets to tread age-related pathologies such as neurodegenerative diseases (Di Micco et al. 2021). Today, for example, we are able to define Alzheimer's disease (AD) with its classic biomarkers, i.e. the presence of high amounts of beta amyloid and phospho-Tau in the brain or the appearance of Lewy bodies in Parkinson's disease (PD) (Seltzer et al. 2001; Savelieff et al. 2019).

In conclusion, it seems to be clear that the scientific contribution of the biology in the field of ageing is needed to be intensified. To date, studying the molecular mechanisms

involved in senescence could improve the lives of patients suffering from neurodegenerative diseases, but more importantly, in the future it could lead to the depression of these age-related diseases or at least further extend the healthy life expectancy of the world's population.

1.2 Cellular senescence and autophagy

Cellular ageing is a phenomenon that has been extensively studied in recent years. Big steps have been made in the understanding of how a cell age (Di Micco et al. 2021). To date, it is clear that senescent cells have a predisposition to avoid apoptosis and cell death (Muller et al. 2007). However, it remains unclear how aged cells manage to escape apoptosis for a time and then die. The pathways that lead a cell to survival or cell death are very similar and often overlap (Bokov et al. 2004). Moreover, it has been shown that this balance between cell death and senescence is dynamic. Indeed, a cell can by as yet unclear stimuli take the senescence pathway via blocking apoptosis and vice versa (Balaban et al. 2005).

The network of pathways that lead a cell to age is enormous and tracing the first step seems almost impossible to date (Sasaki et al. 2010). To summarise the immense molecular network that leads to cellular ageing in biology, the main events have been highlighted: mitochondrial dysfunction with formation of oxidative stress, DNA damage and the decline of autophagy, the main catabolic pathway of cells (Frenk and Houseley 2018; Zhou et al. 2021; Shay and Wright 2000)

The most important function of mitochondria at the cellular level is the production of ATP, which is essential for certain metabolic reactions (Passos and Zglinicki 2005). In the mitochondria, both NADH and $FADH_2$ produced by the β-oxidation of fatty acids and the Krebs cycle are used to produce energy (Richter and Proctor 2007). Through a multi-enzyme complex that functions as a transport chain, electrons are taken from NADH and $FADH_2$ and are transported to the electron transport chain (ETC) in the inner mitochondrial membrane (Trifunovic and Larsson 2008). The ETC consists of four complexes in which electrons are transferred to molecular oxygen (O_2), which is reduced to water (Khacho et al. 2019). During electron transfer, the various transporter proteins undergo conformation changes that allow protons to be transferred from the matrix to the intermembrane space against a concentration gradient (Wong et al. 2019). This proton gradient is then used by ATP synthase, which corresponds to the complex V. The protons are then passed through

the inner membrane again, in a process of facilitated diffusion, by the enzyme ATP synthetase, which thus obtains sufficient energy to produce ATP molecules by transferring a phosphate group to ADP (Janikiewicz et al. 2018). Besides the nucleus, mitochondria are the only organelles to have DNA inside them (Naoi et al. 2019). This DNA is called mitochondrial DNA (mtDNA). It is widely recognized that an accumulation of mtDNA in the cytosol is linked to mitochondrial damage and cellular ageing (Naoi et al. 2019; Janikiewicz et al. 2018). Already 1988, Pikò and colleagues evaluated the cytosolic amount of mtDNA in tissues of animals of different ages and they showed that it was directly proportional to the age of the respective animals (Pikó et al. 1988). Subsequently, this type of experiment was also performed on human tissues such as skeletal muscle and brain. In both cases, it was shown that ageing caused cells to accumulate mtDNA and a decline in mitochondrial respiration functions (Holt et al. 1988).

However, mitochondria are also powerful producers of reactive oxygen species (ROS), because mitochondrial enzymes are the main consumer of cytosolic oxygen (Bazopoulou et al. 2019). Liguori and colleagues showed that 4% of the oxygen used by mitochondria generates ROS (Liguori et al. 2018). During ATP production, complex I and III produce the reactive free radical superoxide anion, i.e. O_2^{-}, which can subsequently be further reduced to OH^-, the hydroxyl radical, and to H_2O_2 (Shields et al. 2021). While OH^- and O_2^{-} are highly unstable and can cause only limited damage, H_2O_2 is a very stable molecule that diffuses freely in the cytosol and nucleus causing oxidative damage in many cellular compartments (Starkov and Fiskum 2003).

During cellular ageing, ROS levels are also clearly increased (Bazopoulou et al. 2019) and has been described in many publications (Stefanatos and Sanz 2018; Schumacher et al. 2021). Indeed, recent research indicates that ROS promote ageing processes and are associated with many diseases such as cancer, diabetes, or brain disorders such as Parkinson's or Alzheimer's disease (Dias et al. 2013; Ahmad et al. 2017). Already in 1994, Shigenaga and colleagues clearly demonstrated that old mitochondria showing altered morphology and functionality produced more oxidants and less ATP than young mitochondria (Shigenaga et al. 1994). More recent research, such as that of Miwa and colleagues, also shows, how during ageing the increase of ROS at the cytosolic level in the mouse brain leads to an accumulation of damaged mitochondria (Stefanatos and Sanz 2018; Miwa and Brand 2003).

As mentioned above, ROS can easily move through the various cellular compartments, even reaching the nucleus and creating DNA damage (Babizhayev and Yegorov 2016; Schumacher et al. 2021).

DNA damage has a central effect on the ageing process and senescent cells, since it has a broad spectrum of actions and consequences at the molecular level, such as genome instability and proteostatic stress that leads to the DNA damage response (DDR) (Schumacher et al. 2021). DDR involves a complex series of molecular reactions that respond to DNA damage, such as activation and induction of inflammation-related pathways, induction of apoptosis or even alteration of autophagy (Vougioukalaki et al. 2022).

The autophagy (derived from Greek, “auto” oneself and “phagy” to eat) process was discovered in 1992 by the team of Yoshunori Ohsumi (Takeshige et al. 1992). Autophagy and lysosomes were first described by Christian De Duve, Nobel Prize winner for Physiology and Medicine in 1974, but autophagy has been remained for a long time a poorly studied process that can only be analysed morphologically by electron microscopy (Sabatini and Adesnik 2013). In 1992, Ohsumi identified the autophagic process in yeast cells by demonstrating under the light microscope that yeast mutants lacking lysosomal digestive enzymes in the absence of nutrients accumulate cellular components within the digestive vacuole corresponding to lysosomes (Takeshige et al. 1992). Ohsumi reasoned that this accumulation should not occur if the autophagy process is defective, and in 1993 he confirmed this hypothesis by identifying a series of mutants of genes essential for autophagy (Tsukada and Ohsumi 1993). These genes encode for proteins required for autophagosome formation and were subsequently identified in the eukaryotic cells of all living organisms, plants, and animals. This genetic screen in yeast allowed to identify 15 autophagy-related proteins (ATGs), essential for the autophagic delivery of cargo to the lysosome (vacuole for yeast) (Tsukada and Ohsumi 1993). From a functional point of view, autophagy is a catabolic process of recycling of various cellular components (Mizushima 2007). Therefore, autophagy plays an essential role in degrading non-functional or damaged protein aggregates and dysfunctional organelles, adapting the cell to different changes in the environment in order to maintain normal cell homeostasis (Tanida et al. 2008). The autophagic process can be induced mainly by growth factor depletion, hypoxia and cellular starvation (Jung et al. 2010).

The initial event of autophagy is the formation of the autophagosome. The autophagosome is a double-membrane structure that recycles proteins and organelles and subsequently

traffics to the lysosomes. Fifteen ATGs participate in the formation of the autophagosome (Takeshige et al. 1992).

Autophagy can be subdivided into different subcategories, for example, macroautophagy, microautophagy, chaperon mediated autophagy or even mitophagy (Satoo et al. 2009). All these sub-classes, although varying in autophagosome content, have in common the process of forming the autophagosome and fusing it with the lysosome to degrade unused or damaged proteins or organelles (Takeshige et al. 1992). The autophagosome formation itself is divided into different steps: autophagy initiation, phagophore elongation, autophagosomes maturation, fusion of autophagosome with lysosome and formation of autolysosome (Yim and Mizushima 2020). The first starting point of the autophagy initiation machinery is the pre-autophagosomal structure (PAS), which is induced by various stimuli, such as starvation and metabolic stress. The main regulator of the initiation phase of autophagy is a serine/threonine kinase, called mammalian target of rapamycin (mTOR) (Deleyto-Seldas and Efeyan 2021). mTOR possesses the ability to regulate cellular metabolism (Deleyto-Seldas and Efeyan 2021). Indeed, mTOR promotes anabolic metabolic processes by interacting with different proteins involved in pathways related to protein nucleotide or lipid synthesis, while on the other hand it could block metabolic processes such as autophagy (Mercer et al. 2009; Deleyto-Seldas and Efeyan 2021). mTOR critically regulates autophagy initiation by activating or deactivating UNC51-like kinase1 (ULK1) via phosphorylation, thereby inhibiting ULK1 kinase activity (Guo et al. 2018). During starvation and other positive stimuli for autophagy, ULK1 is activated via dissociation from mTOR. The ULK complex comprises the ULK1/2 family, the 200 kDa FAK family kinase-interacting protein (FIP200) and ATG13 (Turco et al. 2020). ULK complex is not the only pathway that activates autophagy; in fact, class III phosphatidylinositol-3-kinase (PI3K), also called Beclin1 complex, displays this ability too (Mercer et al. 2009). The Beclin1 complex consists of four proteins, vacuolar protein sorting 34 (Vps34), p15 (VPS15), Beclin1 (ATG6) and ATG14 (Russell et al. 2013; Guo et al. 2018). The autophagic process begins when both PI3K and ULK complex are recruited to the phagophore assembly site (PAS) (Shao et al. 2007; Lippai and Szatmári 2017).

The elongation and closure of autophagosome are regulated by two ubiquitin-like complexes. The first reaction is between ATG5 and ATG7 linking to ATG12 (Cao et al. 2016). Subsequently, this complex binds with ATG16 to form ATG5-ATG12-ATG16 complex, which is responsible for the elongation phase (Cao et al. 2016; Shimizu et al. 2010). The other ubiquitin-like complex consists of the microtubule-associated protein 1

light chain 3 (LC3) (Tanida et al. 2008). LC3 is a protein that must be activated in order to participate in the autophagy process. A protease, ATG4, is the responsible protein that process LC3 to a glycine form, before the lipidation process that involves the conjugation of LC3 and phosphatidylethanolamine (PE), catalysed by two enzymes named ATG3 and ATG7, takes place (Tanida et al. 2004). The newly lipidated LC3 is called LC3-II and can be attached to the inner and outer membrane of the autophagosome and thereby support the closure of the phagophore. LC3 is a well characterized protein as an autophagic marker, because the inactivated form, LC3-I, not yet lipidated and the active form, LC3-II, are very well distinguishable by western blot (Kuma et al. 2007). During the closing phase of the autophagosome, p62 receptor acts as a cargo protein capable of selecting and transporting proteins or organelles for recycling into the autophagosome. Thus, the newly formed autophagosome is enriched for p62 (Bjørkøy et al. 2009). The last step in the autophagic process is the maturation of autophagosomes by their fusion with lysosomes (Korolchuk et al. 2010). Lysosomes have a lumen's pH of about 5 and are rich in hydrolytic enzymes that can break down all organelles or proteins for recycling (Sandri 2013).

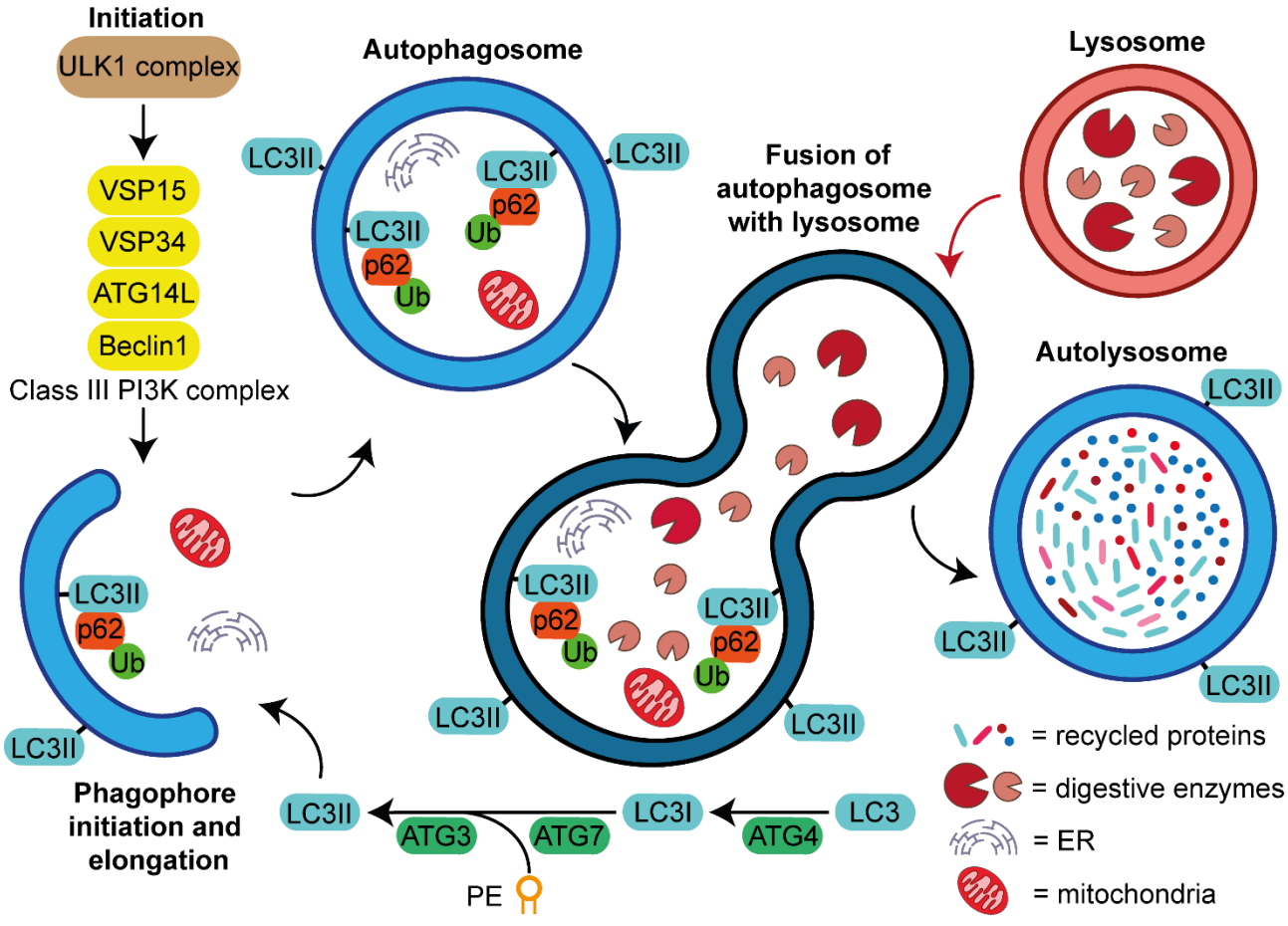

Figure 2: The autophagic process.

After the initiation phase, mediated by the ULK1- and Class III PI3K complex, a phagophore is formed via small releases from the ER and Golgi. In the elongation phase, LC3 plays a very important role. Following its activation and lipidation, LC3-II marks the inner and outer membranes of the autophagosome. p62 is responsible for the transfer of old proteins or disused organelles into the autophagosome. Subsequently, the autophagosome fuses with the lysosome rich in hydrolytic enzymes that disassemble the entire content of the autolysosome.

In recent years, more and more researcher are highlighting the central role of autophagy not only in cellular functions but also in human pathologies like cancer and neurodegenerative diseases (Sato et al. 2018). To date, the autophagic process has been shown to have many links to the development of tumours. The regulation of autophagy overlaps closely with signalling pathways that regulates tumorigenesis (Xu et al. 2020b). The mTOR signalling is inhibited by several tumour suppressor genes like TSC1 or PTEN with a consequent stimulation of autophagy. One of the most important human cancer suppressor gene, p53, increase the autophagic rate in cells with DNA damage (Xu et al. 2020b). From a different perspective, cellular proto-oncoproteins like Bcl-xL and Bcl-2 that are usually overexpressed in human cancer, inhibit autophagy after merging with Beclin1 (Schaaf et al. 2019). Cancer is not the only human disease in which autophagy plays an important role. Indeed, previous research have established the correlation between autophagy and neurodegenerative diseases (Lee et al. 2019; Djajadikerta et al. 2020).

1.3 Autophagy in the brain during ageing and neurodegenerative diseases

Autophagic mechanism appears to be functionally involved in diseases such as Parkinson's disease (PD) or amyotrophic lateral sclerosis (ALS) in which strong accumulations of protein aggregates, such as alpha-synuclein or mutant TAR DNA-binding protein 43 (TDP-43), occur (Mputhia et al. 2019; Rusmini et al. 2019; Strohm and Behrends 2020). A number of studies have a convergence between autophagic lysosomal pathways and the pathogenesis of many neurodegenerative diseases postulated, including also Alzheimer’s disease (AD) (Strohm and Behrends 2020; Overhoff et al. 2021). AD is a neurodegenerative disease in the world and is mainly characterised by amyloid-β accumulation in the brain (Heckmann et al. 2020). It has been shown that brains of healthy

subjects do not show autophagosome vesicles, whereas AD patients have a marked increase in the presence of autophagosomes in the brain probably related to autophagic impairment (Rahman et al. 2020). In PD, which is the second most common neurodegenerative disease in the world, a loss of dopaminergic neurons at the level of the substantia nigra pars compacta and an intracellular increase at the neuronal level of Lowy bodies composed of α-synuclein is characteristic (da Costa et al. 2021). The connections that have been demonstrated between autophagy and PD are manifold (Decressac et al. 2013; Zhu et al. 2019). Already in 2010, Dehay and colleagues found an increase in autophagosomes and impairment of lysosomes at the neuronal level in post-mortem brains of PD patients (Dehay et al. 2010; Lynch-Day et al. 2012). This suggests that problems with the lysosomal and autophagic system induce an increased presence of α-synuclein (Hou et al. 2020; Engelender 2008; Winslow and Rubinsztein 2011). This theory is confirmed by many publications, showing that all forms of α-synuclein are degraded through autophagy. Indeed, it has been shown that an activation of Transcription factor EB (TFEB), which is an important regulator of autophagy, mediates clearance of aggregated α-synuclein, rescuing midbrain dopamine neurons from α-synuclein toxicity (Decressac et al. 2013; da Costa et al. 2021).

The main cell types in the brain are neurons, glial cells, and microglia, characterized by various specific functions and morphologies. For example, neurons are persistent postmitotic cells that are already prenatal developed. Furthermore, neurons display a complex cellular architecture. For these features, a sufficient recycling of organelles and proteins is essential. Thus, autophagy plays a key role in neuronal homeostasis. Indeed, brain ageing, and neurodegenerative diseases have been shown to be closely related to autophagic neuronal impairment. In previous studies on mice and humans brain, a decline of Beclin-1 expression and activity have been found to be related to ageing and neurodegeneration (Shibata et al. 2006; Pickford et al. 2008). Autophagosome closure and fusion with lysosomes are inhibited by neurons by the accumulation of α-synuclein bodies, leading to a decreased protein degradation (Winslow and Rubinsztein 2011; Winslow et al. 2010). Previous research reviled also that *Drosophila* knockdown of *ATG7* and *ATG8* genes reduces lifespan and promotes neuronal accumulation of ubiquitin-positive aggregates (Juhász et al. 2007). Furthermore, transcriptional downregulation of *ATG5*, *ATG7* and *Beclin1* during ageing has conclusively been shown in *post-mortem* human brains (Lipinski et al. 2010).

In parallel, glial cells represent 50% of the resident cells of the CNS and one of their tasks, beside others, is to promote neuronal health and survival. This role includes maintenance of synaptic functions, control of blood pressure, proper nutrition of neurons and regulation of neurotransmitter release. In addition, following injury or ageing, glial cells that are able to reproduce itself, are essential for pursued proper neuronal functioning. To date, comparably less is known about autophagy in glia, but with respect to the importance of these cells in the brain, the research in this field has clearly to be increased. Indeed, autophagy is useful to clear unused or misfolded proteins or organelles in astrocytes and help, especially in pathologies like AD or PD, in which the accumulation of tau, amyloid-β or α-synuclein is the principal characteristic, to improve the viability of the surrounding cells. Already 2014 Wang and colleagues demonstrated the importance of autophagy for the astrocytic homeostasis. They showed that astrocytes from mice with ATG5 knockdown were less differentiated in comparison with that from normal black six mice. On the other side, overexpression of ATG5 led to an excessive astrocytic differentiation *in vivo* (Wang et al. 2014). Additionally, in co-cultures of astrocytes and neurons treated with amyloid-β, astrocytes can suppress inflammation via the activation of autophagy induced by progesterone (Hong et al. 2018).

Another cell type of the CNS are microglia, the resident immune cells of the brain. Because of whose enormous phagocytic power, microglia can eliminate viruses and bacteria during CNS infections by using autophagic processes. Indeed, microglia has been shown to prevent neurodegeneration by clearing neuron-released α-synuclein via selective autophagy (Choi et al. 2020). Furthermore, data from several studies suggest that microglia restrict viral infection using autophagy (Kumar et al. 2020; Waltl and Kalinke 2022). In fact, loss of autophagy leads to increased viral load in the brain of Zika virus infected Drosophila (Liu et al. 2019). Similar results have been reported for CNS infections in Drosophila with Herpes simplex virus 1 (HSV-1) (Liu et al. 2018; O'Connell and Liang 2016). In this context, in a recent study could been demonstrated that during ageing microglial phagocytosis is faulty and the diminished response to brain injury is due to the accumulation of lipid droplets caused by the impairment of autophagy (Loving et al. 2021).

Thus, since impairment of neuronal, glial, or microglial autophagy predisposes animals and humans to infections, degenerative or age-related diseases, pharmacological restoration of brain autophagy could be a valuable tool to ameliorate these pathological conditions.

1.4 The cGAS-STING pathway

The cGAS-STING pathway (cyclic GMP-AMP synthase – stimulator of interferon genes) was discovered in 2013 by Chen and colleagues, where they reported for the first time the isolation of the cGAS protein and its ability to recognize and bind cytoplasmic double-stranded DNA (dsDNA) and activate STING via the production of 2′,3′-cyclic GMP-AMP (cGAMP) (Sun et al. 2013). STING (alternatively known also as MPYS, TMEM173, MITA and ERIS) activation is able to induce interferon regulatory factor 3 (IRF3) and NF-κB (Yum et al. 2021). In addition, TANK-binding kinase 1 (TBK1) is recruited by STING, which also promotes its phosphorylation at Serine 172. Thus, pTBK1 induces phosphorylation of IRF3 at Serine 396. Then, pIRF3 dimerizes, translocates to the nucleus and induces the expression of type I IFNs, interferon-stimulated genes (ISGs), and several other inflammatory mediators (Sun et al. 2013; Guo et al. 2018; Decout et al. 2021; Liu et al. 2021b).

For immune cells, but also other cell types the cGAS-STING pathway is an important signal cascade with essential functions for innate immunity (Xiao and Fitzgerald 2013; Chen et al. 2016; Sun et al. 2013). Thereby, the ability to recognize cytosolic DNA is a fundamental skill for the innate immune response of each individual cell. The pattern recognition receptors (PRRs), such as cytosolic DNA sensors cGAS or STING are the first-line natural barrier of the host for the elimination of pathogenic infections. This pathway takes place in numerous tissue types, of immune and non-immune origin, receiving increased attention in recent years due to the importance in viral response, tumour surveillance, autoimmune diseases, and cellular senescence. In normal conditions, DNA is only present at the level of the nucleus or in the mitochondria of eukaryotic cells. It could be convincingly shown that the presence of DNA in different cellular areas, such as in the cytosol, exponentially increases the innate immune response (West and Shadel 2017). In case of cell malfunction with damage to the nucleus or more frequent mitochondrial damage, the potential of DNA release into the cytosol is very high (Barber 2011). In addition, pathogens, such as viruses and bacteria, can also possess their own DNA that they release into the cytosol during the infection event. In these cases, the cGAS-STING pathway plays a pivotal role (Motwani et al. 2019). cGAS is activated by interacting with dsDNA in a minimal 2:2 complex that induce conformational changes in the protein that allow cGAS to catalyse the transformation of ATP and GTP into 2′,3′-

cGAMP, a cyclic dinucleotide (CDN) comprising both 2′–5′ and 3′–5′ phosphodiester linkages (Zhang et al. 2014). Therefore, 2′,3′-cGAMP is considered a 'second messenger', because the dinucleotide is able to bind and activate STING that has a pivotal role in the innate immune responses (Zhang et al. 2014). During the interaction with 2′,3′-cGAMP, STING is localized in the endoplasmic reticulum (ER) and undergoes a higher-order oligomerization to form tetramers (Ogawa et al. 2018).

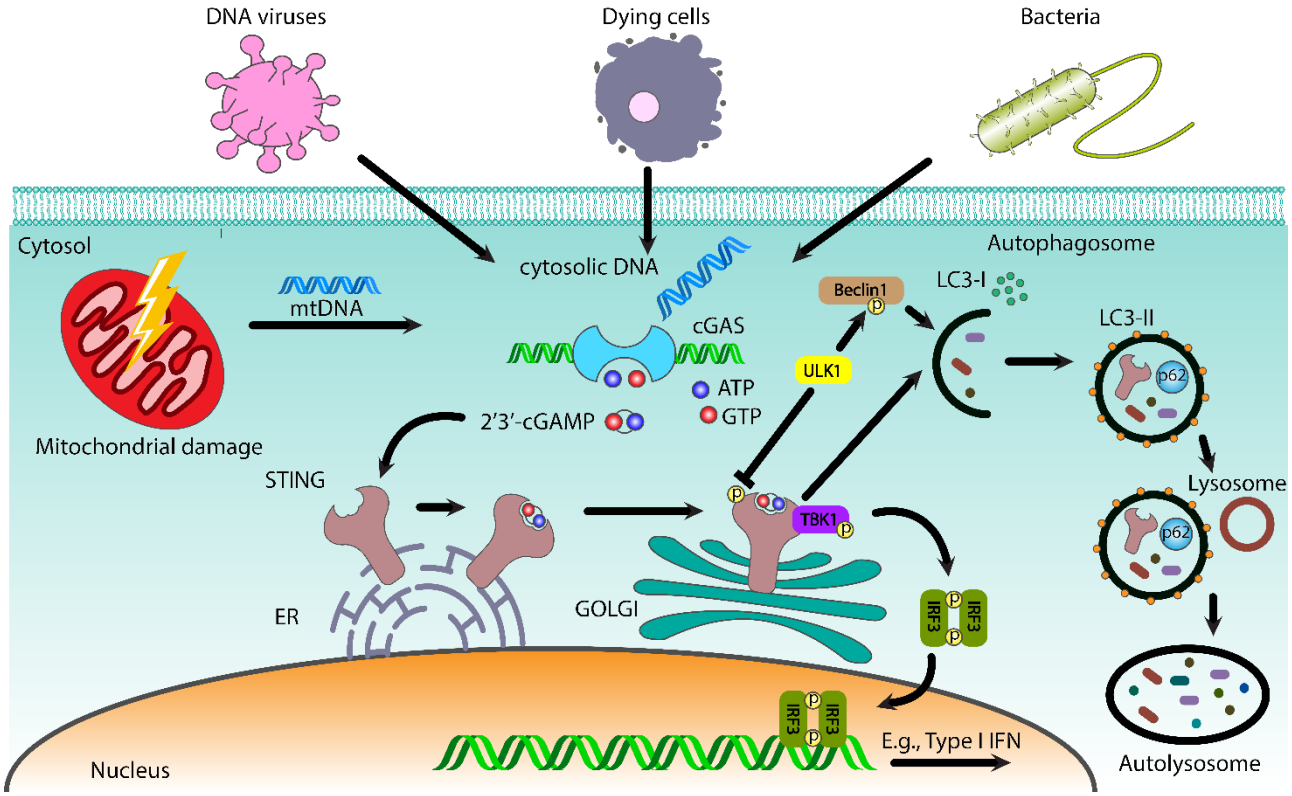

Figure 3: The cGAS–STING signalling pathway.
cGAS binds cytosolic RNA or DNA derived from the nucleus, micronucleus, mitochondria, and viral or bacterial pathogens to produce 2′,3′-cGAMP from ATP and GTP. 2′,3′-cGAMP initiates the signalling cascade by binding to the protein STING, which translocates to the Golgi apparatus, where it binds TBK1, which phosphorylates IRF3. Then, IRF3 translocates to the nucleus and transcribes ISGs. Together, the cytokines and interferons produced mount an immune response against invading pathogens.

In recent years, it has been demonstrated that the binding of STING to CDNs, leads to its translocation from the ER to perinuclear compartments like the Golgi, endosomes, and autophagy-related compartments via coat protein complex II (COPII) (Mukai et al. 2016; Zhang et al. 2020; Dobbs et al. 2015). The trafficking of STING between ER and different cellular compartments has been shown to be crucial for the pathway function. In fact, inhibiting STING trafficking from the ER to the Golgi using Brefeldin A has been shown to block IRF3 phosphorylation and consequently IFN-ß production after STING activation (Taguchi et al. 2021; Mukai et al. 2016; Zheng et al. 2021). Furthermore, in 2016 Mukai

and collaborators demonstrated that palmitoylation of STING at the Golgi is an essential step for the activation of STING (Mukai et al. 2016). After leaving the Golgi, STING has been shown to move to the p62 and LC3-II positive compartments and lysosomal environments, meaning that STING after its inactivation is recycled through the autophagosome (Prabakaran et al. 2018; Liu et al. 2019; Decout et al. 2021). Indeed, degradation of STING can be prevented by interfering with lysosomal functions using chloroquine or bafilomycin A1 treatment (Gonugunta et al. 2017; Fischer et al. 2020). Nevertheless, the exact mechanism by which STING translocates into the autophagosome is still unclear to date.

1.5 The link between autophagy and cGAS-STING pathway

In recent years the cGAS-STING pathway has been discovered to be closely related to autophagy (Sun et al. 2013; Yum et al. 2021; Zheng et al. 2021; Gui et al. 2019). Apart from the activation of processes leading to the production of cytokines and type I interferons, STING trafficking is also able to induce autophagy even before human evolution (Prabakaran et al. 2018; Gui et al. 2019). In fact, Gui and colleagues demonstrated in 2019 that even STING-mediated autophagy induction was found in sea anemone *Nematostella vectensis*, which belongs to a clade that separates from *Homo sapiens* more than 500 million years ago (Gui et al. 2019). Furthermore, the same authors showed that on one hand the activation of the cGAS-STING pathway induced autophagy in these animals, but on the other hand without inflammation and type I interferon expression. That leads to the conclusion that autophagy activation via STING trafficking might be a primordial function of the cGAS pathway (Gui et al. 2019). Furthermore, in the same report the researchers demonstrated that 2’3’-cGAMP-treated BJ cells had a higher number of autophagosomes than untreated cells, suggesting a close link between the cGAS-STING pathway and autophagy function. In fact, loss of cGAS, STING and TBK1 significantly reduced the protein quantity of lipidated and therefore activated LC3 in cells treated with herring testes DNA (HT-DNA) and 2'3'-cGAMP (Gui et al. 2019). Autophagy must also be considered as a factor regulating the activity of the cGAS-STING pathway and vice versa. Prabakaran and colleagues demonstrated that the degradation of STING and therefore the consequent deactivation of the pathway occurs predominantly via autophagy. Specifically, TBK1 is capable of phosphorylating p62 which, once activated, acts as a cargo protein and transfers ubiquitinated STING into autophagosomes

(Prabakaran et al. 2018). Indeed, with the absence of p62, STING is not successfully degraded while high levels of pro-inflammatory genes are still maintained after treatment with 2'3'-cGAMP (Prabakaran et al. 2018). In addition, Prabakaran and colleagues demonstrated that TBK1 and IRF3 are also essential for a correct degradation of STING via autophagy and subsequent degradation in lysosomes, the two proteins that therefore occur in order of activation of the STING pathway. In fact, even proteins essential for the initiation phase of autophagy show a close link with cGAS and STING. For example, an interaction between cGAS and Beclin1 is demonstrated (Liang et al. 2014). cGAS competes with Rubicon on the same binding site as Beclin1. Rubicon can negatively regulate autophagy and is usually linked to Beclin1 when autophagy is inhibited. Following dsDNA treatment, HEK-293T cells activate both the cGAS-STING pathway and autophagy and the amount of cGAS-Beclin1 complex increases with a decrease in the Rubicon-Beclin1 complex (Liang et al. 2014). There is a relatively small body of literature that considers the direct interaction between cGAS and LC3. In 2021, Zhao et al. reported a role of cGAS in the induction of micronucleophagy via cGAS-LC3 complex. They demonstrated on HEK-293T cells that this interaction is essential for the recycling of cytosolic micronuclei (Zhao et al. 2021).

STING is also considered to function as an autophagy receptor, interacting directly with LC3 (Liu et al. 2021a). The physical contact between STING and LC3 that leads directly to the initiation phase of autophagy (Liu et al. 2021a). Further studies have indicated that the activation of STING by phosphorylation is an essential prerequisite for STING-induced autophagy (Gui et al. 2019). As mentioned before in chapter 1.4, activated STING leaves the ER, moves to the ER-Golgi intermediate compartment (ERGIC) and then into Golgi in a process dependent on the COP-II complex (Dobbs et al. 2015). Vesicles budding from the ER and ERGIC could serve as membrane sources for LC3 lipidation and autophagosome biogenesis. For this reason, it is possible that autophagy induced by STING requires the membrane fraction derived from ER or ERGIC as the substrate for LC3 lipidation. Indeed, bafilomycin A1 (BFA) treatment leads to the inhibition of the STING movement and thereby to the reduction of the LC3 lipidation of newly formed autophagosomes (Ge et al. 2013). Studies about STING recycling via autophagy were first carried out by Konno *et al.* in 2013. They demonstrated that STING can be phosphorylated by ULK1 at Serine 366 in order to prevent a continuous activation of innate immunity signalling (Konno et al. 2013). These data are supported by the fact that ULK1 is deregulated under conditions of strong cGAS-STING pathway activation. Indeed, Kemp

and colleagues demonstrated that a strong induction of STING activity by stimulation with ultraviolet wavelengths on keratinocytes led to a decrease in ULK1 protein levels (Kemp et al. 2015). If STING is considered to be essential for the induction of autophagy via cGAS-STING pathway activation, its functioning for TBK1 and IRF3 is different. In fact, more and more publications suggest that the portion of the STING protein responsible for the lipidation of LC3 is separate from that for the phosphorylation of TBK1 and subsequently of IRF3 (Cai and Imler 2021; Yum et al. 2021). The key area of the STING protein for phosphorylation of TBK1 and IRF3 and subsequent induction of type I IFNs is the C-terminal tail (aa 341-379) (Yum et al. 2021). Any S365A mutations in STING result in a phosphorylation deficit of IRF3 but maintained ability to recruit TBK1. In contrast, the L373A mutation of STING results in complete blockade of phosphorylation of both TBK1 and IRF3. Both of these mutations, although essential for the induction of cellular defence mechanisms, do not implicate the role of STING in the induction of autophagy through lipidation of LC3 (Yum et al. 2021). Furthermore, depletion of TBK1 and IRF3 on He La cells does not block the increase in LC3-II (thus active and lipid-rich) after stimulation with poly(dA:dT) (Cai and Imler 2021).

Anyway, a recent study indicates that in TBK1 knockdown cells the formation of the autophagosome via LC3 lipidation was not affected, but STING was not degraded by autophagy due to a lack of the autophagosomes maturation phase (Pilli et al. 2012). A small number of publications have demonstrated the involvement of TBK1 in the autophagic process but as, yet nothing has been published on a possible role instead of IRF3 (Oakes et al. 2017; Le Ber et al. 2015).

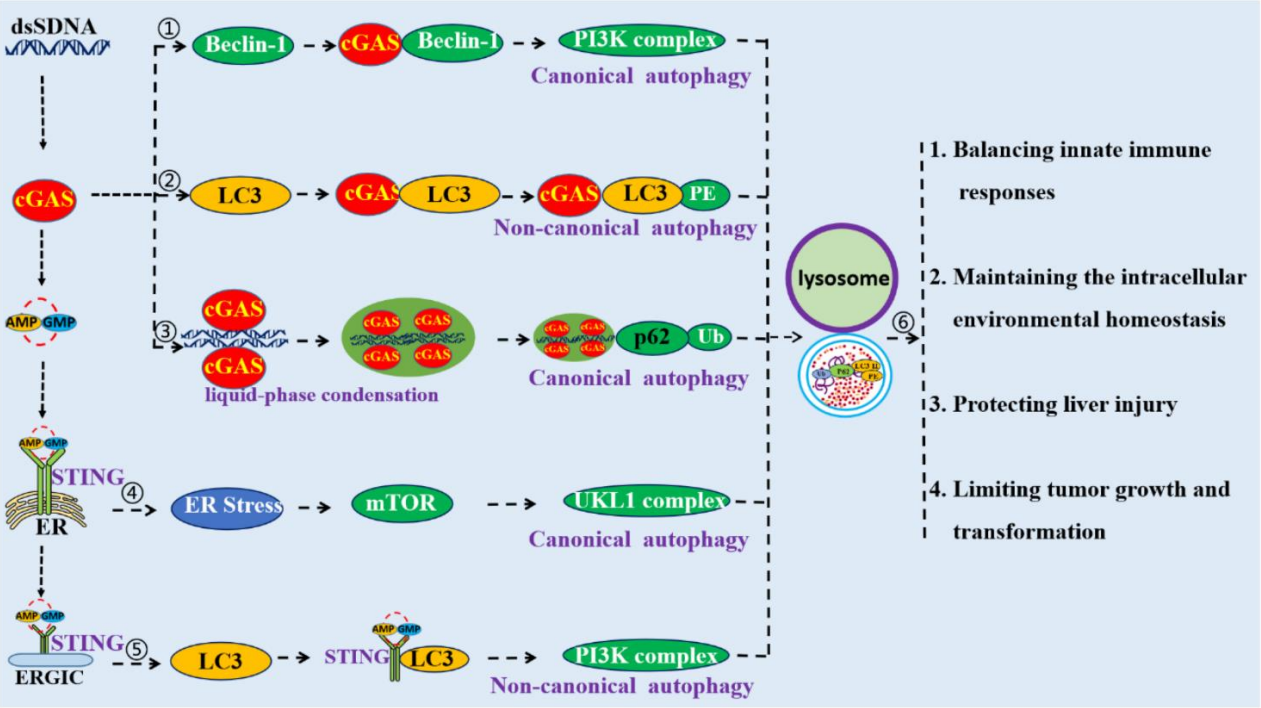

Figure 4: Schematic overview of the close correlation between the cGAS-STING pathway and the autophagic process (Zheng et al. 2021).

1.6 The role of the cGAS-STING pathway in the brain during ageing and neurodegenerative diseases

The relevance of the cGAS-STING pathway in autophagic processes makes it to an important tool in mediating cellular senescence. In fact, to date it is unquestioned that cellular ageing is accompanied by pro-inflammatory states and/or phenomena of damage and loss of cytosolic organelles such as mitochondria. The injury of mitochondria or the formation of micronuclei in pro-apoptotic cells leads to the accumulation of DNA at the cytosolic level. The main proteins involved in the removal of these nucleic acids are pattern recognition receptors (PRRs) and their adaptor proteins that exist in the mammalian brain, including not only cGAS but also the retinoic acid inducible gene I-mitochondrial antiviral signalling protein (RIG1-MAVS) and Toll-like receptor 3/4-TIR-domain containing adaptor inducing interferon β (TLR3/4-TRIF). If MAVS and TLR3 and 4 predominantly recognize cytosolic RNA, essentially released by exogen invaders such as viruses or bacteria, cGAS seems to be mainly predisposed to recognize DNA. As mentioned earlier in Chapter 1.2, DNA damage increases with age and this phenomenon

has also been demonstrated in the brain. In fact, neurons are rich in mitochondria and base their anergy budget predominantly to the function of these organelles. During ageing it has been shown that in practically all brain regions an increase of mutations and cytosolic release of mtDNA can be observed (Corral-Debrinski et al. 1992). The cytosolic accumulation of DNA is extremely toxic to cells and especially to neurons, which are perennial cells and which in the course of evolution have created an excellent resistance to cell death due to the disability of cellular renewal (Corral-Debrinski et al. 1992). Likewise, neurons, astrocytes and microglia also accumulate cytosolic DNA during ageing that must be recycled by the cell. The most important way to eliminate this toxic waste in all neural cell types, is realized by the cGAS-STING pathway and the subsequent activation of inflammatory processes and autophagy. Understanding the functioning of the cGAS-STING pathway could contribute to the identification of effective methods to maintain a lifelong brain function.

The accumulation of toxic materials in the cytosol occurs not only during ageing, but also throughout neurodegenerative diseases. In fact, a recently Jauhari and colleagues points out that *post-mortem striae* of Huntington's disease patients showed very high levels of pro-inflammatory genes and cytosolic DNA. Moreover, these data could be correlated with the activation of the cGAS-STING pathway (Jauhari et al. 2020). Another study indicates that one of the most common mutations in PD patients was found at the level of the gene, coding for the leucine-rich-repeat kinase 2 (LRRK2) protein (Houlden and Singleton 2012). Recently was found that in LRRK2 knockout macrophages an abnormal increase of oxidative stress takes place that is linked to activation of the cGAS-STING pathway with subsequent increase of inflammation and expression of ISGs (Wallings and Tansey 2019; Weindel et al. 2020). Unfortunately, this experiment was realized only on macrophages and not on specific CNS resident cells.

Nowadays, in the different cell populations residing in the brain, the cGAS-STING pathway has mainly been studied in microglia. The reason is due to the immune power that microglia have in defending neurons and glial cells, such as astrocytes. For example, in 2022 could be shown, how activation of the cGAS-STING pathway in microglia contributes to neuroinflammation with the induction of microglial pyroptosis in mice with cerebral venous sinus thrombosis (CVST) (Ding et al. 2022). In other neurodegenerative diseases microglia also plays an important role. For example, in microglia-astrocytes primary cell cultures of intrastriatal αSyn preformed fibril (α-Syn PFF) mouse model of PD, Hinkle *et al.* demonstrated a strong increase of DNA damage that induces cGAS-STING pathway

activity. Furthermore, in this paper they also demonstrated that striatal interferon activation in the α-Syn PFF model is STING-dependent by using STING-deficient mice (Hinkle et al. 2022). Additionally, it has been shown that microglia play an important role in chronic cerebral restraint stress that is mediated via the cGAS-STING pathway. In mice with chronic stress-induced behaviour experiments, induction of STING improved depression-like behaviour during chronic stress via increased microglial phagocytosis (Duan et al. 2022).

Unfortunately, recent experiments regarding the role of the cGAS-STING pathway on the function of the aged or diseased brain were focused only on microglia. To date, the knowledge about the role that the cGAS-STING pathway might have on astrocytes and even more on neurons is missing. Therefore, a focused study on the role of the cGAS-STING pathway on neurons or astrocytes using an *in vitro* and *in vivo* model of brain ageing could be important.

2 Hypothesis

The process of cellular ageing has been studied since many years. However, there are still many unexplored sides of brain ageing to date. The brain is a structurally very intricated organ with functional variations between highly specified areas and cellular differences, thus complexity reflect the challenge of the following study. Moreover, the proliferating cycle of glia cells shows distinctions from the neuronal one. Indeed, microglia and astrocytes, which are mitotic cells behave differently from post-mitotic neurons. Therefore, the focus on the neuronal autophagy is essential to understand the mechanism underling their survival. The discovery of the cGAS-STING pathway in 2013 (Sun et al. 2013) and its intense connection with autophagy (Gui et al. 2019), revealed the need of further investigation in the field of neuronal ageing and homeostasis. Over the past 9 years, the cGAS-STING signalling have been examined intensively and to date, much more is known about its functioning. However, regarding its role in the CNS comparable less is known and so far, the only one cell type studied is microglia, the brain resident immune cells. Thanks to various, rare reports concerning HSV-1 or Zika virus infection in the brain (Liu et al. 2019; Yamashiro et al. 2020; Reinert et al. 2016), we received some information about the significant aspect of the cGAS-STING regarding the defence of the brain against invading pathogens. Considering the relationship between the cGAS-STING pathway and cellular senescence, demonstrated in many experiments on cell types, such as HeLa, HEK 293T cells or keratinocytes (Li and Chen 2018), comparably little is known about how this pathway may influence neuronal homeostasis and ageing. Furthermore, the morphological, structural, and functional differences between the various cell types residing in the CNS leads to the question, whether the cGAS-STING pathway plays a different role within neurons, astrocytes, and microglia.

To date, the consequence of STING deficiency with subsequent deactivation of the entire pathway on neuronal homeostasis is completely unknown. Understanding how the cGAS-STING pathway may alter the brain ageing process and neuronal homeostasis might contribute to the development of new therapies for neurodegenerative diseases and provide insights into the brain, and more specifically neuronal ageing processes.

3 Materials and Methods

3.1 Materials

3.1.1 Chemicals and solutions

The experiments were performed by using Cell Signalling, Merck, Invitrogen, Peprotech, Proteintech, R&D Systems, Roche, Roth, Sigma Aldrich, SYnaptic SYstems, Thermo Scientific and Tocris products in pro analysis or molecular-biology grade. In the method description, supplier and composition information of special chemicals and solutions are mentioned. Roti®CELL water (Carl Roth, cat. no. 9186.2) was used for protein biochemical experiments. For all other requirements, such as buffer preparation, bi-distilled water (ddH_2O) from the Milli-Q Direct (Merck Millipore, cat. no. Y00Q0V0WW) was used. Special chemicals and solutions are mentioned at the beginning of each corresponding methods section.

Table 1. Primary antibodies for WB

Western Blot					
Primary Antibodies	**Species**	**WB**	**IF/IHC**	**Catalog N°.**	**Supplier**
α-β-actin	Mouse, monoclonal	1:2000	/	**#3700**	Cell Signalling
	Rabbit, monoclonal	1:2000	/	**#8457**	Cell Signalling
α-Bassoon	Guinea Pig, polyclonal	1:1000	/	**161 004**	SYnaptic SYstems
α-Beclin1	Rabbit, polyclonal	1:1000	/	**#3495**	Cell Signalling
α-phospho-Beclin1 (Ser30)	Rabbit, polyclonal	1:1000	/	**#84966**	Cell Signaling
α-cGAS	Rabbit, monoclonal	1:1000	/	**#31659**	Cell Signaling
α-Cleaved Caspase3	Rabbit, monoclonal	1:1000	1:300	**MAB835**	R&D Systems
α-Glial Fibrillary Acidic Protein (GFAP)	Chicken, polyclonal	1:1000	1:1000/ 1:500	**ab4674**	Abcam
	Rabbit, monoclonal	1:1000	/	**170 002**	SYnaptic SYstems
α-Golgi matrix protein (GM) 130	Mouse, monoclonal	1:1000	1:500	**610822**	BD Biosciences
α-Gluthathione S Transferase	Goat, polyclonal	1:1000	/	**ab53942**	Abcam
α-Homer1	Rabbit, polyclonal	1:1000	/	**160 003**	SYnaptic SYstems

α-Ionized calcium Binding Adaptor molecule 1 (IBA-1)	Chicken, polyclonal	1:1000		**234 009**	SYnaptic SYstems
α-Interferon Regulatory transcription Factor 3 (IRF3)	Rabbit, monoclonal	1:1000	1:250	**ab68481**	Abcam
α-phospho-IRF3 (Ser396 or 385)	Rabbit, monoclonal	1:1000	/	**#PA5-38285**	Invitrogen
α-Microtubule-associated proteins 1A/1B light chain 3A (LC3A/B)	Rabbit, polyclonal	1:1000	/	**#4108S**	Cell Signaling
α-Microtubule Associated Protein 2 (MAP2)	Mouse, monoclonal	1:1000	1:1000/ 1:500	**M4403**	Sigma-Aldrich
	Guinea Pig, monoclonal	1:1000	1:1000/ 1:500	**188 004**	SYnaptic SYstems
α-Neuronal Nuclear protein (NeuN)	Guinea Pig, polyclonal	1:1000	1:1000/ 1:500	**266 004**	SYnaptic SYstems
α-p62	Rabbit, polyclonal	1:1000	/	**#5114**	Cell Signaling
	Mouse, polyclonal	/	1:300	**ab56416**	Abcam
α-phospho-p62 (Ser403)	Rabbit, monoclonal	1:1000	/	**#39786**	Cell Signaling
α-PSD95	Mouse, monoclonal	1:1000	/	**ab30645**	Abcam
α-Signal transducer and activator of transcription 1 (STAT1)	Rabbit, polyclonal	1:1000	/	**#9172**	Cell Signaling
α-phospho-STAT1 (Ser727)	Rabbit, polyclonal	1:1000	/	**#9177**	Cell Signaling
α-phosphor-STAT1 (Y701)	Rabbit, polyclonal	1:1000	/	**ab30645**	Abcam
α-STAT2	Rabbit, polyclonal	1:1000	/	**ab32367**	Abcam
α-phospho-STAT2 (Tyr690)	Rabbit, polyclonal	1:1000	/	**SAB4503836-100UG**	Sigma-Aldrich
α-Shank3	Guinea pig, polyclonal	1:1000	1:300	**162 204**	SYnaptic SYstems
α-Synaptophysin 1	Guinea Pig, polyclonal	1:2000	1:500	**101 004**	SYnaptic SYstems
α-Stimulator of	Rabbit,	1:1000	1:300/	**19851-1-**	Proteintech

interferon genes (STING)	polyclonal		1:200	**AP**	
α-TAU1	Mouse, monoclonal	1:1000	1:1000	**MAB3420**	Sigma-Aldrich
α-TANK-binding kinase1 (TBK1/NAK)	Rabbit, polyclonal	1:1000	/	**#29047**	Cell Signalling
α-phospho-TBK1/NAK (Ser172)	Mouse, monoclonal	1:1000	/	**#5483**	Cell Signaling
α-Translocase of outer membrane (TOM) 20	Rabbit, monoclonal	1:1000	/	**#42406**	Cell Signaling
α-Unc-51 Like Autophagy Activating Kinase 1 (ULK1)	Rabbit, monoclonal	1:1000	/	**#8054**	Cell Signaling
α-phospho-ULK1 (Ser555)	Rabbit, polyclonal	1:1000	/	**#14202**	Cell Signaling
ds-Deoxyribonucleic Acid (DNA)	Mouse, monoclonal	/	1:1000	**ab27156**	Abcam

Table 2. Secondary antibodies for WB

Western Blot				
Secondary antibodies	**Species**	**Dilution**	**Catalog N°.**	**Supplier**
α-rabbit IgG, horseradish peroxidase (HRP) conjugated	donkey	1:7500	115-035-152	Jackson ImmunoResearch
α-mouse IgG, HRP conjugated	goat	1:7500	115-035-146	Jackson ImmunoResearch
α-chicken IgG, HRP conjugated	goat	1:7500	103-035-155	Jackson ImmunoResearch
α-guinea pig IgG, HRP conjugated	donkey	1:7500	706-035-148	Jackson ImmunoResearch
α-goat IgG, HRP conjugated	donkey	1:7500	705-035-147	Jackson ImmunoResearch

Table 3. Secondary antibodies for immunofluorescence and immunohistochemistry

Immunofluorescence and Immunohistochemistry (IF and IHC)

Secondary antibodies	Species	IF/IHC	Catalog N°.	Supplier
α-rabbit IgG (H+L) Alexa Fluor 488	donkey	1:2000/ 1:1000	A-21206	Invitrogen
α-guinea pig IgG (H+L) Alexa Fluor 488	goat	1:2000/ 1:1000	A-11073	Invitrogen
α-mouse IgG (H+L) Alexa Fluor 488	donkey	1:2000/ 1:1000	A-21202	Invitrogen
α-chicken IgG (H+L) Alexa Fluor 647	donkey	1:2000/ 1:1000	703-606-155	Jackson ImmunoResearch
α-guinea pig IgG (H+L) Cy™5	donkey	1:2000/ 1:1000	715-175-151	Jackson ImmunoResearch
α-rabbit IgG (H+L) Cy™3	donkey	1:2000/ 1:1000	711-165-152	Jackson ImmunoResearch
α-mouse IgG (H+L) Cy™3	donkey	1:2000/ 1:1000	715-165-150	Jackson ImmunoResearch
α-guinea pig IgG (H+L) Cy™3	donkey	1:2000/ 1:1000	706-165-148	Jackson ImmunoResearch

3.1.2 Animals

In this study, Wistar rats (*Rattus norvegicus*/) and C57BL/6J and B6(Cg)-Sting$^{1tm1.2Camb}$/J (STING$^{-/-}$ mice) (*Mus musculus*) from the animal facility of the Institute of Pharmacology and Toxicology (Magdeburg, Germany) were used. Adult mice and rats were housed in groups of 5-6 animals, under a regular 12 h light-dark schedule (lights on 6 AM-6 PM) with food and water available *ad libitum* at constant temperature (22±2°C) and relative humidity (40-60%). All animal experiments were performed in compliance with international guidelines regarding the care and use of animals for experimental procedures (2010/63/EU) and procedures were approved and conducted under established standards of the German federal state of Sachsen-Anhalt (Institutional Animal Care and Use Committee: Landesverwaltungsamt Sachsen-Anhalt; License No. 42505-2-1507 UniMD Germany in accordance with the European Communities Council Directive; 86/609/EEC). Any effort was made to minimize the number of animals used and their suffering during experiments.

3.2 Methods

3.2.1 Cell Culture

- Poly-d-lysine (PDL): 150mM borate buffer pH 8.5, poly-d-lysine (100µg/mL);
- DMEM^{+}: DMEM + 4.5g/L D-Glucose, 2 mM L-glutamine (Gibco, cat. no. 25030081); 10 % (v/v) foetal calf serum (Capricorn Scientific, cat. no. FCS-62A);
- Neurobasal™ medium^{+}: Neurobasal™ medium (Gibco, cat. no. 21103049), 1xB-27 (Gibco, cat. no. A3582801), 0.8mM L-glutamine (Gibco, cat. no. 25030081).

Primary cortical cells were obtained from embryonic E19 rats (Wistar) or mice (C57BL/6J, STING$^{-/-}$) and were prepared as essentially described in Banker & Goslin (1988) or Kaech & Banker (2006) with slight modifications (Banker and Goslin 1988; Kaech and Banker 2006). In brief: female pregnant animals were anaesthetized with Isofluran CP (cp-pharma, cat. no. 1214) for 2 minutes and sacrificed by decapitation. Embryos were decapitated without anaesthesia prior isolation of the cortex. After shearing the cortical tissue, samples were treated with trypsin for 7 min and later with DNAse. Following DNAse digestion, a mechanical dissociation was performed using a syringe with different cannulas (0,9x40 mm and 0.45x25 mm).

The primary cortical cells were counted and cultured in Dulbecco's Modified Eagle Medium^{+} (DMEM^{+}) using different well plate sizes (Avantor, 6 well plate cat. no. TPPA9246; 12 well plate cat. no. TPPA92412; 24 well plate cat. no. TPPA92412) and T75 flasks (Sarstedt, cat. no. 83.3911.002) pre-coated with Poly-D-Lysine (PDL). The medium was exchanged by Neurobasal™ medium^{+} for the first time 3h after seeding and a second time after 24h. Cell viability was maintained by adding 10% fresh Neurobasal™ medium^{+} once a week. For PCR experiments, cells were seeded into flask at a density of 3 million cells. For immunocytochemistry experiments, cells were seeded into 24 well plates containing glass coverslips with a diameter of 12 mm (Thermo Fisher, cat.no. CDAD00120RA120MNZ#0) on the bottom of each well at a density of 20.000, 40.000 or 80.000 cells per well. For Western blot experiments, cells were seeded into 6 well plates at a density of 300.000 cells per well. Cells were cultured in an incubator (Thermo Fisher, Heracell^{TM} 150i) at 37°C, 5% CO_2 and 95% humidity.

3.2.2 Drugs and treatment of primary cortical cells from mice

- 2'3'-cGAMP (InvivoGen, cat. no. tlrl-nacga23-1) 25 µg/ml for 2 h;

- Chloroquine (CQ, Sigma-Aldrich, cat. no. C6628-25G): 50 µM for 4 h;
- H151 (InvivoGen, inh-h151): 4 µg/ml for 2 h;
- Recombinant murine Interferone (IFN) γ (Peprotech, cat. no. 315-05): 100 ng/ml for 24 h.

3.2.3 Protein extraction from mouse brains

- Homogenisation buffer: 1x PBS pH 7.4, Protease inhibitor (Roche, cat. no. 04693132001), PhosStop (Roche, cat. no. 04906837001);
- 4x protein sample buffer (SDS): 250mM Tris-HCL pH 6.8, 4% (v/v) SDS, 40% (v/v) glycerol, 20% (v/v) ß-mercaptoethanol, 0.004% (v/v) bromophenol blue.

Brains were homogenised using a potter machine (Potter S, Sartorius cat. no. 8533024) with a volume of 10 ml for 1 g of brain tissue using the M-PER (in case of ELISA) or the homogenisation buffer in case of western blot. After the dilution of the sample using the homogenisation buffer, the 4xSDS were added in a proportion 1:4. The brain lysates were incubated at 95°C for 5 min and stored at -20°C until further use.

3.2.4 Protein extraction from primary cortical cells

- Phosphate buffered saline (PBS)-MC: 1 x PBS pH 7.4, 0.1 mM $CaCl_2$, 1 mM $MgCl_2$;
- 4x protein sample buffer: 250mM Tris-HCL pH 6.8, 4% (v/v) SDS, 40% (v/v) glycerol, 20% (v/v) ß-mercaptoethanol, 0.004% (v/v) bromophenol blue;

Primary cortical cells grown in 6 well plates at a density of 300.000 cells per well were washed once with 1mL of ice-cold Phosphate Buffered Saline-MC and then lysed in 80µL 1x protein sample buffer and transferred into a reaction tube. The cell lysates were incubated at 95°C for 5 min and stored at -20°C until further use.

3.2.5 Amido black protein assay

The amido black protein assay (Heda *et al.* 2014) was conducted in a transparent white border 96-well plate (Eppendorf AG, cat. no. 951040005) to determine the total protein concentration of the respective lysates. The assay was performed in triplicates for both, the samples, and Bovine Serum Albumin (BSA, Carl Roth, cat. no. 8076.5) standards respectively. The BSA standard was diluted from a 0.5 mg/mL stock solution to reach a final concentration of 2, 4, 8, 12, 16 and 20 µg of total protein in a final volume of 100 µL,

according to the scheme in Table 3. Therefore, 5 µL of each protein lysate sample was diluted in 95 µL molecular biology graded H_2O. According to the protocol 200µL of amido black solution was added to each well and incubated for 10 min at RT. Centrifugation was carried out at 3220xg (Eppendorf AG, centrifuge 5810R), followed by a 10 min incubation at RT. The supernatant was carefully decanted, 300 µL of washing solution was added to the pellets and the plate was centrifuged with the same settings as described before. This step was repeated twice and then the pellets were air-dried after decanting. Resuspension of the pellets was conducted with 300 µL of 0.1M NaOH with gentle agitation. Excitation at 620 nm was measured with a spectrophotometer (Tecan, Infinite® F50) and the read out displayed with the Magellan™ standard software (Tecan, version 2.0). All the lysates were diluted to reach a final concentration of 0.5 or 1 µg/µL.

Table 4. BSA standard of amido black

Row	µl ddH_2O	µl BSA (conc.1mg/mL)	µg BSA
A	100	0	0
B	96	4	2
C	92	8	4
D	84	16	8
E	76	24	12
F	68	32	16
G	60	40	20

3.2.6 Sodium Dodecyl Sulfate Polyacrylamide Gel Electrophoresis (SDS-PAGE)

Table 5. Composition of SDS-PAGE Tris Glycine gradient (5-20%) gels

	Volume (mL) for Separating gel			Volume (mL) for Stacking gel
Components	**5%**	**20%**	**Components**	
1.8 M Tris-HCl pH 8.8	6.84	6.84	0.5 M Tris-HCl pH 6.8	9.00
40% (v/v) acrylamide+ 0.8% (w/v) bisacrylamide	4.06	16.20	Rotiphorese® Gel 30	5.76
Double distillate H_2O	18.94	1.39		11.88
10% (v/v) SDS	0.3168	0.3168		0.360

0.2M EDTA pH 8.0	0.3168	0.3168		0.360
87% (v/v) glycerol	1.8	7.2		8.28
0.8% (v/v) Bromophenol blue	-	0.150	0.5% (w/v) Phenol red	0.175
10% (w/v) APS	0.1152	0.072		0.2223
TEMED	0.0216	0.0216		0.0273

Table 6. Composition of SDS-PAGE Tris Glycine (10%) homogeneous gels

	Volume (mL) for Separating gel	Volume (mL) for Stacking gel	
Components	**10%**	**Components**	
1.8M Tris-HCl pH8.8 + 0,4% SDS	10	0.5 M Tris-HCl pH 6.8	5.2
Rotiphorese® Gel 30	13.33		3.41
Double distillate H_2O	13.36		7.25
0.8% (v/v) Bromophenol blue	0.01667	0.5% (w/v) Phenol red	0.1035
87% (v/v) glycerol	3		4.74
TEMED	0.02667		0.0296
10% (w/v) APS	0.2667		0.1184

- Electrophoresis buffer: 0.25M Tris-base, 1.92M glycine, 1% (v/v) SDS);

SDS-PAGE was conducted according to the standards described by Laemmli 1970 (LAEMMLI 1970). SDS-PAGE gradient gels (5-20%; Table 4) and SDS-PAGE homogeneous gels (10%; Table 5) were placed together with the electrophoresis buffer into the Hoefer™ Mighty Small System SE250 basic unit electrophoresis chamber from Hoefer™ (Fisher Scientific, cat. no. 03-500-483). Samples were loaded into the pockets of the gel at a concentration of 0.5 or 1 μg/μl for a total of 10 or 20 μg/μl per sample loaded. The protein separation was carried out at a voltage of 12 mA per gel and a constant temperature of 4°C. The PageRuler™ prestained protein ladder (4 μL, ThermoFisher Scientific, cat. no. 26617) was used as marker for molecular weight in SDS-PAGE.

3.2.7 Coomassie Brilliant Blue R250 staining

- Coomassie staining solution: 0,125% (w/v) Coomassie Brilliant Blue R250, 50% (v/v) methanol, 10% (v/v) acetic acid;
- Destaining solution: 7% (v/v) acetic acid;
- Gel drying solution: 50% (v/v) methanol, 5% (v/v) glycerol.
- 0,1 M NaOH

After SDS-PAGE, the gels were incubated with staining solution overnight at RT and then destained with the destaining solution. The gels were destained until distinct protein bands were clearly visible and finally incubated overnight in dd$H_2$0. The gels are imaged and analysed using the ArtixScan F2 (Microtek) scanner and SilverFast software (Silverfast, version 8). Finally, the gels were incubated in gel drying solution for 5 min and then stretched on a frame between two sheets of cellophane (Carl Roth, cat. no. K422.1) to dry.

3.2.8 Western Blot (WB)

- Blocking solution: 1x Tris buffered saline (TBS), 5% (w/v) dry milk;
- Primary antibody solution: 1x TBS supplemented with 0.1% (v/v) Tween® 20 (TBS-T), 0.02% (v/v) Azide, 0.1% (w/v) BSA;
- Ponceau staining solution: 0.5% (w/v) Ponceau, 3% (v/v) acetic acid;
- Western Blot buffer: 0.25M Tris-base, 1.92M glycine, 0.2% (v/v) SDS.

WBs were performed in order to identify and quantify the amount of a specific protein in different samples. Proteins from SDS gels were transferred to the nitrocellulose membrane using the sandwich method (Towbin, 2015). To obtain the sandwich, the gels and nitrocellulose (NC) membranes were closed with Whatman paper and sponge and finally placed in the chamber with transfer buffer. The proteins were transferred to the NC membrane (Protran BA85, 0,22 µm, Li-Cor Biosciences, cat. no. 926-31092) using a Hoefer™ Mighty Small System SE250 at 200 mA for 1.5 h at standard temperature of 4°C and with constant stirring of the buffer. Subsequently, membranes were incubated for 10 min with Ponceau staining solution for protein visualization. The stain was removed by few washings in ddH_2O and 1xTBS. To avoid unspecific binding of the primary antibody, the membrane was blocked with 5 % dry nonfat milk (for all antibodies) in TBS for 1h at RT under constant and gentle agitation. After two times rapid washing with 1xTBS, primary

ABs were incubated overnight at 4 °C under permanent agitation. On the next day, membranes were washed for 10 min with 1xTBS, 10 min with 1xTBS-T, 5 min with 1xTBS-T and 5 min with 1xTBS. Afterwards, the membranes were incubated with the corresponding secondary HRP-conjugated AB (1:7500 in 5 % milk in TBS-T) for 2h at RT under gentle agitation, followed by the same washing procedure. Immunoblotting was visualized either directly for fluorescent secondary ab's in an Odyssey Fc (LI-COR® Biosciences GmbH, model: 2800), with exposure times set to 2 or 5 min, or membranes were developed with ECL Pierce™ detection solution, Pierce™ SuperSignal West Dura or Pierce™ SuperSignal West Femto (ThermoFisher Scientific, cat. no. 32209, 34076, 34096) according to the manufacturer's instructions. Lastly, chemiluminescence was detected with the Odyssey Fc luminescence detector with exposure times set to 10 min for the proteins of interest and 5 min for β-actin used as control.

3.2.9 Immunostaining

3.2.10 Fixation and immunofluorescence

- Periodate-lysine-paraformaldehyde (PLP) fixative: 4% (v/v) PFA, 2.16% (w/v) glucose, 1.83% (w/v) lysine hydrochloride, 0.2 M phosphate buffer pH 7.4, 0.336% (w/v) sodium (meta) periodate (see McLean & Nakane, 1974);
- B-Block: 10% (w/v) normal horse serum, 5% (w/v) sucrose, 2% (w/v) BSA, 1x PBS pH 7.4, 0.2% (v/v) Triton-X-100;
- Mowiol: 10% (w/w) Mowiol (Carl Roth, cat. no. 0713.1), 25% (v/v) Glycerol, 100 mM Tris-HCl pH 8.5, 2.5% (w/v) DABCO.

Cells were washed once in ice-cold PBS before they were incubated in PLP fixative, prepared as described by McLean and Nakane (1974), for 30min at RT. After three washing steps with 1x PBS pH 7.4 for 10min, cells were incubated with B-Block for 1h at RT. Subsequently, cells were incubated with primary antibodies diluted in B-Block overnight at 4°C. The next day, cells were washed three times with 1x PBS pH 7.4 for 10min each and then incubated with the respective secondary antibody diluted in B-Block for 1 h at RT. Following this step, cells were incubated with DAPI (Invitrogen) in 1x PBS pH 7.4 for 10 min at RT (This step is not necessary for every staining performed). After three times washing with 1x PBS pH 7.4, the coverslips were briefly rinsed in ddH2O and then mounted in Mowiol (8-9 µL for 12 mm coverslips), with cells facing the object slide.

3.2.11 Metabolic labelling of nascent neural proteins using AHA

- HBSS: 1 x HBSS (Gibco, cat. no. 14025092);
- L-Methionine: 200 mM (Sigma-Aldrich, cat. no. 1.05707) in ddH_2O;
- L-Azidohomoalanine (AHA): 200 mM (synthesized by P. Landgraf) in ddH_2O;
- Hibernate medium -Met: recipe in Brewer & Price, 1996;
- PBS-MC: 1 x PBS pH 7.8, 0.1 mM $CaCl_2$, 1 mM $MgCl_2$;
- 4 % PFA (w/v), 1x PBS pH 7.4.

To incorporate non-canonical amino acids into the proteins of primary neural cells, the cultures were washed once with warm HBSS and incubated for 30 min at 37°C and 5 % CO_2 with Hibernate medium (without methionine) to deplete the methionine stores inside the cell. Subsequent labelling with AHA (or methionine as control) was performed for 3 h at a final concentration of 4 mM in Hibernate medium. Neural cells were washed with PBS-MC and were fixed with 4 % PFA for FUNCAT.

3.2.12 Fluorescent noncanonical amino acid tagging (FUNCAT)

- PLP fixative: 4% (v/v) PFA, 2.16% (w/v) glucose, 1.83% (w/v) lysine hydrochloride, 0.2 M phosphate buffer pH 7.4, 0.336% (w/v) sodium (meta) periodate;
- B-Block: 10% (w/v) normal horse serum, 5% (w/v) sucrose, 2% (w/v) BSA, 1x PBS pH 7.4, 0.2% (v/v) Triton-X-100;
- TAMRA-alkyne tag: 200 mM in DMSO (Invitrogen, cat. no. 85190);
- Copper sulfate: 200 mM in ultra pure H_2O (Carl Roth, cat. no. 9186.1);
- Triazol-ligand (Tris[(1-benzyl-1H-1,2,3-triazol-4-yl)methyl]amine): 200 mM in DMSO;
- TCEP: Tris(2-carboxyethyl)phosphine hydrochloride, 500 mM in ultrapure H_2O (Carl Roth, cat. no. HN95.1);
- FUNCAT wash buffer: 0.5 mM EDTA, 1 % (v/v) Tween-20 in 1x PBS pH 7.8;
- Mowiol: 10 % (w/v) Mowiol, 25 % (v/v) Glycerol, 100 mM Tris-HCl pH 8.5, 2.5 % (w/v) DABCO.

After incorporation of AHA, primary neural cells were fixed for 7 min at RT with 4 % PFA. Cells were washed three times with 1 x PBS pH 7.4, blocked with B-Block for 1.5 h under gentle agitation and subsequently washed three times with 1 x PBS pH 7.8 at RT. The click reaction mix was prepared by first adding the triazol-ligand (1:1000) to 1x PBS pH 7.8

and mixed by strong vortexing. Next, TCEP (1:1000) was added to the click reaction mix and vortexed for 10 s followed by the TAMRA-tag (1:10000) and mixing for further 10 s. After adding the copper sulfate solution (1:1000) and mixing for 30 s the reaction solution was transferred to a 24-well plate (400 µl per well). The coverslips were placed on top of small paraffin dots with cells facing down to prevent accumulation of precipitates and incubation was performed overnight at RT under gentle agitation. To stop the click reaction, cells were washed two times with FUNCAT wash buffer and three times with 1x PBS pH 7.4 for 10 min each. Afterwards, immunocytochemistry was performed to counterstain for different proteins of interest as described under 3.2.10, starting with the primary antibody incubation step.

3.2.13 Mitotracker staining

At DIV 21, C57BL/6J and STING$^{-/-}$ neurons were treated with Mitotracker Red CMXRos (Thermo Fisher, cat. no. M7512). The concentration used was 100 nM and the incubation period at 37°C was 15 minutes. Mitotracker was diluted in DMSO and therefore the control group was treated with the same volume of DMSO used for the Mitotracker-treated cells. At the end of the incubation time, the procedure was carried out as already described in chapter 3.2.10 by performing an immunostaining in association with the neuronal marker MAP2.

3.2.14 Lysotracker staining

At DIV 21, 40 and 60, C57BL/6J cells were treated with Lysotracker Red DND-99 solved in DMSO (Thermo Fisher, cat. no. L7528) using a final concentration of 50 nM or with DMSO only as a control. Then, the cells were incubated for 1 hour in the incubator at 37°C. At the end of the incubation time, the procedure was carried out as already described in chapter 3.2.10 by performing an immunostaining in association with the neuronal marker MAP2.

3.2.15 Senescence ß-Galactosidase Cell Staining

To analyse the amount of ß-Galactosidase *in vitro*, the Senescence ß-Galactosidase Staining Kit (Cell Signaling, cat. no. #9860) was used. Cells were washed once in ice-cold 1x PBS pH 7.4 before they were incubated in fixative solution (provided with the kit) for 15 min. After three washes with 1x PBS pH 7.4, cells were incubated with ß-Galactosidase staining solution at 37°C overnight. The day after, three times washing with 1x PBS pH 7.4

were done and the coverslips were briefly rinsed in ddH2O and finally mounted in Mowiol (8-9 µL for 12 mm coverslips), with cells facing the object slide.

3.2.16 Terminal deoxynucleotidyl transferase dUTP nick end labelling (TUNEL) assay

For the TUNEL assay the *In Situ* Cell Death Detection TMR rot kit (Roche, cat. no. 12156792910) was used. As positive control, cells were treated with DNase I for 10 minutes at 37°C to induce DNA strand breaks. During the first stages of the experiment, the fixation and blocking step described in chapter 3.2.10 was followed. Subsequently, 50 µl of TUNEL reaction mixture (substance supplied by the kit) was added to the coverslip with the cells. After a 60 minutes incubation at 37°C in a humidified and dark atmosphere, the cells were washed three times in PBS for 5 minutes each.

3.2.17 Immunohistochemistry

- PLP fixative: 4% (v/v) PFA, 2.16% (w/v) glucose, 1.83% (w/v) lysine hydrochloride, 0.2M phosphate buffer pH 7.4, 0.336% (w/v) sodium (meta) periodate;
- Sucrose solution: 30% (w/v) sucrose, 14% (v/v) 0,2 M $NaH_2PO_4*H_2O$, 36% (v/v) 0,2 M $Na_2HPO_4*H_2O$
- TPBS: 0,12% (w/v) Tris, 0,9% (w/v) NaCl, 0,025% (w/v) $NaH_2PO_4*H_2O$,
- TPBS-T: 0,12% (w/v) Tris, 0,9% (w/v) NaCl, 0,025% (w/v) $NaH_2PO_4*H_2O$, 0,3% (v/v) Triton X-100
- Avidin-biotin complex (ABC) solution, Vectastain ABC Kit (Vector Laboratories, cat. no. PK-4000) (0,5% solution A, 0,5% solution B in TPBS-T)
- Biotin-tyramin (BT) solution: 0,15% (w/v) biotin-tyramine, 0,03% (v/v) of 30% H_2O_2 in TPBS-T.

For immunohistochemical stainings, C57BL/6J and $STING^{-/-}$ mice were sacrificed at different age after being anaesthetised with an intraperitoneal injection of 4% chloral hydrate solution (150 µl/10 g body weight). Subsequently, the mice were perfused transcardially, first with 20 ml of 0.9% NaCl, followed by another 20 ml of PLP fix solution repeated three times. Then, animals were decapitated and brains removed. Brains were fixed in PLP fixative overnight at RT in a 15 ml Falcon tube (Corning Incorporated, cat. no. 352070). The day after, the PLP fixative was removed and replaced by sucrose solution at a volume sufficient to cover the entire brain. The incubation process took place at 4°C and

lasted three days in order to protect brains during the cooling process. The brains were then cut into 20 µm thick sections using a cryostat machine (Leica, CM3050). Ultimately, the sections were stored in 12 well plates and immersed in TPBS solution with Azide 0.1% (w/v) until staining was performed.

For the staining process selected brain slices were washed 3 times in TPBS for 5 min each under constant gentle shaking. Later, the samples were incubated in a TPBS-ethanol solution (1:1) for 30 min. After this, further three washes in TPBS for 5 min each were carried out. Later, the sections were blocked in TPBS-T containing 3% horse serum for 1 h. Following this step, cells were incubated overnight with primary antibodies in the dark and at 4°C (diluted in TPBS-T with 1% horse serum). On the next day, the sections were washed four times in TPBS-T for 5 minutes each and then incubated for 2 hours with the biotin-conjugated IgG at a dilution of 1:500 in TPBS-T containing 1% horse serum. Afterwards, the sections were washed three times with TPBS-T for 5 min and subsequently incubated with ABC solution for 1 hour, followed by washing with TPBS-T three times for 5 min each, and incubated with BT solution for 20 min. After washing three more times with TPBS-T for 5 min each, the sections were incubated overnight at 4°C in the dark with Alexa Fluor 488-conjugated streptavidin (1:2000 in TPBS-T with 1% horse serum) and other primary antibodies. On the third day, the sections were washed four times with TPBS-T for 5 min and incubated with the respective secondary antibodies (all 1:1000 in TPBS-T with 1% horse serum) for 4 h at 4°C in the dark. The sections were mounted on gelatine-covered slides (SuperFrost White, 26 x 76 mm, Carl Roth cat. no. 1879.1) and dried for 30 min at 37°C in the dark. The slides were then incubated for 2 min in 70, 80, 90, 100 % isopropanol and then twice for 5 min each in Roti-Histo (Carl Roth, cat. no. 6640.1). The slides were dried and covered with Neo-Mount (Sigam-Aldrich, cat. no. 109016) and cover slips (24 x 50 mm, Menzel glass).

3.2.18 2’3’-cGAMP ELISA

The 2’3’-cGAMP ELISA (Cayman Chemical, cat. no. 501700) was performed on cortices 8-, 24- and 108-weeks old mice. Animals were deeply anaesthetized with Isofluran CP prior decapitation. One cerebral hemisphere was taken to perform the ELISA. The cortex was homogenised with the Potter at 12 strokes and 900 rpm, using the diluent N-PER™ solution (Thermo Scientific, cat. no. 87792) at a ratio of 1g tissue/10ml N-PER™. Subsequently an incubation at 95°C for 5 min, the samples were centrifuged at 14000 x g

and 4°C for 20 min. Then, the supernatant was transferred into a new Eppendorf tube and an amido black protein assay was performed as already described in chapter 1.2.5. The assay was performed following the protocol provided by the manufacturer using a sample concentration of 1 mg. Finally, the plate was measured at a wavelength of 450 nm with the photometer Infinite F50 (Tecan).

3.2.19 Quantitative Real Time Polymerase Chain Reaction (qRTPCR)

3.2.19.1 RNA extraction

The Qiagen RNeasy® Plus Mini Kit (Qiagen, cat. no. 74134) was used to extract the RNA from mouse cerebral cortex obtained from C57BL/6J and STING$^{-/-}$ mice at different age. The extraction was performed as per manufacturers protocol.

The “Transcriptor First Strand cDNA Synthesis Kit” by Roche (cat. no. 04379012001) was used to reverse transcribe total RNA isolated from mice cortex. Each 1 μg RNA for mouse cerebral cortex were used. The reverse transcription was performed according to the manufacturers protocol. Briefly, the following reaction components (see Table 7) were added in a nuclease free microcentrifuge tube placed on ice.

Table 7. cDNA Template-Primer Mix

Reagent	Original concentration	Volume (μL)	Final concentration
Anchored-oligo(dT)$_{18}$ Primer	50 pmol/μL	1	2.5 μM
Random Hexamer Primer	600 pmol/μL	2	60 μM
Water, PCR Grade		variable	
Final Solution Volume		13	
Total RNA		variable	0.5 or 1 μg/μL

The Template-Primer Mix was denatured by heating the tube for 10 min at +65°C in a block cycler with a heated lid. Afterwards, the tubes were put on ice and the remaining components of the reverse transcriptase mix were added (see Table 8). Samples were placed in a thermal block cycler (Professional Thermocycler Biometra 070-851) and incubated for 10 min at 25°C followed by 60 min at 50°C. Finally, to inactivate the reverse transcriptase, the samples were heated at 85°C for 5 min and chilled on ice, before the remaining products were stored at -20°C for further uses.

Table 8. Remaining components of the Template-Primer Mix

Reagent	Original concentration	Volume (μL)	Final concentration
Transcriptor Reverse Transcriptase Reaction Buffer	5X	4	1X 8mM $MgCl_2$
Protector RNase Inhibitor	40 U/μL	0.5	20 U/μL
Deoxynucleotide Mix	10 mM	2	1mM
Transcriptor Reverse Transcriptase, (Vial 1)	20 U/μl	0.5	10 U/μL
Final Solution Volume		20	

3.2.19.2 qR-TPCR

Quantitative PCR was performed in triplicate assays using a Roche LightCycler® 96 System (Roche Molecular Systems Inc., Switzerland) and self-designed primers (see Table 9). The housekeeping gene glyceraldehyde 3-phosphate dehydrogenase (GAPDH), served as an internal control. All runs consisted of 50 cycles, each of 15s at 95°C and 1 min at 60°C and were preceded by a 2 min 50°C decontamination step with uracilN-glycosidase.

Table 9. List of primers used for qRT-PCR

Gene	Forward 5' to 3'	Reverse 5' to 3'
GADPH (m)	TGA CCT CAA CTA CAT GGT CTA CA	CTT CCC ATT CTC GGC CTT G
IFN α (m)	GAC CTC CAC CAG CAG CTC AA	ACC CCC ACC TGC TGC AT
IFN β (m)	CTT CTC CGT CAT CTC CAT AGG	CAC AGC CCT CTC CAT CAA CT
ISG 54 (m)	GCG TGA AGA AGG TGA AGA GG	GCA GGT AGG CAT TGT TTG GT

3.2.19.3 qRTPCR data analysis

The mean cycle threshold (CT) values obtained were used for the relative quantification of the expression levels for the different DNA sequences analysed according to the ddCT method described by Livak and Schmittgen (Livak and Schmittgen 2001). Briefly, the expression values of the gene of interest (ISG 54, IFNα and IFNβ) were normalized to

GAPDH, used as internal control that refers to the starting amount of cDNA, obtaining the dCT.

$$\mathrm{dCT\ (gene\ of\ interest)} = \mathrm{(CT\ gene\ of\ interest)} - \mathrm{(CT\ GAPDH)}$$

The averaged dCT values of the CTR group were averaged and the mean CTR dCT value was subtracted from each dCT value of the samples, to obtain the ddCT of the control and treatment group.

$$\mathrm{ddCT\ (gene\ of\ interest)} = \mathrm{(dCT\ gene\ of\ interest)} - \mathrm{(mean\ dCT\ GAPDH)}$$

The qRT-PCR is based on an exponential function, therefore the ddCT value for each treatment group was transformed in the Relative Quantification value (RQ).

$$\mathrm{RQ\ (gene\ of\ interest)} = 2^{-\mathrm{ddCT(gene\ of\ interest)}}$$

3.2.20 Software

NCBI blast® (https://blast.ncbi.nlm.nih.gov/Blast.cgi) and LightCycler 96 (Roche Diagnostics International Ltd, version 1.1.0.1320) were used for examination of DNA. FIJI was used for the analysis of immunofluorescence and immunohistochemical pictures. Maximum intensity projections of immunofluorescence images are displayed in this thesis. Please note that the brightness and contrast of immunofluorescence signals were not adjusted in FIJI (version 2.0). Microsoft PowerPoint (version 2020) was used to rotate, size and annotate images.

3.2.21 Image acquisition and quantitative analysis

Protein quantities were analysed using Image Studio Lite software (LI-COR® Biosciences GmbH, version 5.2.5). Briefly, the densitometry bands were segmented using the “Rectangle selections” tool. After creating the rectangles, the software automatically shows the densitometry values. Subsequently, these densiometric values were transferred to Mircosoft Excell for analysis. For the analysis, first a normalisation was carried out on the control group and then the proteins of interest were normalised with the ß-actin values.

All the ICC stainings were performed in minimum three independent experiments with minimum of two coverslips per conditions. A minimum of 30 pictures per experiment per condition was taken (a minimum of 10 pictures per coverslip). Maximum intensity projections confocal pictures (89,97x89,97µm – 1024x1024 pixels) were processed and analysed in FIJI (version 2.0).

To analyse the number of positive signals (for p62, Lysotracker, Mitotracker), each picture was manually segmented. Briefly, to count the puncta in the soma of the neurons, a standard “Oval selections” tool of the same size for each image, was used to segment the area of the soma. To count the puncta in the main dendrite, the first 50μm of the main dendrite was manually segmented using the “New image” tool with a width of 568 pixels. The area outside the selected soma or dendrite was “deleted” and filled with black and the image was split into the different channels. The channel displaying the puncta of interest (p62, Lysotracker, Mitotracker) was converted in 8 bit and a threshold was set. The standard value of the threshold was selected analysing the conditions of the control group pictures over the three biological replicates. Puncta were counted using the “Analyze particles” tool. The settings used to define the particles were a size comprised between 3-75μ2 in pixel units and a circularity of 0.05-1. In other experiments such as staining for cleaved caspase3 the signal intensity was evaluated. In this case too, FIJI software was used. Firstly, the standard “Oval selections” tool of the same size for each image, was used to segment the area of the soma. The channel displaying the signal of interest (ß-galactosidase, cleaved caspase 3, STING) was converted in 8 bit and the intensity of the signal was evaluated using the “Measure” tool. During the analyse process the intensity values of all different sample groups were normalized using the average of the control group.

For the Sholl analysis of neurons, MAP2 stainings were converted in 8 bits using the FIJI software. The plugin Simple Neurite Tracer (SNT) created by Prof. Tiago A. Ferreira was used (Arshadi et al. 2021). Inside this plugin is possible to find a tool called “Sholl analysis” that evaluates the number of intersections between an imaginary circle and the dendrites of neurons at a regular distance of 10 μm. The number of intersections and their distance from the soma were then saved in Microsoft Excel to be used for statistical analysis.

For the analysis of synapses, another plugin for FIJI was used. It was called SynQuant created by Dr. Yizhi Wang (Wang et al. 2020).

3.2.22 Microscopy

A confocal microscope from Axioplan 2 imaging (Carl-Zeiss Jena) was used for imaging the cells and z-stack pictures were captured with the CCD camera Spot RT camera and the ZEN 2012 SP5 FP1 (black) software (Carl-Zeiss Jena, version 14.0.9.201). The objective EC Plan Neofluar 63x/1.40 Oil DIC M27 (AA=0.19mm) as well as EC Plan Neofluar 40x/1.30 Oil DIC M27 (AA=00.21mm) filter sets (Carl-Zeiss Jena) were used.

For Sholl analysis, a fluorescence microscope Leica DM6000 B (Leica) was used. The software used was LAS X core (Leica, version 5.0) and the objective HC PL Apo 20x/0.80 WD 0.4mm.

3.2.23 Statistics

Data are presented as mean ± standard error of the mean (SEM) for data displaying Gaussian distribution or median values alone. ANOVA tests, Bonferroni's multiple comparison and Tukey post-test were employed for testing for significant differences of the age groups. Statistical analysis was performed with Prism version 8 (GraphPad Software, USA). p values, as indicated in detail in the figure legend in the results section, of $p < 0.05$ were considered statistically significant with *: $p < 0.05$; **: $p < 0.01$; ***: $p < 0.001$; ****: $p < 0.0001$.

4 Results

4.1 Ageing *in vitro*

More than 100 years have passed since Carrel isolated and cultured chicken cells in 1911 to study their ageing processes for the first time in history (Carrel 1911). In his conclusions, he reported that death was a multicellular process and that the single cell proves immortal when grown with the right conditions. Many years later, Hayflick and Moorehead in 1961 proved Carrol's theory wrong (Hayflick and Moorhead 1961). They showed that single cells can age and that they have a limited chance of proliferation, a phenomenon known today as the Hayflick limit. Furthermore, the researchers showed that cells only started to look old when they proved incapable of further replication (Hayflick and Moorhead 1961). It is thanks to people like Carrel, Moorehead and Hayflick that today cell cultures are frequently and habitually used in basic research.

Over the years, thousands of publications have focused on ageing, much less on the possibility of using cells *in vitro* as models of ageing. To date, neural cells aged *in vitro* has received scant attention in the research literature and much information is still missing (Pike et al. 1991; Lesuisse and Martin 2002). Knowing that not everything on this world is black and white, these results will not be presented with the unscrupulousness of saying that *in vitro* neurons age like *in vivo*, but rather with the desire and passion to analyse the behaviour of neuronal cells during their time *in vitro*, considering the similarities but also the clear differences that this *in vitro* ageing model shows compared to the normal neuronal ageing process that takes place inside the human or mouse brain.

To investigate ageing *in vitro*, mouse neural cells (comprising mainly neurons and glia) were used. Based on the maturity of neurons and on the maximum time point at which it is still possible to find living and functioning neurons, three main time points were analysed: day *in vitro* (DIV) 21, representing mature neuronal cells, DIV 40 representing older neurons and DIV 60, representing aged neural cells.

To establish an *in vitro* model of ageing, it is important to have good hallmarks of senescence and one of the most analyzed and reliable one is beta-galactosidase. Beta-galactosidase is an enzyme that catalyses the hydrolysis of beta-galactosidase into monosaccharides and Lee and colleagues demonstrated that this enzyme is usually overexpressed and accumulated in the lysosomes of senescence cells (Lee et al. 2006). As can be seen from figure 5, in the ageing *in vitro* model, beta galactosidase accumulated in the cells proportional to the number of days *in vitro*.

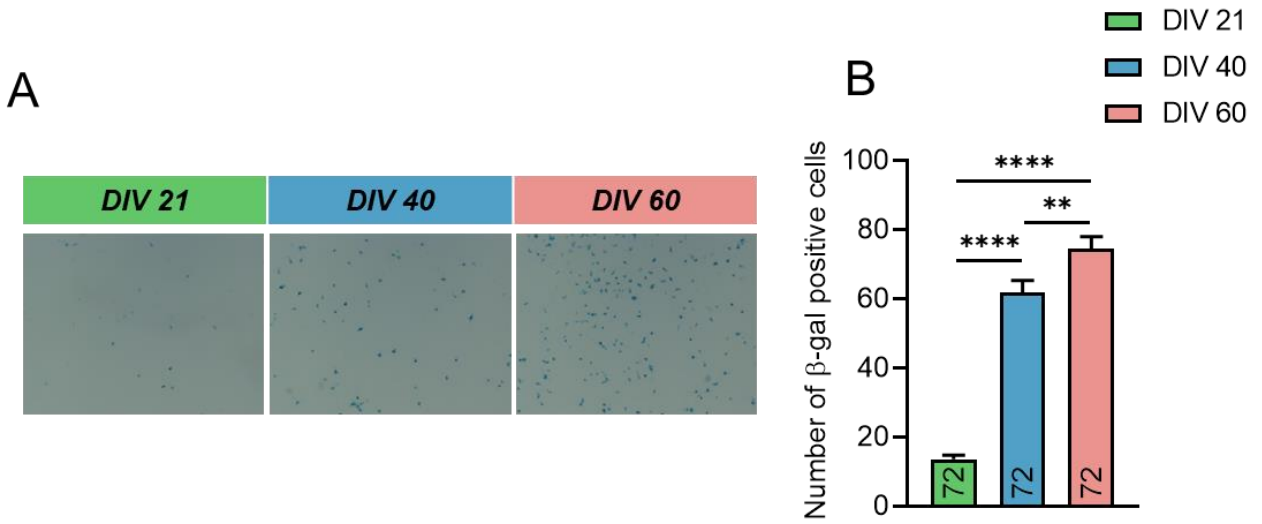

Figure 5: Primary cortical cultures acquire beta-galactosidase senescent features.
Primary neural mice cultures were stained with beta-galactosidase in order to evaluate a senescent feature at different time points (DIV 21, DIV 40 and DIV 60). Quantification of the staining showed a significant increase in the amount of positive blue cells in aged neurons compared with cultures at DIV 21 and DIV 40. Data are presented as mean ± SEM. The statistical analysis was performed by one-way ANOVA followed by Tukey post hoc multiple comparison test (**$P < 0.01$, ****$P < 0.0001$, 18 figures done for each group from four independent experiments).

Next, the morphological change of neurons during ageing *in vitro* was analyzed. For this purpose, Sholl analysis was used, which allows the evaluation of the number of dendritic branches and the maximum length reached by the dendrites present in a single neuron. As can be seen in figure 6, DIV 60 neurons had a clear statistical decrease in the number of dendrites present around the soma compared to the DIV 40 and 21 group. The maximum dendritic length was also significantly shorter in the DIV 60 group than in the DIV 21 group. Interestingly, neurons at DIV 40 had a similar dendritic arborization till 170 µm distance from the soma like at DIV 21 but showed a significant difference in maximum dendritic length.

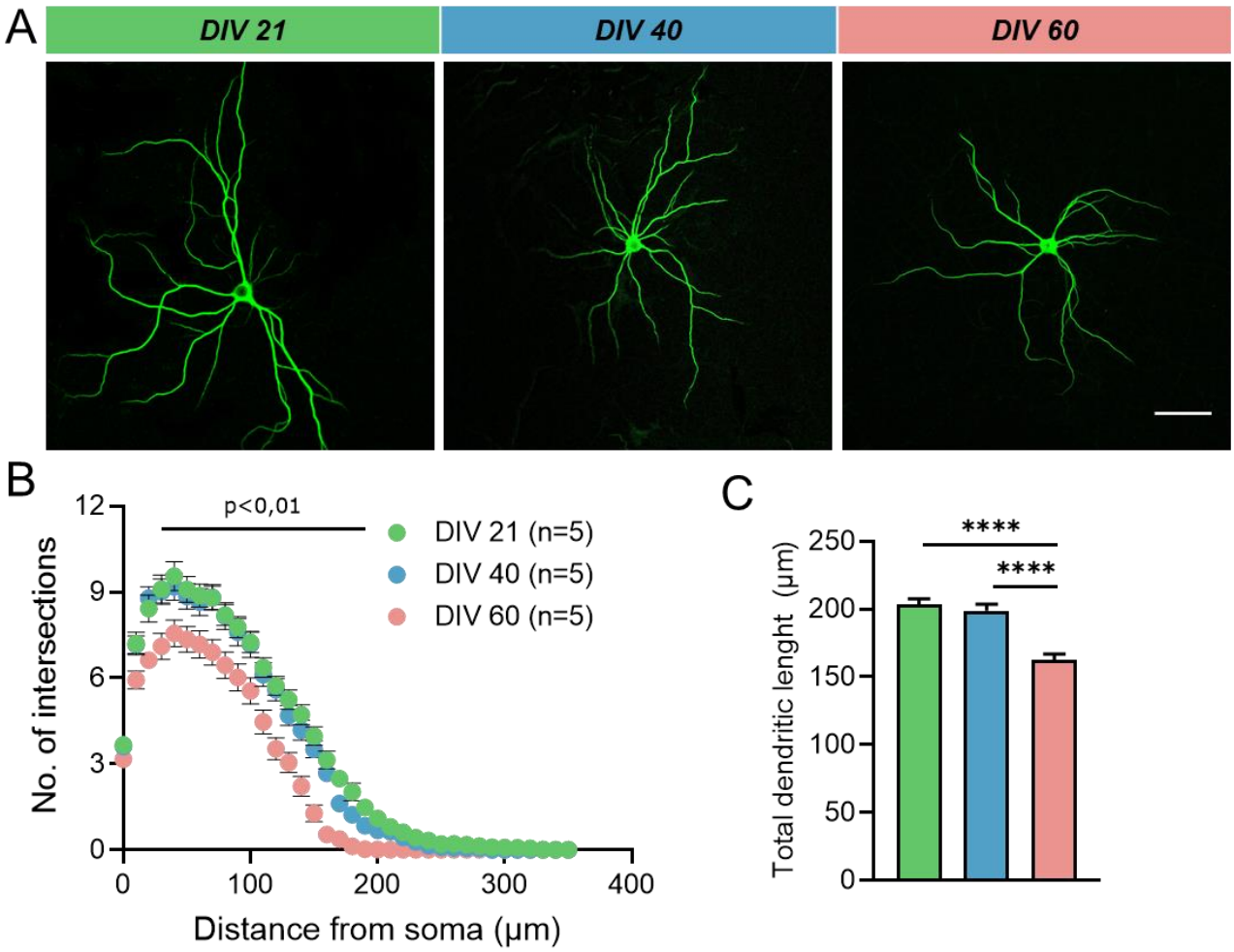

Figure 6: Relevant morphological effects of ageing neurons *in vitro*.
Primary neural mice cultures were stained with MAP2 in order to evaluate morphological changes at different time points (DIV 21, DIV 40 and DIV 60). Scale bar: 50 µM (A). Quantification of Sholl analysis showed a significant reduction of dendritic arborisation (B) and length (C) in aged neurons compared with neurons at DIV 21 and DIV 40. Data are presented as mean ± SEM. The statistical analysis was performed by two-way ANOVA followed by Tukey post hoc multiple comparison test (****P < 0.0001, n=15 in each group from five independent experiments).

Beside the Sholl analysis, cellular composition within the well plates was investigated during the selected time points. The protein levels of the main markers for neurons, axons, and glial cells, MAP2, TAU1 and GFAP, were analysed by WB (Figure 7). Strong evidence of loss of MAP2 protein was found when the cell culture reached DIV 60. Additionally, TAU1 protein showed a marked decrease at DIV 60 compared to DIV 40 and 21 indicating that the protein levels of axonal marker, as well as MAP2-labelled soma and dendrites, tended to drop. Finally, astrocytes were analysed. WB analyses have demonstrated that

the protein amount of GFAP increased significantly in the DIV 60 group compared to both DIV 21 and DIV 40.

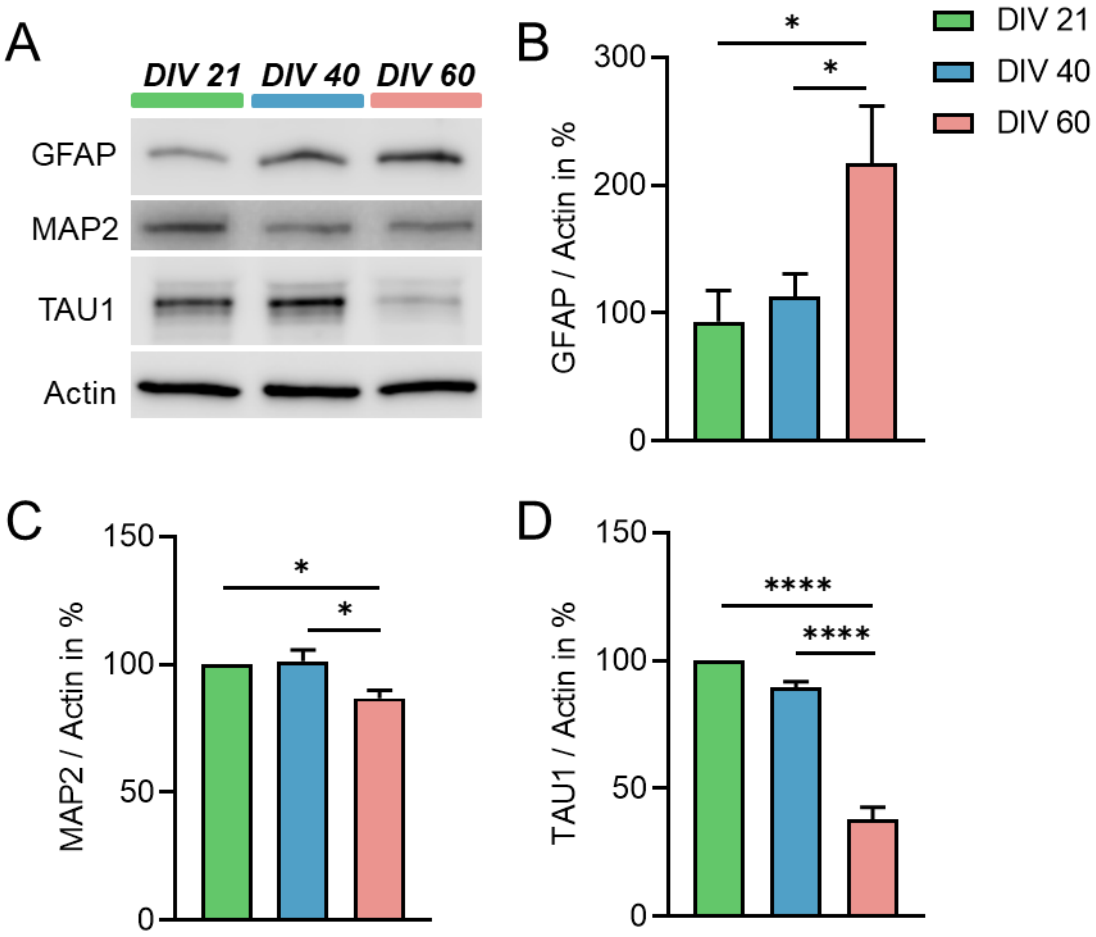

Figure 7: WB analysis of selected marker proteins from aging primary neural cultures
Representative immunoblots of selected proteins (A). Quantitative WB revealed a reduction of neuronal marker MAP2 and axonal marker TAU1 and a statistical increase of the glial marker GFAP in aged cultures (B). Data are presented as mean ± SEM. The statistical analysis was performed by one-way ANOVA followed by Tukey post hoc multiple comparison test (*P < 0.05, ****P < 0.0001, n=3 in each group from three independent experiments).

Based on these data, it was analysed whether the loss of MAP2 protein was related to a decrease in dendritic complexity or to a subsequent neuronal death. To answer this question, a TUNEL assay was performed. TUNEL staining relies on the ability of the enzyme terminal deoxynucleotidyl transferase to incorporate labelled dUTP into free 3'-hydroxyl termini generated by the fragmentation of genomic DNA into low molecular weight double-stranded DNA and high molecular weight single stranded DNA (Loo 2002). The results, as shown in figure 8, indicate that the DIV 60 group showed a marked increase of TUNEL positive cells in comparison with DIV 21 and DIV 40. However, a clear identification of which cell type was emanating this TUNEL positive signal was not

possible. For this reason, additional immunofluorescence staining with cleaved caspase 3, MAP2 and GFAP was performed. Cleaved caspase 3 was used in this experiment as it is considered to be an excellent marker for apoptotic cells in which the process of apoptosis has been already started (Mazumder et al. 2008). Indeed, as can be seen in figure 8 C and D, following irreparable damage, cells started to become apoptotic. The signal from cleaved caspase 3 in DIV 60 neurons (co-stained with MAP2) was much more intense than the signal from younger neurons (DIV 21 and 40). Furthermore, GFAP-labelled glial cells did not show any positive signal for cleaved caspase 3 (data not shown).

These results demonstrate that increasing age of neuronal cells *in vitro* tend to undergo cell death via apoptosis, while glial cells remain proliferating without showing significant effects of cell damage.

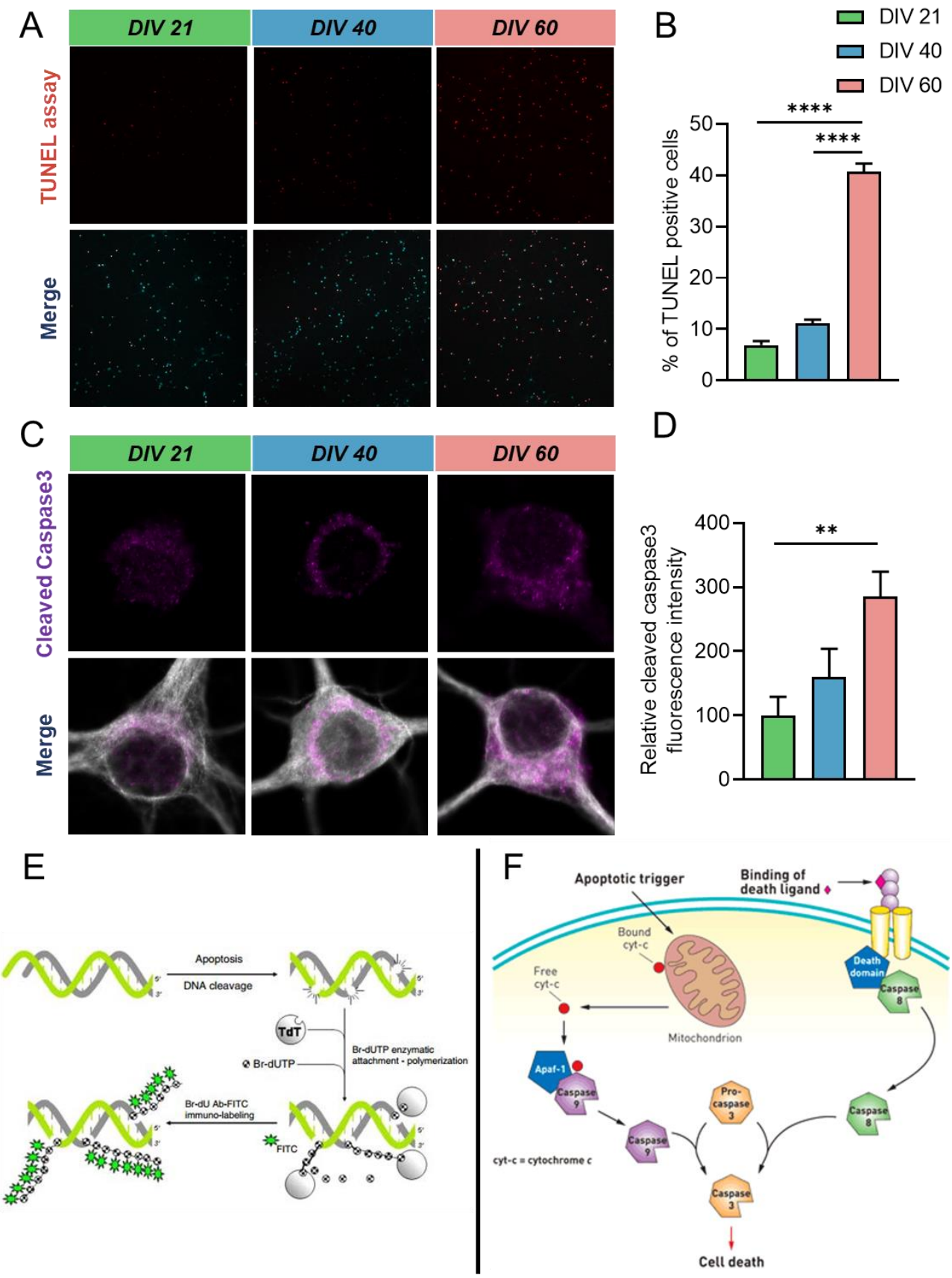

Figure 8: Apoptosis was activated in primary neural cells during ageing *in vitro*.
Cells were stained with TUNEL assay (FITC, red). The signal of DAPI is marked in blue. Scale bar: 50 μM (A). TUNEL assay probing for the increased number of death cells at DIV 60 in comparison

with DIV 21 and DIV 40. Data are presented as mean ± SEM. The statistical analysis was performed by one-way ANOVA followed by Tukey post hoc multiple comparison test (****P < 0.0001, n=10 pictures in each group from three independent experiments) (B). Cleaved Caspase 3 (purple) staining on cortical neurons co-stained with MAP2 (white) (C). Statistical increase in cleaved caspase 3 protein signal intensity on neurons during ageing *in vitro.* Data are presented as mean ± SEM. The statistical analysis was performed by one-way ANOVA followed by Tukey post hoc multiple comparison test (**P < 0.01, n=15 in each group from three independent experiments) (D). Schematic illustration of the TUNEL Assay functionality (Darzynkiewicz et al. 2008) (E). Graphic illustration of the main apoptotic pathway (Putt et al. 2006) (F).

Since neurons at DIV 60, compared to neurons at DIV 40 and DIV 21, showed an increase in the intensity of the dsDNA signal within the soma (Figure 9A and C), we decided to explore the role of mitochondria regarding the increase of DNA within the soma. Therefore, the presence of the mitochondrial marker TOM20 was assessed. TOM20 is a fundamental component of the translocase of outer membrane (TOM) receptor complex. The role of TOM20 is the recognition and translocation of cytosolically synthesized mitochondrial preproteins. TOM20 is a protein already used as a mitochondrial marker in some papers (Ward and Cloonan 2019; Cassina et al. 2020). Using antibodies directed against TOM20, a lower content of mitochondria in old cell cultures could be demonstrated (Figure 9B, D).
A consequence of mitochondria damage or loss is the accumulation of peroxides and reactive oxygen species (ROS) (Marí et al. 2009). One of the main antioxidative defence mechanism against ROS in most mammalian cells is the glutathione (GSH) redox system (Ribas et al. 2014). The process of detoxification can be analysed by performing WBs on Glutathione S Transferase (GST), an enzyme essential for the maintenance of the cellular GSH level and the conjugation of the reduced form of glutathione to xenobiotics for whose subsequent detoxification (Raza 2011). Curiously, opposite to the amount of the mitochondrial markers, the GST concentration was increased in a significant way at DIV 60 in comparison with DIV 40 and DIV 21 (Figure 9B, E).

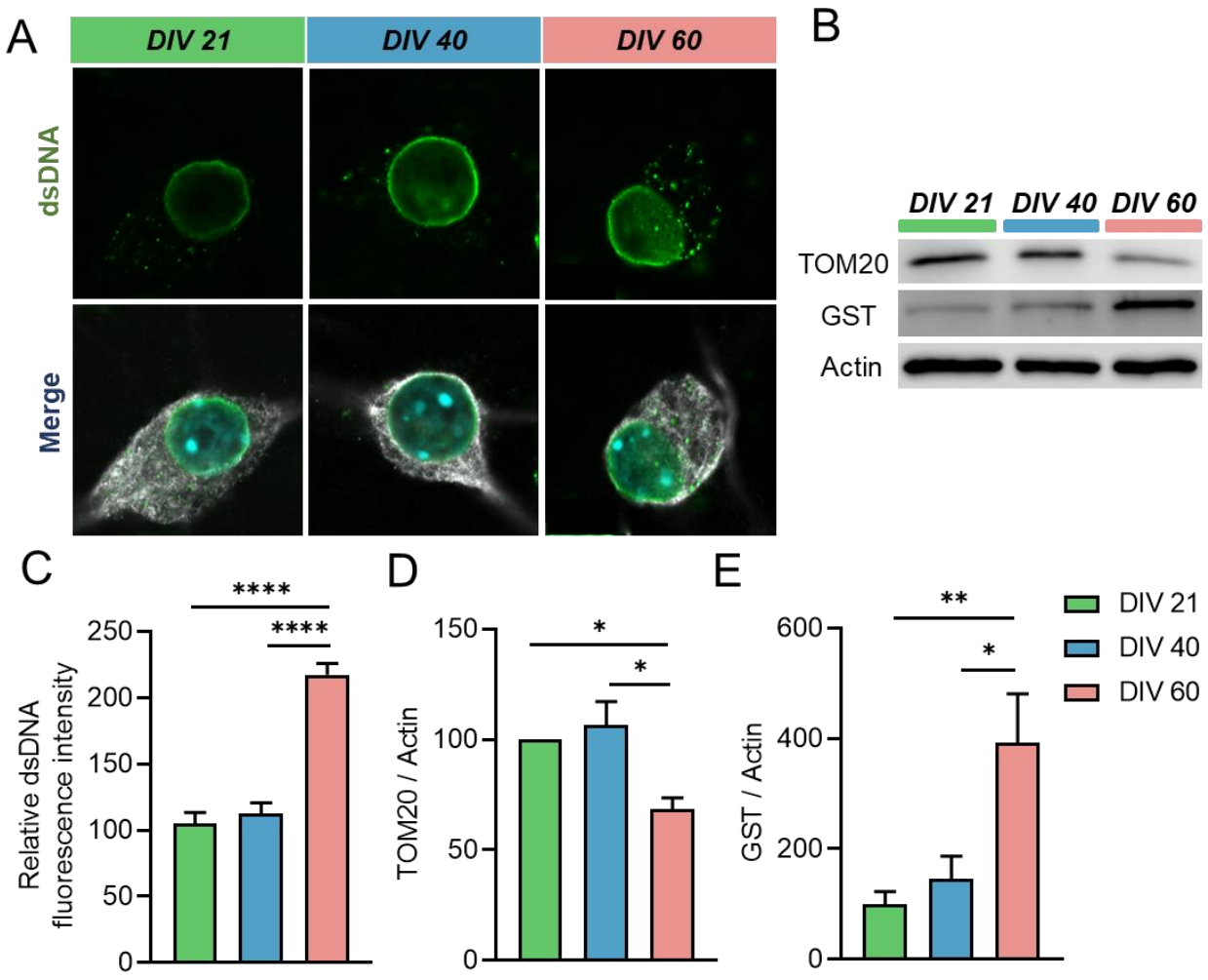

Figure 9: Mitochondrial damage and DNA release into the cytosol of old neural cultures. Neurons stained with dsDNA (green), MAP2 (white) and DAPI (cyan). Scale bar: 20 μM (A). Graphical results of the evaluation of the amount of neuronal dsDNA (C). During ageing *in vitro* it was possible to evaluate the increase of dsDNA in neurons. Data are presented as mean ± SEM. The statistical analysis was performed by one-way ANOVA followed by Tukey post hoc multiple comparison test (****$P < 0.0001$, n = 15 in each group from three independent experiments). WB of TOM20, GST and of the Actin control (B). Quantitative analysis of TOM20 (D) and GST level (E) on WBs normalized to actin. Quantification of TOM20 protein level that decreased in the DIV 60 cultures compared to DIV 21 and 40, indicating a mitochondrial imbalance (D). In contrast, GST increased during ageing, suggesting a higher demand of cell detoxification (E). Data are presented as mean ± SEM. The statistical analysis was performed by one-way ANOVA followed by Tukey post hoc multiple comparison test (*$P < 0.05$, **$P < 0.01$, n=3 in each group from three independent experiments). Data are presented as mean ± SEM. The statistical analysis was performed by one-way ANOVA followed by Tukey post hoc multiple comparison test (****$P < 0.0001$, n = 15 in each group from three independent experiments).

While continuing the characterisation of the *in vitro* ageing model, we decided to focus on another important aspect of cellular senescence, namely autophagy. Autophagy is

necessary for the recycling of old or unused intracellular components. Degeneration of these proteins leads to the formation of new macromolecular precursors and energy production (Glick et al. 2010). The most widely used markers for understanding possible impairments of this important catabolic pathway are p62 and LC3. p62 is a cargo protein important for the connection of ubiquitinated proteins to the autophagic machinery in order to enable their degradation in the lysosome (Glick et al. 2010). p62 is itself degraded by autophagy and can directly interact with LC3 during the formation of autophagosomes. LC3 is a soluble protein, and it is incorporated in the membrane of the budding autophagosomes, after the addition of a phosphatidylethanolamine (PE) group that transforms it in its LC3-II form, and it remains associated with the autophagosomes membrane through degradation. Therefore, measuring the ratio of the LC3-II over LC3-I form of this protein can give a clue about the amount of autophagosomes formation at a given point (Evans and Holzbaur 2019; Evans et al. 2019). Based on these concepts, an analysis of the autophagic flux of the cells was performed. As shown in figure 10A and B, during ageing *in vitro* the fluorescence intensity of p62 on a MAP2 mask was more as doubled at DVI 60 in comparison with DIV 21. Interestingly, the WB of p62 showed just a tendency without any significance, possibly due to the presence of glial cells in the cellular homogenate (11C and D). The protein amount of LC3 was analysed via WBs only. Evaluation of the protein content of LC3 in both the inactivated and PE-linked forms was carried out by calculating a ratio with the actin protein control and the ratio between LC3II and LC3I as well. The LC3II/LC3I ratio is a specific indicator of the changing relation of a particular LC3 version. If the amount of LC3II protein is larger than LC3I, most of the LC3 protein is found in the autophagosome, whereas if LC3I exceeds LC3II, LC3 is more inactivated and therefore not present in the autophagosome. Consistent with the results obtained for p62, LC3 in both, the activated and inactivated forms, showed only an upward trend (not statistically relevant) with increasing days *in vitro.* Furthermore, the LC3II/LC3I ratio was assessed and showed a significant increase between DIV 21 and DIV 60. This result combined with that obtained for p62, leads to the conclusion that cells aged mainly at DIV 60 had a clear impairment in cell autophagy.

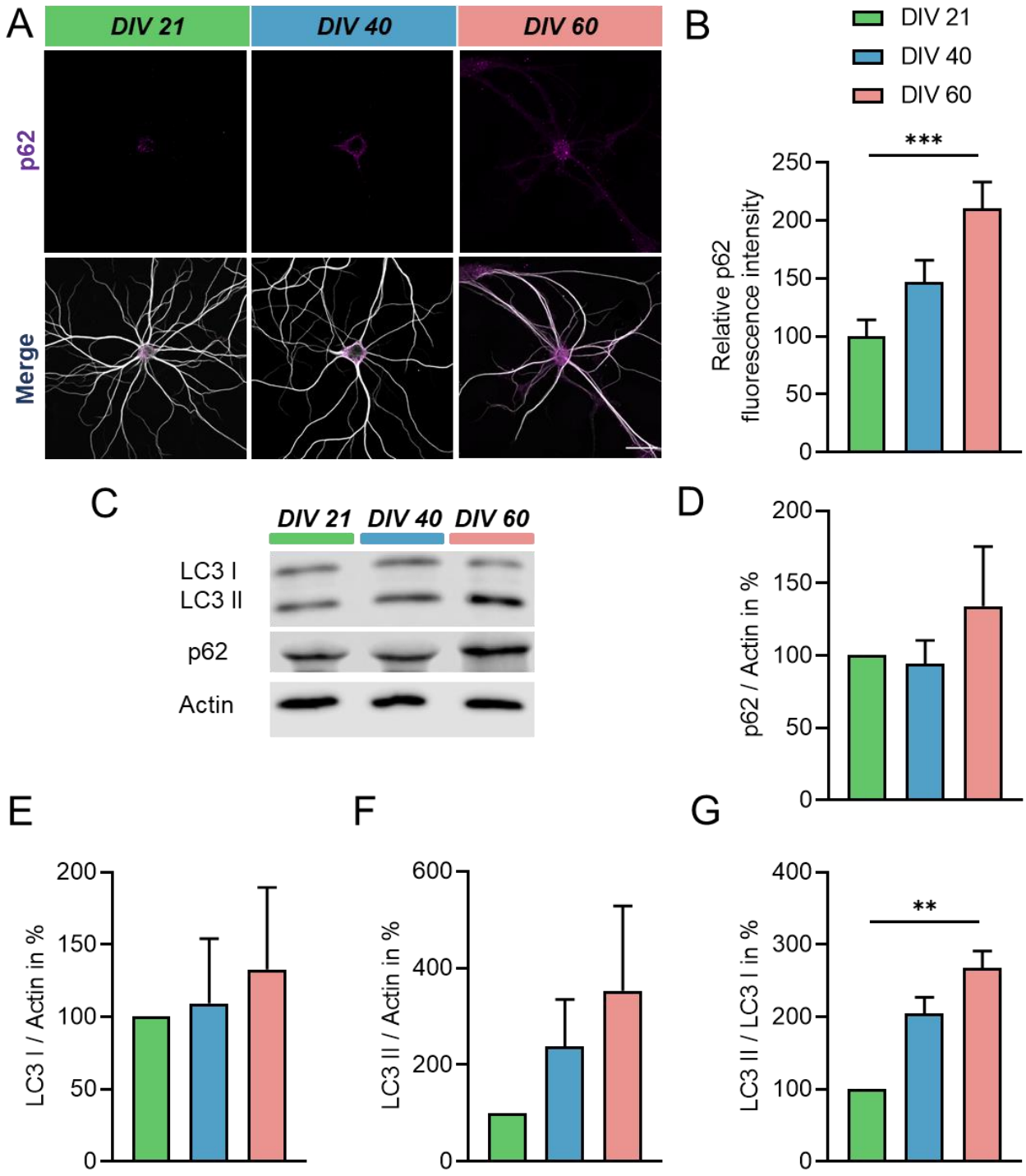

Figure 10: Ageing of neural cells *in vitro* leads to an impairment of the autophagic flux. Neurons stained with p62 (magenta) and MAP2 (white). Scale bar: 20 μM (A). Evaluation of the relative intensity of p62 that show a statistical increase of this protein during the ageing *in vitro.* Data are presented as mean ± SEM. The statistical analysis was performed by one-way ANOVA followed by Tukey post hoc multiple comparison test (****P* < 0.001, n=15 in each group from three independent experiments) (B). WB images of LC3 I and II, p62 and actin (control) (C). In the case of WB, the protein amount of p62, while showing an increasing trend in the DIV 60 group, loses significance as assessed by immunofluorescence (D). Although there is no significance in the LC3 I and LC3 II graphs, the ratio of LC3 II to LC3 I shows a statistical tendency for LC3 II to increase over LC3 I during ageing *in vitro*. Data of WB are presented as mean ± SEM. The statistical

analysis was performed by one-way ANOVA followed by Tukey post hoc multiple comparison test (**P < 0.01, n=3 in each group from three independent experiments) (E).

Based on the experiments concerning cellular autophagy, we decided next to analyse the role of lysosomes in neural aging. Lysosomes are membrane-bound organelle present in the cytosol. They contain hydrolytic enzymes that are active at a pH between 4 and 5, responsible for the hydrolysis of internal bonds of molecules like proteins in order to recycle them and create new nutrients for the cells (Ballabio and Bonifacino 2020). During the final part of autophagy, autophagosomes must fuse with lysosomes to form autolysosomes in order to recycle ubiquitinated proteins (Klionsky et al. 2014). Using Lysotracker allows the staining of lysosomes in order to assess their amount at cellular level (Zhitomirsky et al. 2018). In the following experiments, 50 nM of Lysotracker Red DND-99 was used. As shown in figure 11, neuronal cells show a strong accumulation of lysosomes at DIV 60. Already at DIV 40 the number of lysosomes per cell was statistically higher than in adult DIV 21 neurons.

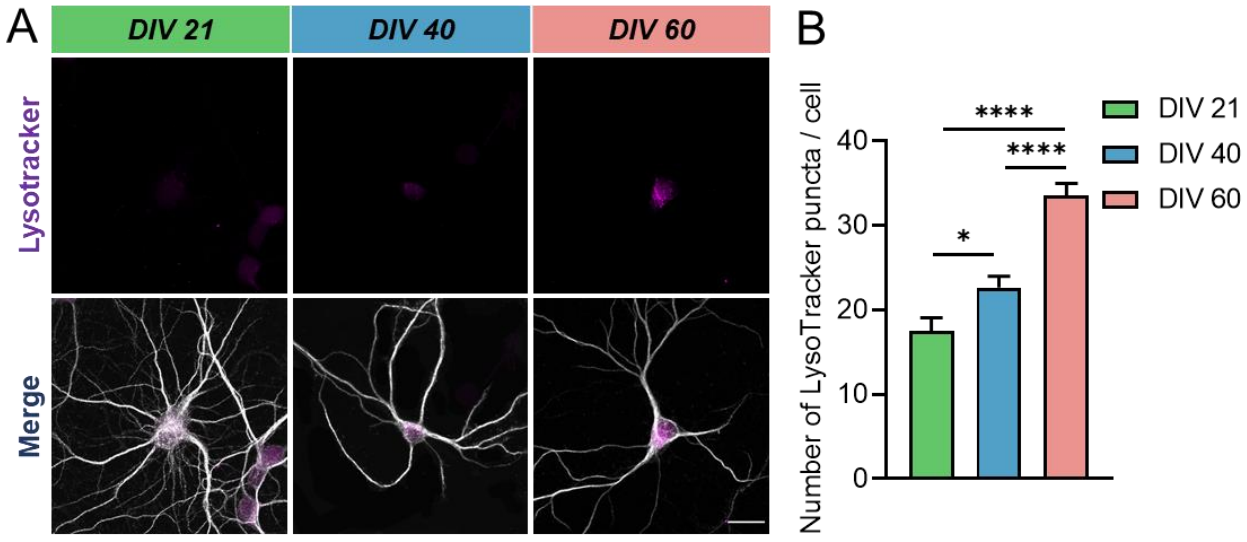

Figure 11: Accumulation of lysosomes in neurons during ageing *in vitro.*
Neurons were stained with Lysotracker (magenta) and MAP2 (white) at different time point DIV 21, 40 and 60. Scale bar: 20 μM (A). Assessment of the numbers of Lysotracker puncta that are expressed mainly in the soma. Data are presented as mean ± SEM. The statistical analysis was performed by one-way ANOVA followed by Tukey post hoc multiple comparison test (****P < 0.0001, n=15 of each group from three independent experiments) (B).

Since it is known from literature that lysosomes originate by budding off from the membrane of the cis and trans-Golgi complex (Bruce Alberts et al. 2002), the question was whether it would be possible to observe changes during ageing *in vitro* at the level of the

Golgi apparatus morphology. In order to answer this question, cells were stained with GM130, an marker of the cis Golgi network (Nakamura et al. 1995). In this experiment, the size of the cis-Golgi body was assessed. While there was no difference between DIV 21 and DIV 40, a statistically significant difference between DIV 21 and DIV 40 compared with DIV 60 was evident, with a markedly reduction in the size of the cis-Golgi (Figure 12).

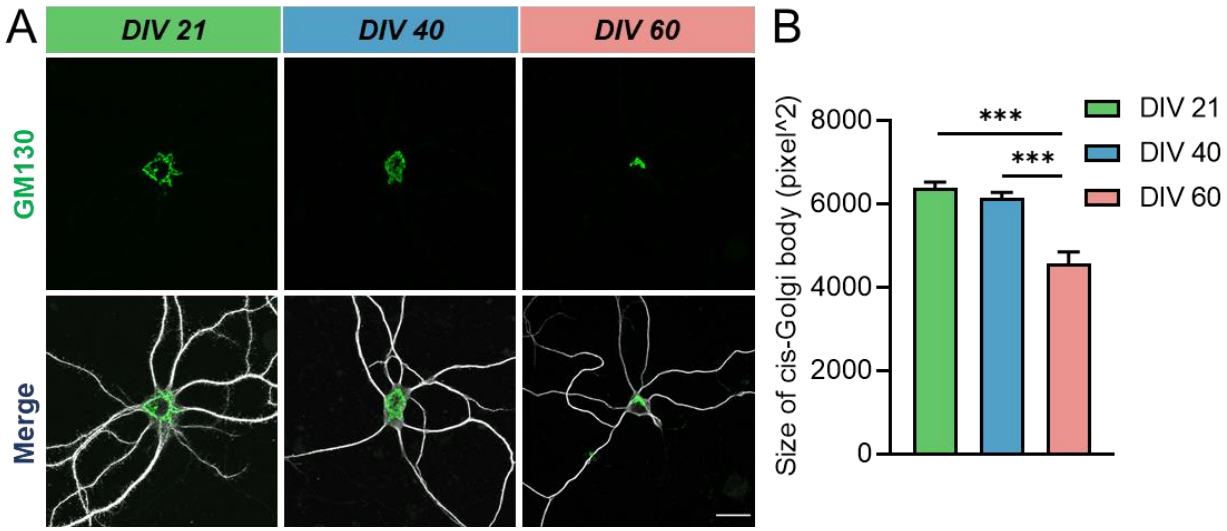

Figure 12: Reduction of cis-Golgi size in old neurons (DIV 60).
Neurons were stained with GM130 (green) and MAP2 (white) at different time point DIV 21, 40 and 60. Scale bar: 20 μM (A). Assessment of the numbers of Lysotracker puncta that are expressed mainly in the soma. Data are presented as mean ± SEM. The statistical analysis was performed by one-way ANOVA followed by Tukey post hoc multiple comparison test (***P < 0.001, ****P < 0.0001, n=10 in each group from three independent experiments) (B).

The obtained data points towards an age-dependent impairment of neurons in recycling and degrading proteins, especially with deficits in the formation of autophagosomes and in removing accumulated lysosomes. In order to complete the total view of proteostasis, it was necessary to analyse, how manly *de novo* proteins these cells are able to synthesise. To determine these changes, the FUNCAT technology was used. Shortly, the non-canonical amido acid azidohomoalanine (AHA) was metabolically incorporated as a surrogate for methionine into the newly synthesised polypeptide chain of nascent proteins. With the use of click chemistry, the azide group of AHA was tagged with the alkyne-bearing TAMRA fluorophore in order to visualize protein synthesis capacities (Dieterich et al. 2010). Subsequently, the TAMRA signal can be detected using fluorescence microscopy. In this experiment, cortical neuronal cultures at DIV 21, 40 and 60 were labelled with AHA for 2 h using a methionine-free Hibernate medium and were afterwards stained with TAMRA and MAP2. In young neurons a high quantity of newly synthesised

proteins was detected, both at soma and dendrite level. At DIV 40 the dendrites showed already less *de novo* protein synthesis in comparison with DIV 21, but this phenomenon didn't occur in the soma. However, in old neuronal cells (DIV 60) the TAMRA signal was significantly lower than from neurons at DIV 21 and DIV 40 in both, soma, and dendrites (Figure 13).

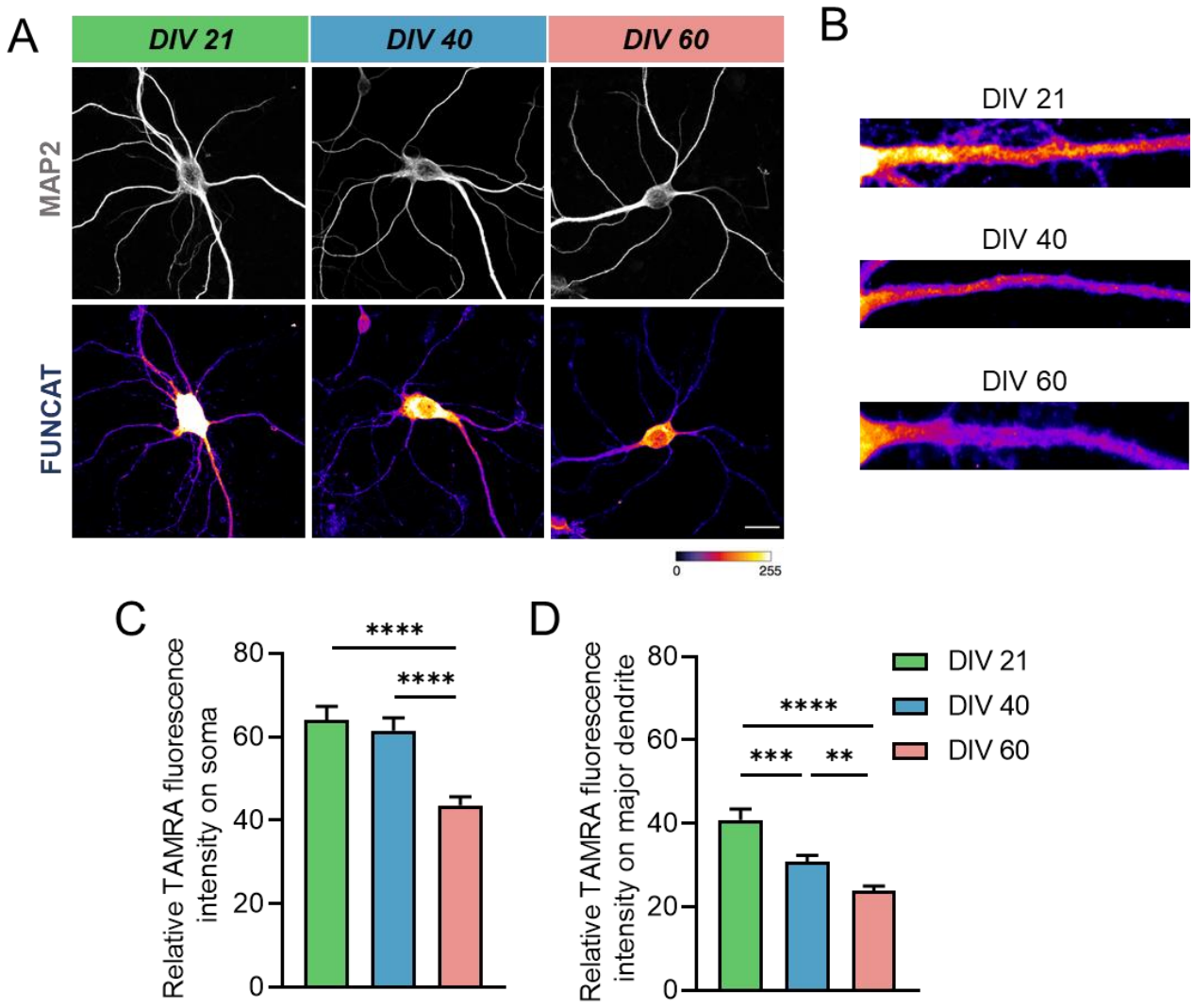

Figure 13: Decrease of the *de novo* protein synthesis in old neurons.
Neurons were metabolically labelled with the non-canonical amino acid AHA for 2 h in Hibernate at different time point DIV 21, 40 and 60. Newly synthesised proteins were visualised with the TAMRA fluorophore using FUNCAT technology. Neurons were stained with MAP2 (white). Scale bar: 20 μM (A). Enlarged image to appreciate the changes in the TAMRA signal at the dendritic level (B). Data are presented as mean ± SEM. The statistical analysis was performed by one-way ANOVA followed by Tukey post hoc multiple comparison test (***P* < 0.01, ****P* < 0.001, *****P* < 0.0001, n=12-20 in each group from five independent experiments) (C and D).

In conclusion, the presented *in vitro* model is an effective method for reproducing neuronal ageing. Among the various markers analysed, phenomena such as modification of neuronal morphology with dendritic loss, activation of apoptotic processes, increase in dsDNA at cytosolic level with obvious problems of mitochondrial respiration and cellular detoxification, completed by a slowdown in protein turnover at neuronal level with impairment of the autophagic flux, lysosomal accumulation and decrease in protein synthesis were described.

4.2 cGAS-STING pathway during brain ageing

Due to the successful establishment of ageing in neural *in vitro* cultures, continuing experiments were focused on age-dependent differences within the cGAS-STING pathway. Briefly, the presence of DNA in aberrant locations, such as cytosol, is believed to trigger immune response. cGAS is activated by interacting with double-stranded DNA (dsDNA) in a sequence-independent manner. This reaction induces conformational changes that allow cGAS to catalyse ATP and GTP into the cyclic di-nucleotide 2′,3′-cGAMP. The second messenger 2′,3′-cGAMP then activates STING. Subsequently, STING phosphorylates TBK1 which in turn phosphorylates IRF3. Finally, a dimer of pIRF3 can translocate to the nucleus and interact with specific DNA promotor regions. In recent years, there has been an increasing amount of literature on the role of cGAS-STING pathways in other molecular processes. For example, it has been observed that STING is a very important element in the process of cellular autophagy and that cGAS and IRF3 are also significant regulators of apoptotic pathways (Gui et al. 2019) (Ning et al. 2019). So far, however, very little attention has been paid to the role of the cGAS-STING pathway in CNS and especially in glial cells and neurons. Nearly nothing is known about its role in brain ageing or in brain diseases such as Alzheimer's and Parkinson's disease.

4.2.1 cGAS-STING pathway in primary neural cultures from mice

The lack of literature concerning the cGAS-STING pathway and its functioning on neurons or astrocytes led us to investigate its main proteins *in vitro*. For this reason, the first step was to analyse the presence of certain key proteins in the neuron. Knowing that neurons have weak defence mechanisms, it is considered to study immunity predominantly in other cell types residing in the CNS (Mathur et al. 2017) (Jin et al. 2021). In figure 14, however, the presence of STING and IRF3 is very clearly demonstrated for neurons *in vitro*. Their presence mirrors the shape of MAP2, indicating that both proteins are present in the

cytosol of the soma and dendrites. Additionally, IRF3 seems to colocalise with axons, labelled with TAU1 (Figure 14A). Based on these findings, we decided to investigate the role of the cGAS-STING pathway in ageing neural cultures *in vitro*.

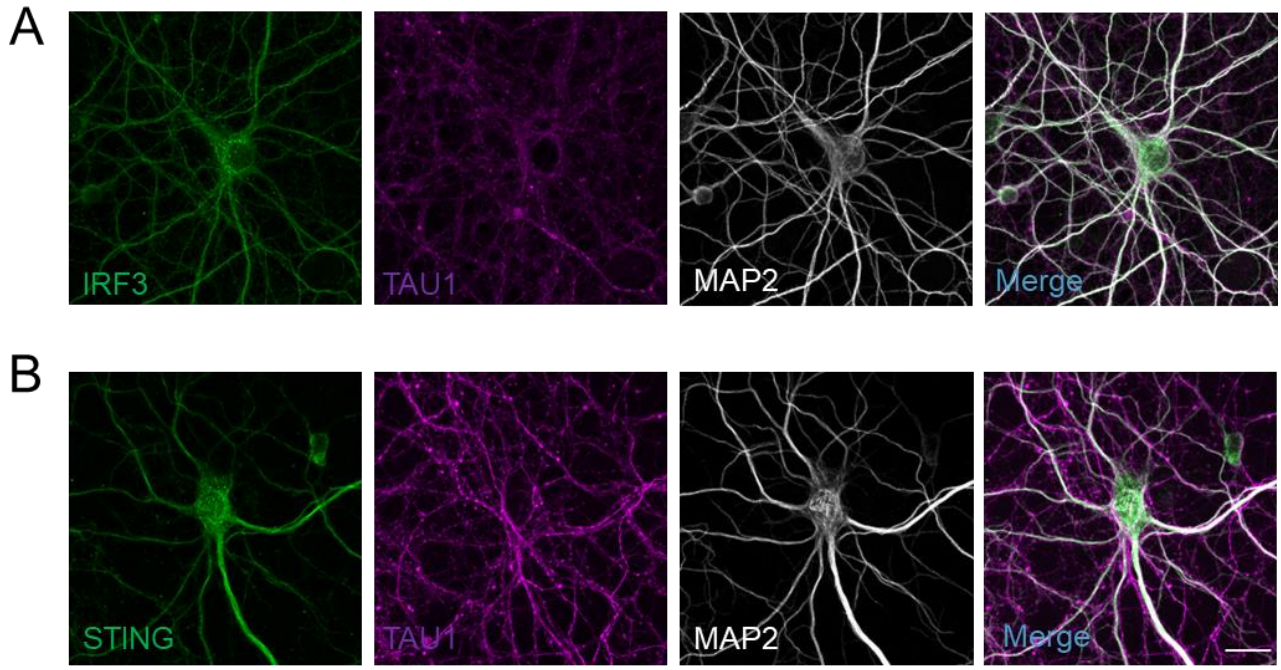

Figure 14: IRF3 and STING are present in neurons of primary cortical cultures.
Mature neurons (DIV 21) were labelled with IRF3 (A) or STING (B; green), TAU1 (magenta) and MAP2 (white). Scale bar: 20 μM.

To identify a potential role of the cGAS-STING pathway during neuronal ageing the expression profile of representative proteins of the pathway were probed in lysates of primary cortical cells using WB. Starting with the first protein of this pathway, cGAS, a clear decrease during ageing *in vitro* with the lowest levels found in the DIV 60 group could be shown. A statistically significant difference was found between the younger DIV 21 group and the older DIV 60 cultures. STING protein levels did not differ between the three analysed groups, while TBK1 and pTBK1 showed a tendency to decrease during ageing *in vitro*. Surprisingly, a completely different situation was found for IRF3 and its phosphorylated component. Indeed, whereas the protein concentration of IRF3 did not appear to be particularly affected by ageing *in vitro*, a statistically significant decrease in pIRF3, the final signalling protein, often used as a marker of cGAS-STING pathway activity, was observed. In addition, the ratio of pIRF3/IRF3 decreased markedly during aging *in vitro*, demonstrating that the phosphorylated IRF3 protein amount is lower in DIV 40 and DIV 60 than in DIV 21.

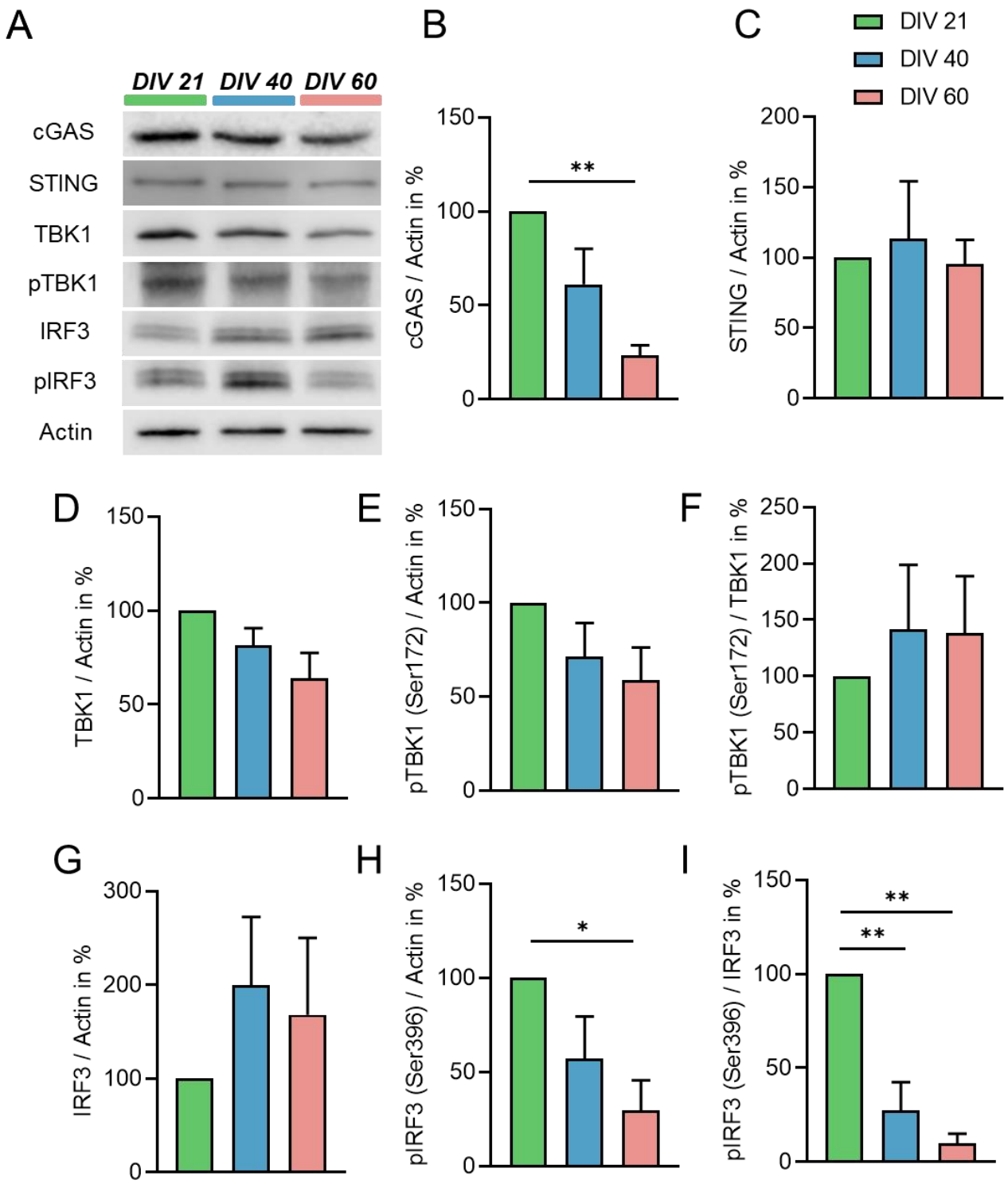

Figure 15: WBs and quantitative analysis of selected cGAS-STING pathway-proteins during ageing *in vitro.*

Representative blots of proteins involved in cGAS-STING signalling and Actin as an internal control (A). Determination of the protein levels related to the pathway. The data indicated impairment of the cGAS-STING pathway during ageing *in vitro,* mainly by revealing the protein loss of cGAS and pIRF3 (B-I). Data are presented as mean ± SEM. The statistical analysis was performed by one-way ANOVA followed by Tukey post hoc multiple comparison test (*$P < 0.05$, **$P < 0.01$, n=3 in each group from six independent experiments) (B).

WBs results clearly indicates that the cGAS-STING pathway exhibited an age-dependent tendency towards inactivation. While proteins, such as STING and TBK1, seems to be not involved in the ageing process *in vitro*, others, such as cGAS and IRF3, especially in its activated form, i.e., with a phosphorylation at the Ser396 position, were found to be involved in the ageing process of primary neural cultures.

The role of the cGAS-STING pathway in neurobiology is poorly understood. Knowing the relevance of proteins such as cGAS, STING, TBK1 and IRF3 in many biological processes beyond innate immunity such as autophagy, apoptosis and inflammation, it becomes more important than ever to understand their mechanism of action in post-mitotic cells such as neurons (Mathur et al. 2017; Ning et al. 2019; Krivega et al. 2021). Based on these gaps in the literature, I decided to analyse how far pharmacological manipulations involving the cGAS-STING pathway could impact on the cellular function of neurons and glial cells *in vitro*. In a first set of experiments, neurons were treated for 24 hours with recombinant murine interferon (IFN) γ at a concentration of 100 ng/ml, because previous publications have shown that treatment with IFN-γ induces STING protein synthesis in various cell types (Reinert et al. 2016; Larkin et al. 2017). Because there is still uncertainty, however, whether IFN-γ has an effect on neurons or glial cells, immunofluorescence labeling was performed on neurons using STING and MAP2 antibodies on primary cortical cells at DIV 21,40 and 60. Due to the fact that there were no age-related differences observed (data not shown), only analyses carried out on mature DIV 21 neurons were proposed. Interestingly, treatment with IFN-γ increases the STING protein amount also in neurons, as shown in figure 16A and C. Additionaly, quantitative analysis by WBs were used to determine, whether other proteins of the cGAS-STING pathway were also influenced by IFN-γ treatment. As demonstrated in the WB graphs of figure 16 D-N cGAS, STING, TBK1, IRF3 and also ULK1 were found to be increased after 24h IFN-γ treatment. Interestingly, however, the treatment seems not result in a cGAS-STING pathway activation of DIV 21 cell cultures, because no statisticaly significant differences in the phosphorylation of TBK1, IRF3 and ULK1, could be observed after IFN-γ stimulation compared to the unstimulated control. However, this experiments has shown that both neural cultures (containing glial cells and neurons) and the neurons themselves can be stimulated by IFN-γ at the level of the cGAS-STING pathway.

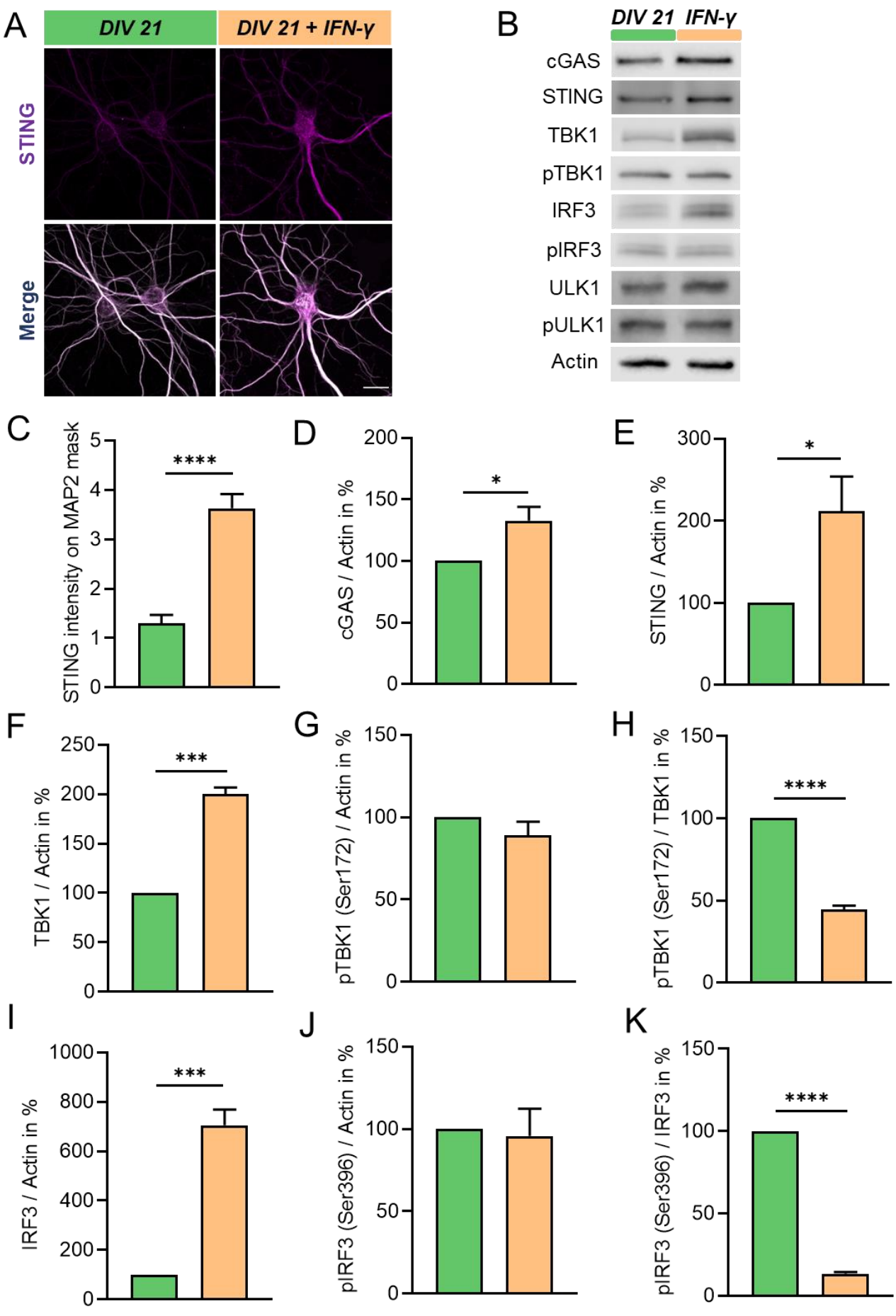
A
DIV 21
DIV 21 + IFN-γ
STING
Merge
B
DIV 21
IFN-γ
cGAS
STING
TBK1
pTBK1
IRF3
pIRF3
ULK1
pULK1
Actin
C
STING intensity on MAP2 mask
****
D
cGAS / Actin in %
*
E
STING / Actin in %
*
F
TBK1 / Actin in %
***
G
pTBK1 (Ser172) / Actin in %
H
pTBK1 (Ser172) / TBK1 in %
****
I
IRF3 / Actin in %
***
J
pIRF3 (Ser396) / Actin in %
K
pIRF3 (Ser396) / IRF3 in %
****

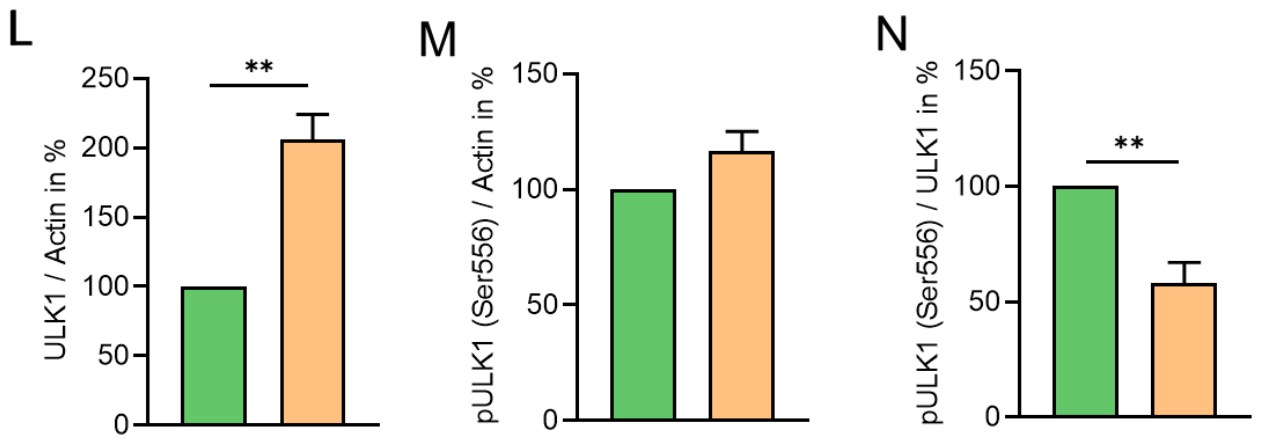

Figure 16: IF and WB analysis of cGAS-STING pathway proteins after IFN-γ stimulation *in vitro.*

Representative IF stainings of STING and MAP2 in DIV 21 cortex cultures with and without IFN-γ treatment for 24 h. Scale bar: 20 μM (A). The STING signal intensity from the neurons following IFN-γ treatment was significantly increased compared to the control (C). Representative blots of all major phosphorylated and non-phosphorylated proteins of the cGAS-STING pathway (B). Evaluation of the protein levels related to the cGAS-STING pathway (D-N). In green are represented the DIV 21 control data and in orange the DIV 21 data after 24h treatment with IFN gamma. Data are presented as mean ± SEM. The statistical analysis was performed by unpaired t-test followed by Tukey post hoc multiple comparison test (*$P < 0.05$, **$P < 0.01$, ***$P < 0.001$, ****$P < 0.0001$, n=3 for WB and n=15 for IF in each group from three independent experiments) (D-N).

For further analysis of the cGAS-STING pathway an agonist and an inhibitor of one of the main proteins, STING was used. The agonist chosen was 2′,3′-cGAMP, which activates the cGAS-STING pathway by binding STING and promoting its degradation following phosphorylation by ULK1 (Prabakaran et al. 2018). Regarding the STING inhibitor, I decided for H151. H151 is a novel covalent small molecule that can inhibit the action of STING (Haag et al. 2018). To study the reaction of mature cortex cell cultures at DIV 21 to a treatment with STING agonist and antagonist, 4 µg/ml H151 and 25 µg/ml 2'3'-cGAMP were applied for 2 hours. In 2019, Giu and colleagues demonstrated on HEK293T, HeLa, MEF, L929, Vero, THP1 and BJ-hTERT cells that the treatment with cGAMP induces an inhibitory phosphorylation on STING carried out by ULK1 (Gui et al. 2019). This phosphorylation was also demonstrated by us using co-cultures of cortex neurons and astrocytes as shown in figure 17. Furthermore, analysing the WB's of the figure 17 it can be demonstrated that the inhibition of STING leads to whose accumulation in contrast to the inhibition of autophagy as shown by the reduction of LC3 II. At the same time after 2 hours of H151 treatment the phosphorylation of TBK1 and IRF3 is inhibited. Interestingly, a certain amount of pIRF3 is also expressed on Ser366 in the DIV 21 control group. The

obtained data forced our interest for studying the role of the cGAS-STING pathway in the brain also *in vivo*.

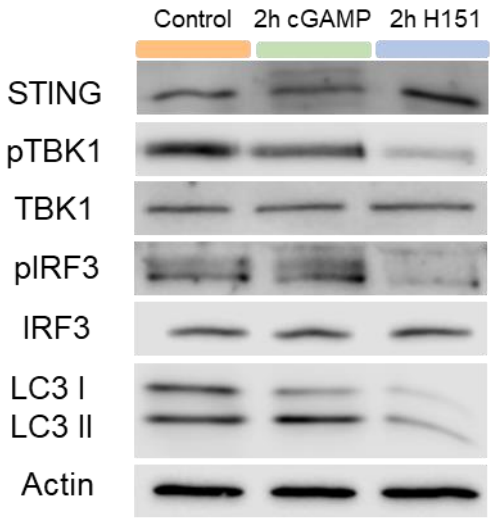

Figure 17: Modulation of cGAS-STING pathway in neural culture.
Representative WB correlating activation and inhibition of the cGAS-STING pathway and autophagic process in primary cortical cultures.

4.2.2 Relevance of the cGAS-STING pathway during ageing *in vivo*

In recent years, the literature linking the cGAS-STING pathway to ageing has increased significantly (Glück and Ablasser 2019; Glück et al. 2017; Loo et al. 2020). Indeed, proteins such as cGAS are thought to be crucial in senescence processes. For example, it has been shown that there is a cGAS-dependent regulation of senescence following irradiation and oncogene activation *in vivo* (Glück et al. 2017; Yang et al. 2017). STING has also been shown to be a central protein in regulating microglial neuroinflammation and alleviating diseases such as Alzheimer's disease and ataxia telangiectasia (Aguado et al. 2021; Hou et al. 2021). Given recent publications and our observations that the cGAS-STING pathway seemed to be clearly disbalanced during ageing *in vitro,* forebrains of mice at different ages were used for quantitative WB analysis *in vivo*. Therefore, the brains of three different age groups of mice were taken: 8-week-old, 24-week-old, and 108-week-old. This part of the results was completed in close collaboration with the medical student Shananthan Kethiswaran and will therefore also be part of his doctoral thesis. First analysis was carried out by using protein extracts of the cerebral cortexes for quantitative WBs in order to determine components of the cGAS-STING pathway. As can be seen in figure 18, there was a disbalance of the cGAS-STING pathway found, represented by a significant increase of the cGAS protein in the 108-week-old mice compared to the 24- and 8-week-old groups. Simultaneously, the protein concentration of STING exhibited an

opposite trend in cerebral cortices, with a significant reduction during ageing. TBK1 and its phosphorylated and thereby activated form pTBK1 showed any age-related trends. In contrast, a completely different situation was found for IRF3 and pIRF3 in the brain. In fact, the amount of IRF3 showed a statistically significant decrease in 108-week-old mice compared to 8-week-old young mice. In contrast, the pIRF3 protein, i.e., the form putatively activated by the cGAS-STING pathway, showed a clear increase in older mice compared to both young and adult mice at 24 weeks of age. As several papers have shown, the predominantly used markers for determining the activation of the cGAS-STING pathway are the phosphorylation of STING, IRF3 but also the amount of 2′,3′-cGAMP present in the cell cytosol. Therefore, the amount of 2′,3′-cGAMP was analysed by using ELISA. The results depicted in image 19B illustrates that 2′,3′-cGAMP levels surprisingly decrease significantly during ageing, with a statistically significant reduction in the cortices of 108-week-old mice compared to 24- and 8-week-old mice.

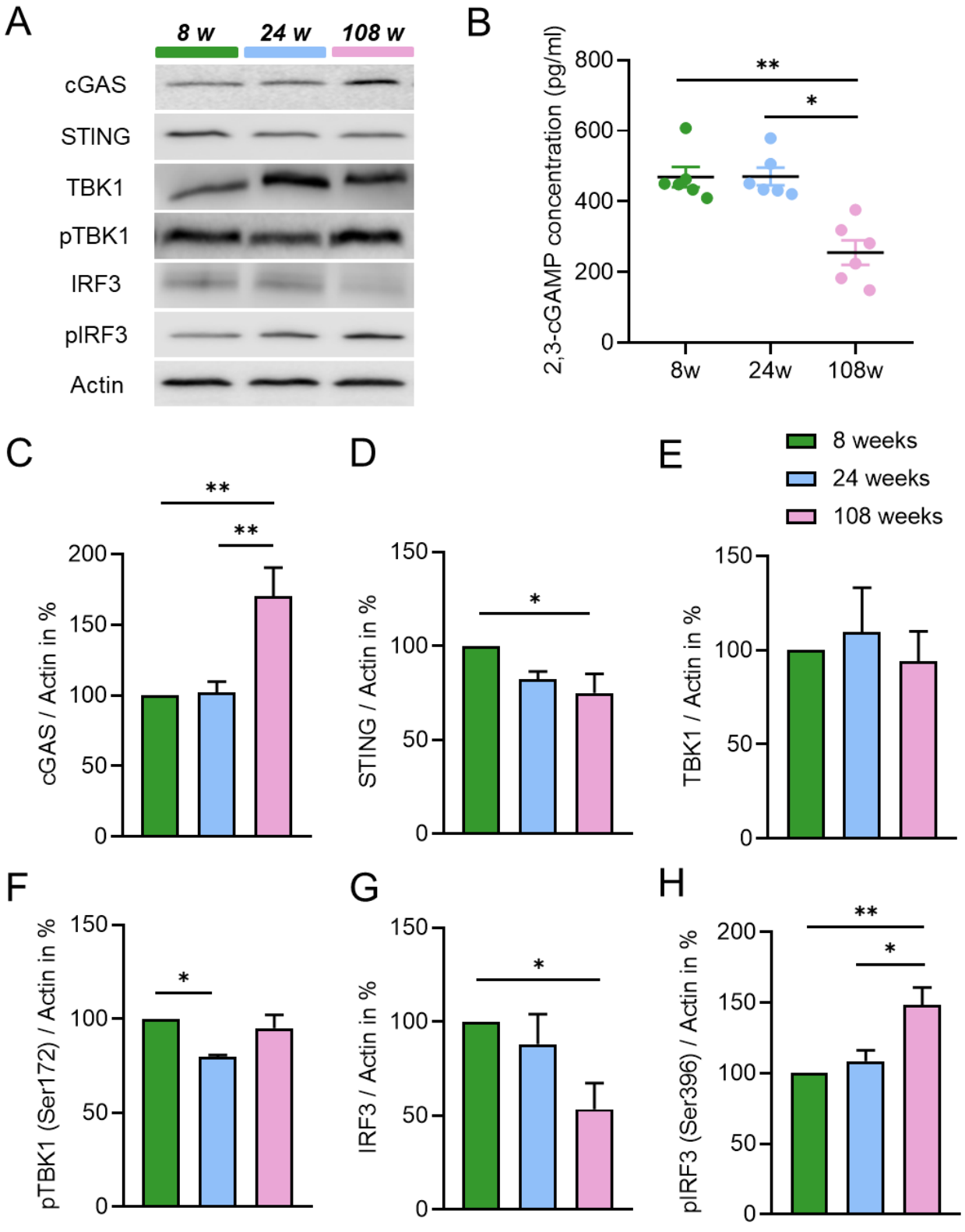

Figure 18: Quantitative changes of 2′,3′-cGAMP and cGAS-STING pathway proteins during ageing *in vivo*.

Representative blots of proteins involved in cGAS-STING signalling and Actin as an internal control (A). Quantification of the 2′,3′-cGAMP concentration via ELISA. The graphs indicated that the cGAS product was decreased in the cerebral cortex of older mice compared to young and mature mice (B). Determination of the protein levels related to the pathway. The data indicated impairment of the cGAS-STING pathway during ageing *in vivo* with increased protein levels of cGAS and

pIRF3. Simultaneously, STING and IRF3 proteins showed a clear decrease in 108-week-old mice in comparison with 8-week-old group (C-H). Data are presented as mean ± SEM. The statistical analysis was performed by one-way ANOVA followed by Tukey post hoc multiple comparison test (*P < 0.05, **P < 0.01, n=3 in each group from six independent experiments).

Because of the strong interconnections that the cGAS-STING pathway has with autophagy related proteins, especially ULK1 and Beclin1, the concentration of these proteins was analysed. As shown in figure 19, the level of ULK1 and Beclin1 are not changed during ageing. In addition, the levels of two phosphorylated proteins pULK1 (Ser555) and pBeclin1 (Ser30) were determined by WB. Although they have many phosphorylation sites, these two antibodies were chosen because of recent discoveries in the molecular relationship between the cGAS-STING pathway and autophagy (Konno et al. 2013; Liu et al. 2019; Zheng et al. 2021). Indeed, ULK1 has an important regulatory function in the cGAS-STING pathway. This protein can phosphorylate STING, thereby inactivating the subsequent phosphorylation of IRF3, which is an indicator of STING activation. Phosphorylation of ULK1 at serine 555 promotes the inactivation of ULK1's inhibitory role on STING. On the other hand, Beclin1 is one of the most important proteins in the autophagy initiation phase and is phosphorylated on serine 30, activating and promoting autophagy. The main protein capable of phosphorylating Beclin1 at Ser 30 is ULK1.

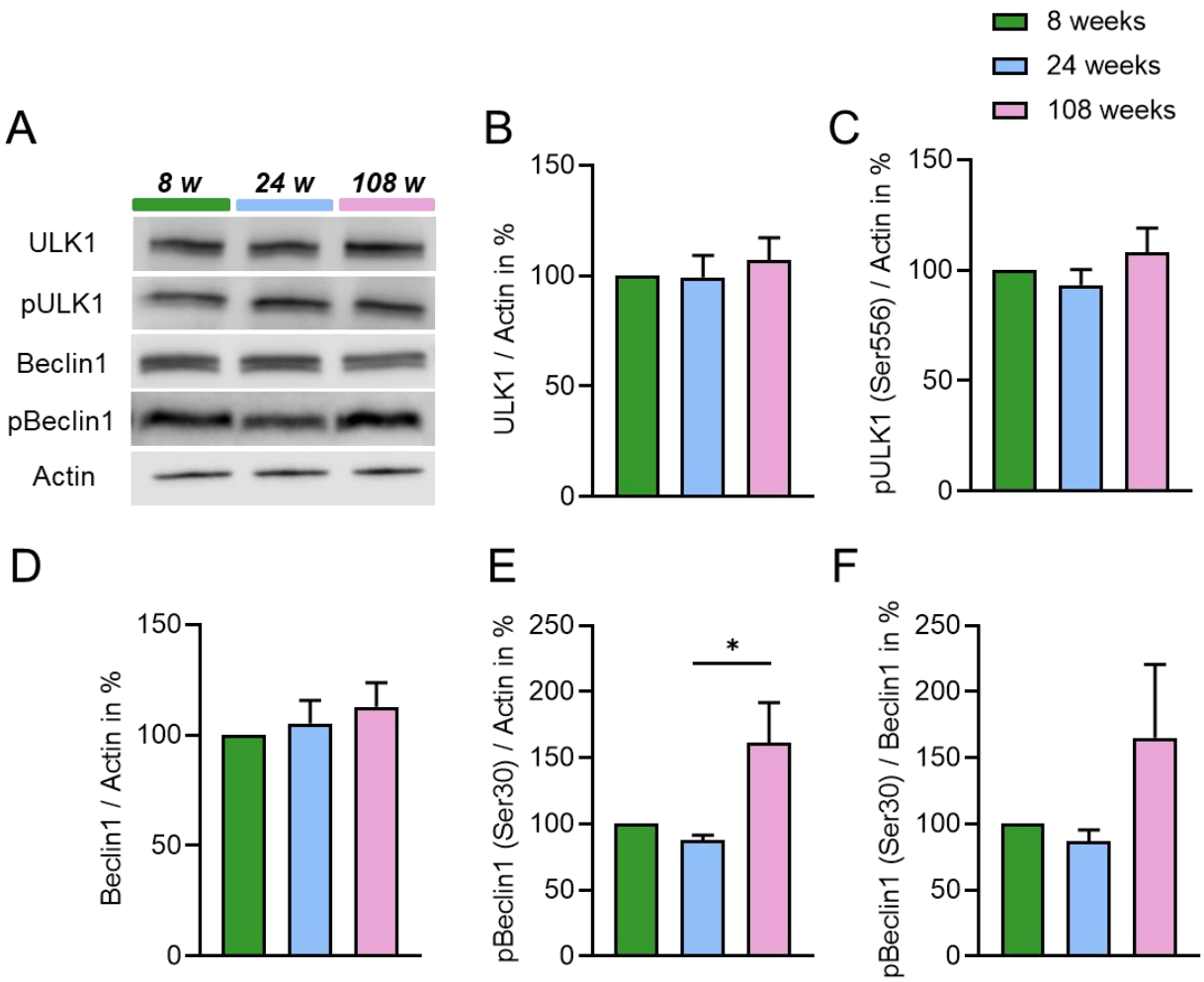

Figure 19: The main interconnecting proteins between autophagy and cGAS-STING pathway and their variation during ageing *in vivo*.
Representative blots of ULK1 and Beclin1 with the associated phosphorylated proteins. Actin was used as internal control (A). The data indicated a clear increase of pBeclin (Ser30) in 108-week-old group in comparison with 24-week-old animals. Data are presented as mean ± SEM. The statistical analysis was performed by one-way ANOVA followed by Tukey post hoc multiple comparison test (*$P < 0.05$, n=3 in each group from three or six independent experiments) (B).

Based on these results, we sought to understand whether the increase in IRF3 phosphorylation during ageing was also followed by a rise in type I IFN release. As demonstrated in figure 20 the main nucleic interaction site of IRF3, ISG54, was not increased during ageing and the same result was seen for IFNα and IFNβ. Furthermore, the absence of an induction of IFNα and IFNβ genes indicate that the cGAS-STING pathway does not appear to be activated regarding the induction of inflammatory processes during brain ageing, albeit with previously discordant results for example pIRF3 protein levels (see figure 18). In addition, these graphs indicate that during normal brain

ageing there was no large increase in interferon release indicating that in 108-week-old mice there might be an absence of neuroinflammation mainly related to IFNs.

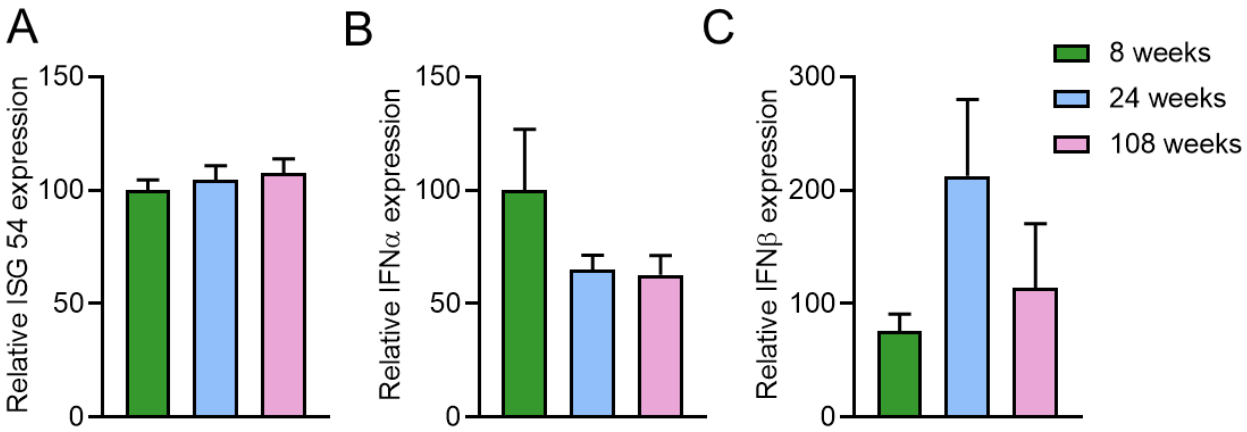

Figure 20: Quantitative RT-PCR of the principal target proinflammatory genes ISG 54, IFNα and IFNβ of the cGAS-STING pathway during ageing *in vivo*.
Graphs of relative ISG 54, IFNα and IFNβ expression in the cerebral cortex of 8-week-old, 24-week-old and 108-week-old mice (A, B, C). The housekeeping gene used was GAPDH. Analyses showed any strong state of IFN type I mediated inflammation during ageing *in vivo*, related to the genes on which the cGAS-STING pathway acts. Data are presented as mean ± SEM. The statistical analysis was performed by one-way ANOVA followed by Tukey post hoc multiple comparison test (n=3 in each group from three independent experiments) (A, B, C).

In a next set of experiments, we aimed to analyse the spatial and temporal expression of STING in the mouse brain. It has been shown in the literature that signals of the STING antibody strongly colocalize with IBA1, the microglial marker (Mathur et al. 2017).

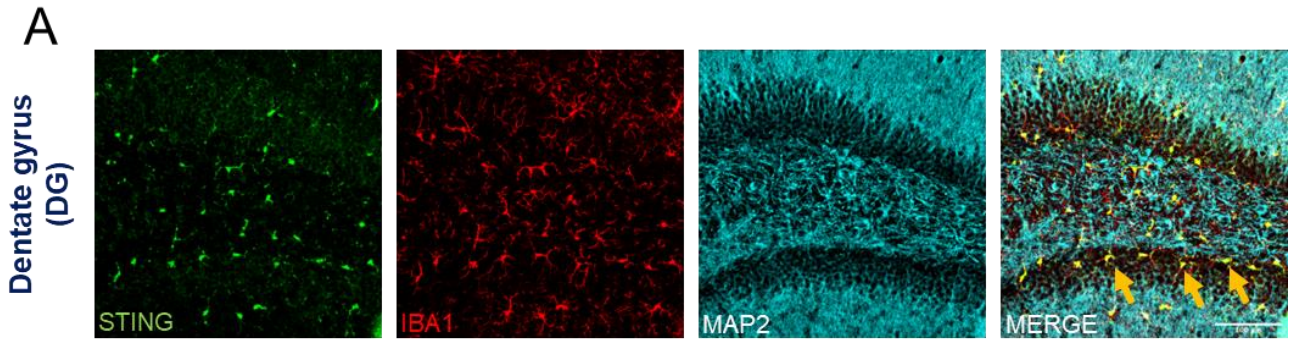

Figure 21: Immunohistochemical co-staining of STING, IBA1 and MAP2 at the level of the dentate gyrus.
Frontal brain slices with a size of 20 µm from 8 weeks old mice were immunohistochemically stained using antibodies raised against STING (green), IBA1 (red) and MAP2 (blue). Depicted are images from the dentate gyrus, showing strong overlap between STING and IBA1 positive microglia cells. Figure representing a signal overlap between IBA1 and STING showing that microglia are the main location of the cGAS-STING pathway in the CNS. Scale bar: 100 µM (A).

Further immunostaining analysis of STING and IBA1, were focused on three brain areas, the somatosensory cortex (SCX), the Cornu ammonis (CA1) and the dentate gyrus (DG), because they are critically affected by ageing. The somatosensory cortex, on the other hand, is the area responsible for receiving sensory stimuli. CA1 and DG are part of the hippocampus, an important region for short- and long-term memory and for spatial and orientation memory. In these fundamental regions, the intensity of IBA1, the intensity of the STING signal on an IBA1 mask and the number of STING and IBA1 positive cells were analysed to determine changes of the STING concentration and the number of microglial cells. Firstly, the results obtained on the SCX are shown in figure 22.

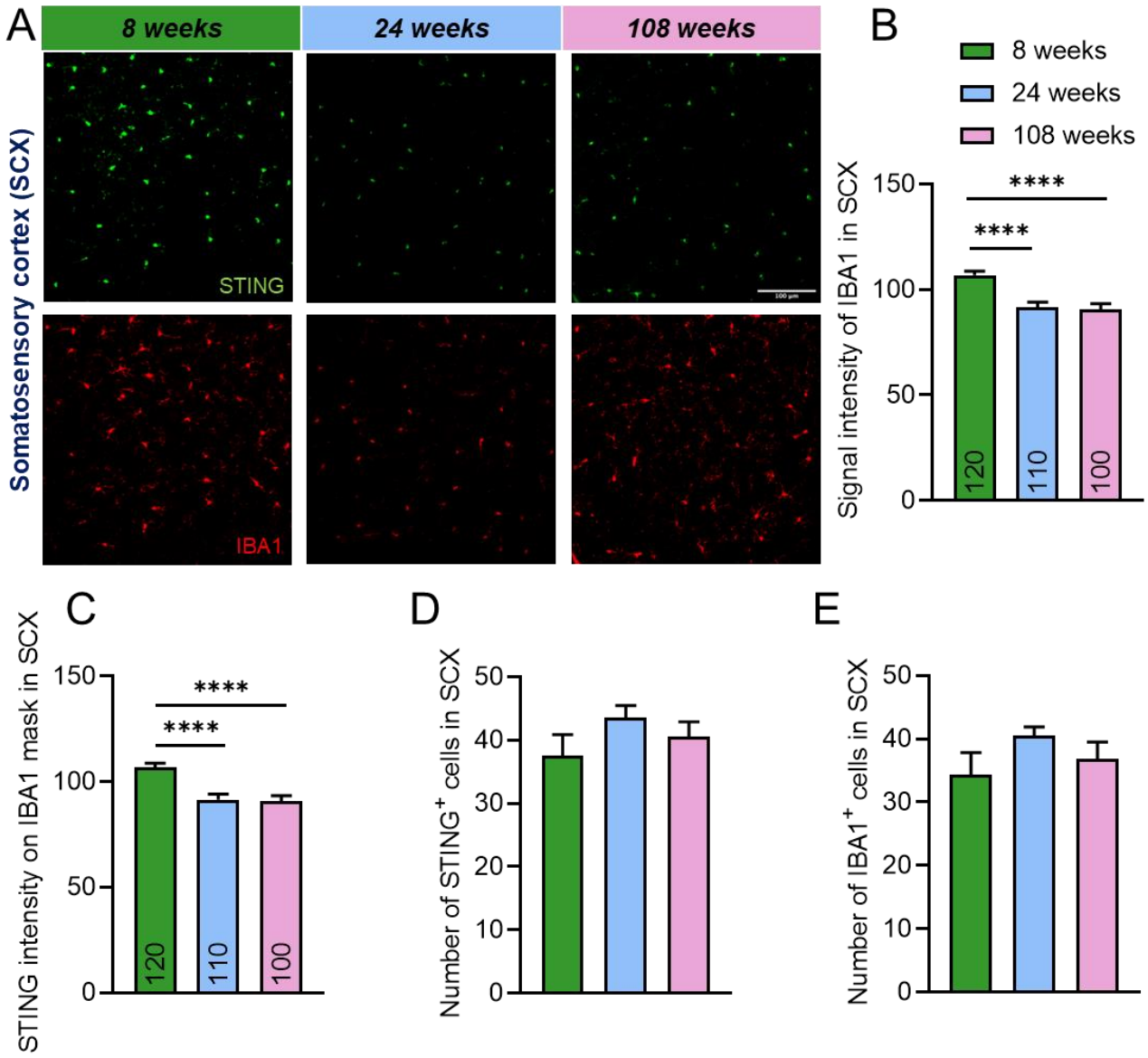

Figure 22: High intensity of STING and IBA1 in SCX of 8-weeks-old mice.
Representative images of STING and IBA1 positive cells in the SCX of 8-, 24- and 108-weeks-old mice. Scale bar: 100 μM (A). During ageing *in vivo* and especially already in the 24-week-old group of mice a decrease in the signal intensity of IBA1 and STING was found compared to the 8-week-

old group of mice (B-C), whereas the total number of STING positive microglia cells seams to increase (D-E). Data are presented as mean ± SEM. The statistical analysis was performed by one-way ANOVA followed by Tukey post hoc multiple comparison test (****P < 0.0001, n=3 in each group from three independent experiments) For the intensity analysis 100-120 cells were used (B).

In the SCX region, it was noted that the signal intensity of IBA1 and consequently also of STING decreased during ageing, with 24 and 108-week-old mice showing a significant decrease in the intensity of these two proteins (Figure 22B, C). In addition, no significant trend in the number of STING and IBA positive cells was visible (Figure 22D, E). Subsequently, the CA1 region of the hippocampus was analysed (Figure 23). This area, important for memory formation and consolidation, did not show an increase in IBA1 intensity (Figure 23B). At the same time, an increase in STING signal intensity was noted in 108-week-old mice compared to 24-week-old mice (Figure 23C). While STING-positive cells in this region significantly increased during ageing, there was only an upward trend in the number of microglia in the 108-week-old groups compared to the 8-week-old groups (Figure 23D, E).

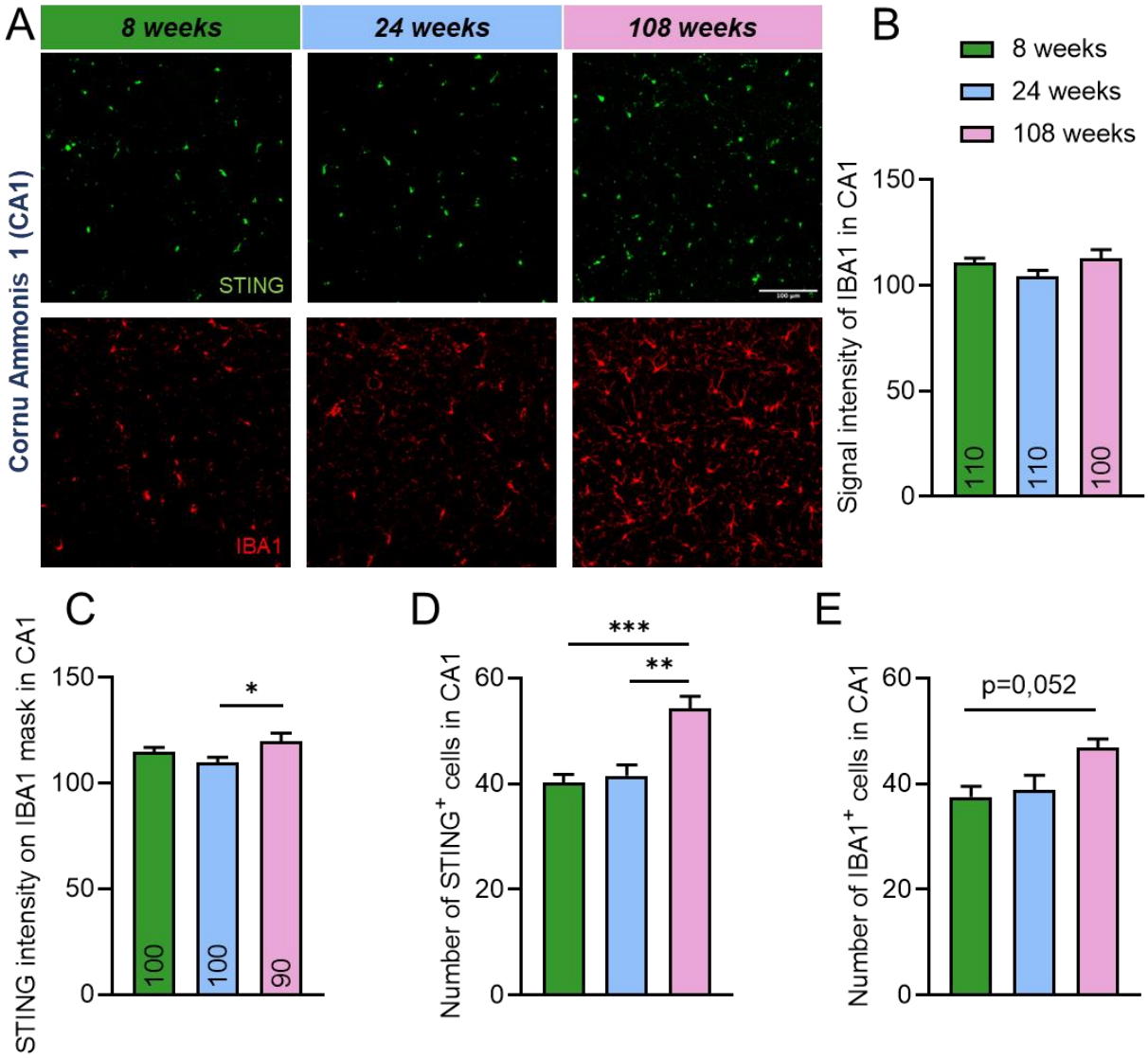

Figure 23: Increase in the number of STING-positive cells in CA1 during ageing *in vivo*. Representative images of STING and IBA1 positive cells in the CA1 region of 8-, 24- and 108-week-old mice. Scale bar: 100 μM (A). A strong increase of the number of STING-positive cells was detected during ageing *in vivo* (D). The same trend was observed for microglial cells, but it was not significant (E). Furthermore, the STING intensity was higher in the CA1 region of 108-weeks-old mice in comparison with 24-weeks-old ones (C). Data are presented as mean ± SEM. The statistical analysis was performed by one-way ANOVA followed by Tukey post hoc multiple comparison test (*$P < 0.01$, **$P < 0.001$, ***$P < 0.001$), two images per animal were acquired, one image for each hemisphere. The experiment was repeated at least three times and animals used were six. For the intensity analysis 90-110 cells were used (B-C).

Finally, the region of the DG was investigated, another region that undergoes strong changes during ageing and supposed to be fundamental for memory and learning (Dillon et al. 2017). Analyses showed a statistical relevant decrease between 8-week-old and 24-

weel-old in the signal intensity of STING, while the intensity of IBA1 demonstrated no difference in this area between the three age groups tested (Figure 24).

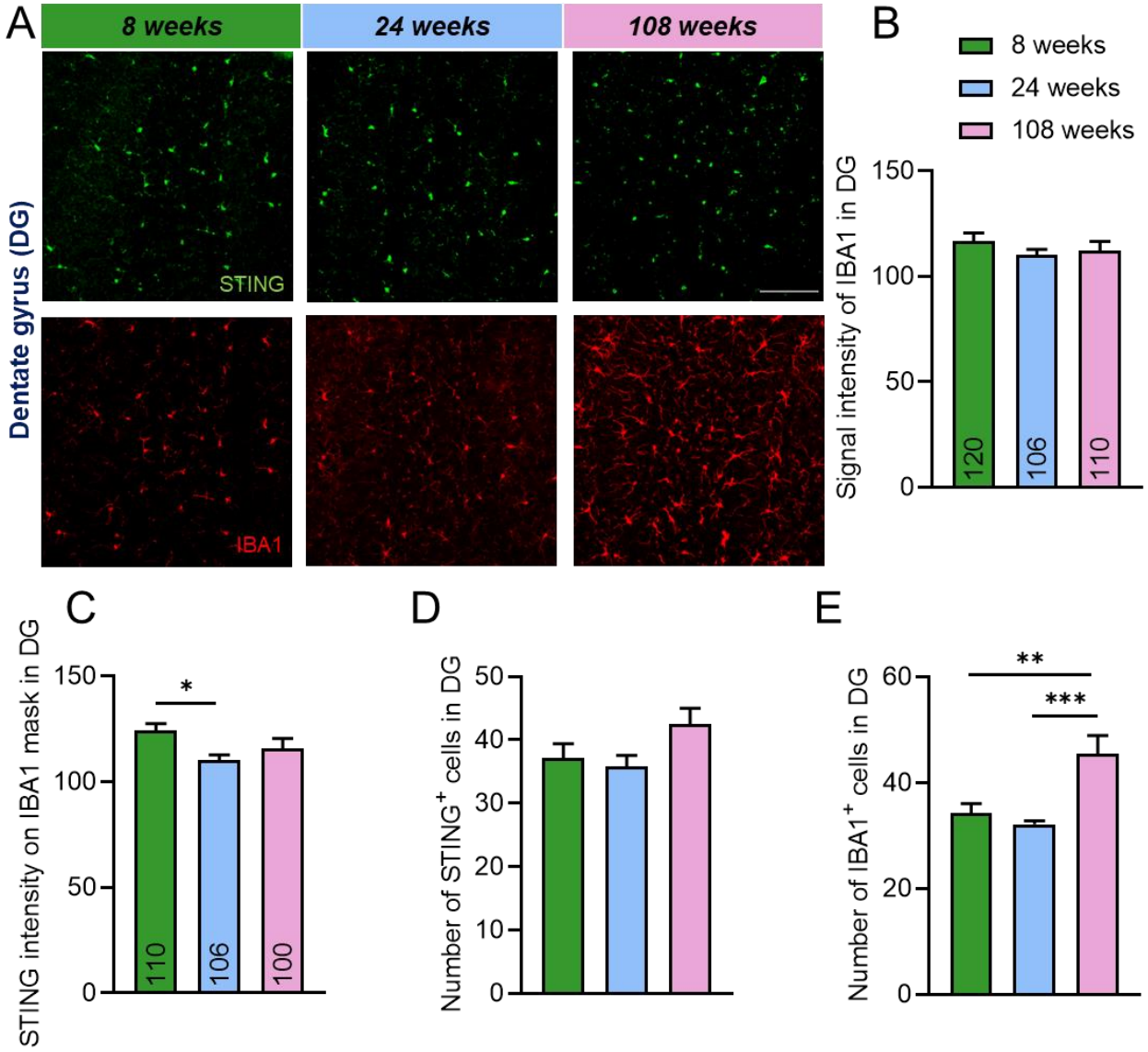

Figure 24: Migration or proliferation of IBA1-positive cells in DG during ageing *in vivo*. Representative figures of STING and IBA1 in the DG of 8-, 24- and 108-week-old mice. Scale bar: 100 μM (A). An abnormal increase in microglial cells was observed at the level of the DG in the 108-week-old mice groups compared to 24- and 8-week-old mice (E). Data are presented as mean ± SEM. The statistical analysis was performed by one-way ANOVA followed by Tukey post hoc multiple comparison test (**$P < 0.001$, ***$P < 0.001$), n=3, two images per animal were acquired, one image for each hemisphere. The experiment was repeated at least three times and animals used were six. For the intensity analysis 90-110 cells were used (B-C).

Interestingly, although the number of STING-positive cells did not change during ageing, at the same time the group of 108-week-old mice showed a marked increase in IBA1-positive cells compared to the groups of 8- and 24-week-old mice. The analyses of these areas led

to the conclusion that STING might not only be present in IBA1 positive microglia but also on GFAP and MAP2 positive cells, as shown in figure 25. Therefore, astrocytic, and neuronal markers were analysed using Pearson coefficient value (Figure 26).

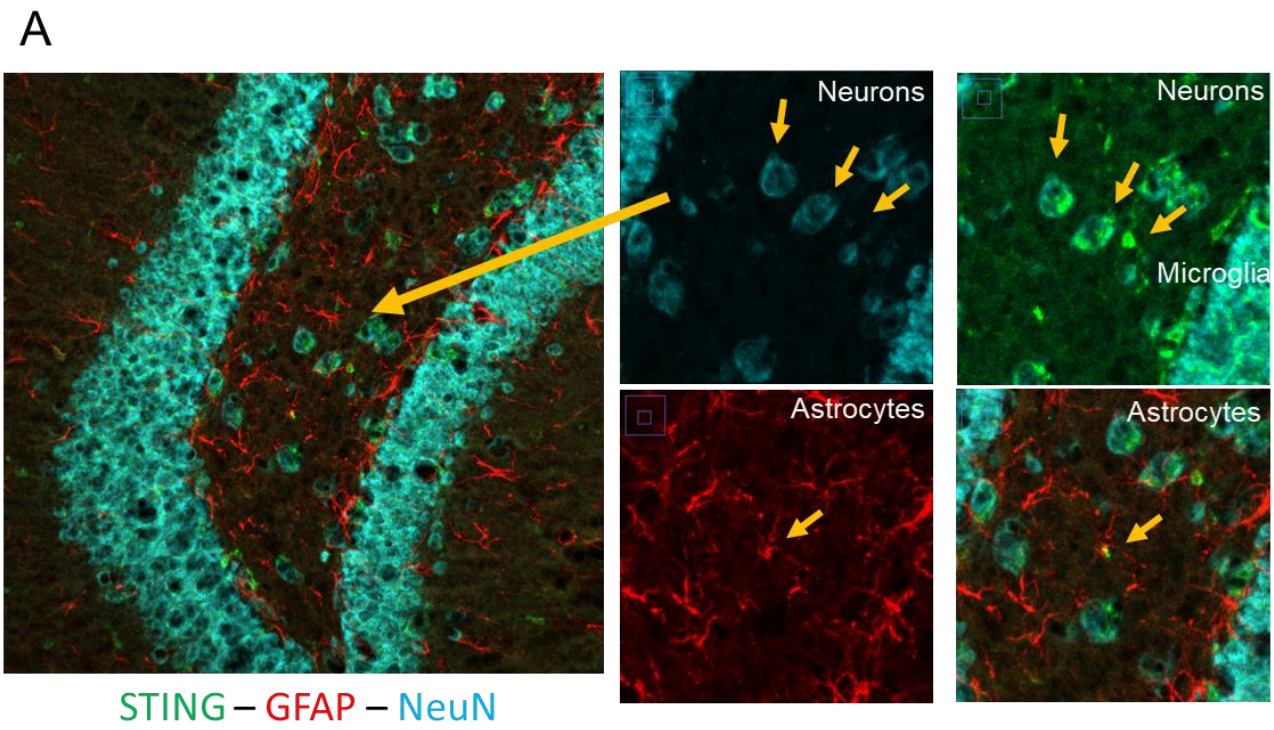

Figure 25: Representation of the colocalization between STING/astrocytes (GFAP) and STING/neurons (NeuN) in DG
Representative image with relative enlargement of the DG of 24-weeks-old mouse brain stained with STING (green), GFAP (red), and NeuN (cyan) to demonstrate that the STING signal is presence in neurons and astrocytes too (A).

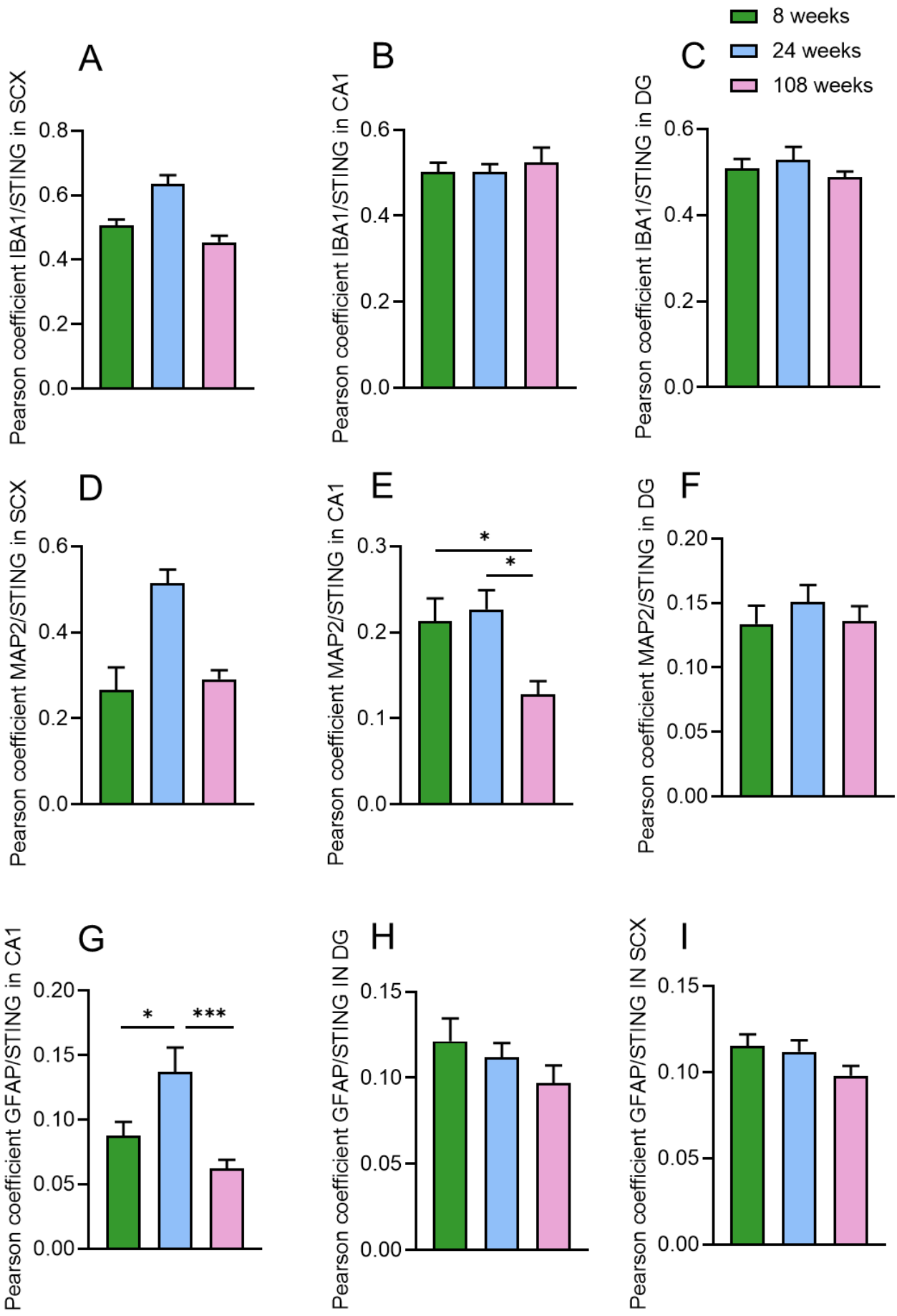
A
B
C
D
E
F
G
H
I
8 weeks
24 weeks
108 weeks
Pearson coefficient IBA1/STING in SCX
Pearson coefficient IBA1/STING in CA1
Pearson coefficient IBA1/STING in DG
Pearson coefficient MAP2/STING in SCX
Pearson coefficient MAP2/STING in CA1
Pearson coefficient MAP2/STING in DG
Pearson coefficient GFAP/STING in CA1
Pearson coefficient GFAP/STING IN DG
Pearson coefficient GFAP/STING IN SCX
*
*
*
***

Figure 26: Colocalization analysis between STING and IBA1, GFAP and MAP2 in different brain areas and during ageing.
Graphs representing the value of the Pearson coefficient between the different experimental groups related to ageing in the three areas examined. The combinations were IBA1/STING (A-C), MAP2/STING (D-F) and GFAP/STING (G-I). Data are presented as mean ± SEM. The statistical analysis was performed by one-way ANOVA followed by Tukey post hoc multiple comparison test (*P < 0.05, ***P < 0.001), two images per animal were acquired, one image for each hemisphere. The experiment was repeated at least three times and animals used were six (A-I).

The obtained data demonstrate changes in the localisation of STING in the selected brain areas during ageing. Thereby a particular significant trend towards loss of co-staining between MAP2 and STING in CA1 in the 108-week-old mouse groups compared to groups 8 and 24-week-old could be observed and the same trend was shown using the astrocytic marker GFAP on DG and SCX with a statistical difference between 24-week-old and 108-week-old in CA1 (Figure 26).

4.3 Functional role of STING in the mouse brain and neurons

In a next set of experiments the importance of the cGAS-STING pathway in brain physiology was analysed. Since most of the publications focuses on the role of the cGAS-STING pathway in microglial homeostasis, especially following CNS infections, a systematic understanding of how the cGAS-STING pathway contributes to the physiology of astrocytes and neurons, particularly during aging, is still missing (Reinert et al. 2016; Song et al. 2019; Ferro et al. 2019; Nazmi et al. 2019).
Based on this, a characterisation of the cortex of 24-week-old adult STING$^{-/-}$ mice was performed and compared to C57BL/6J WT mice. The analysis was carried out by WB for proteins involved in the cGAS-STING pathway and by ELISA to determine the amount of 2,3-cGAMP in the cerebral cortex. Strong evidence for decreased cGAS protein level were found in the STING$^{-/-}$ mice compared to C57BL/6J mice (Figure 27A, B). Similar results were obtained with TBK1 showing lower level in STING$^{-/-}$ mice. Interestingly, the phosphorylated protein seems to exhibit an opposite trend, with a non-significant increase in STING$^{-/-}$ mice compared to WT mice. Also, IRF3 and its phosphorylated component on serine 396 is significantly decreased when the STING protein is absent. Interestingly, the ratio between pIRF3 and IRF3 protein showed an increase in STING$^{-/-}$ mice compared to WT mice. Finally, despite the low protein concentration of cGAS, there was a statistically

significant increase of cytosolic 2,3-cGAMP levels in the cerebral cortexes of STING$^{-/-}$ mice (Figure 27I), probably due to the absence of the only protein capable of binding this CDN, i.e., STING.

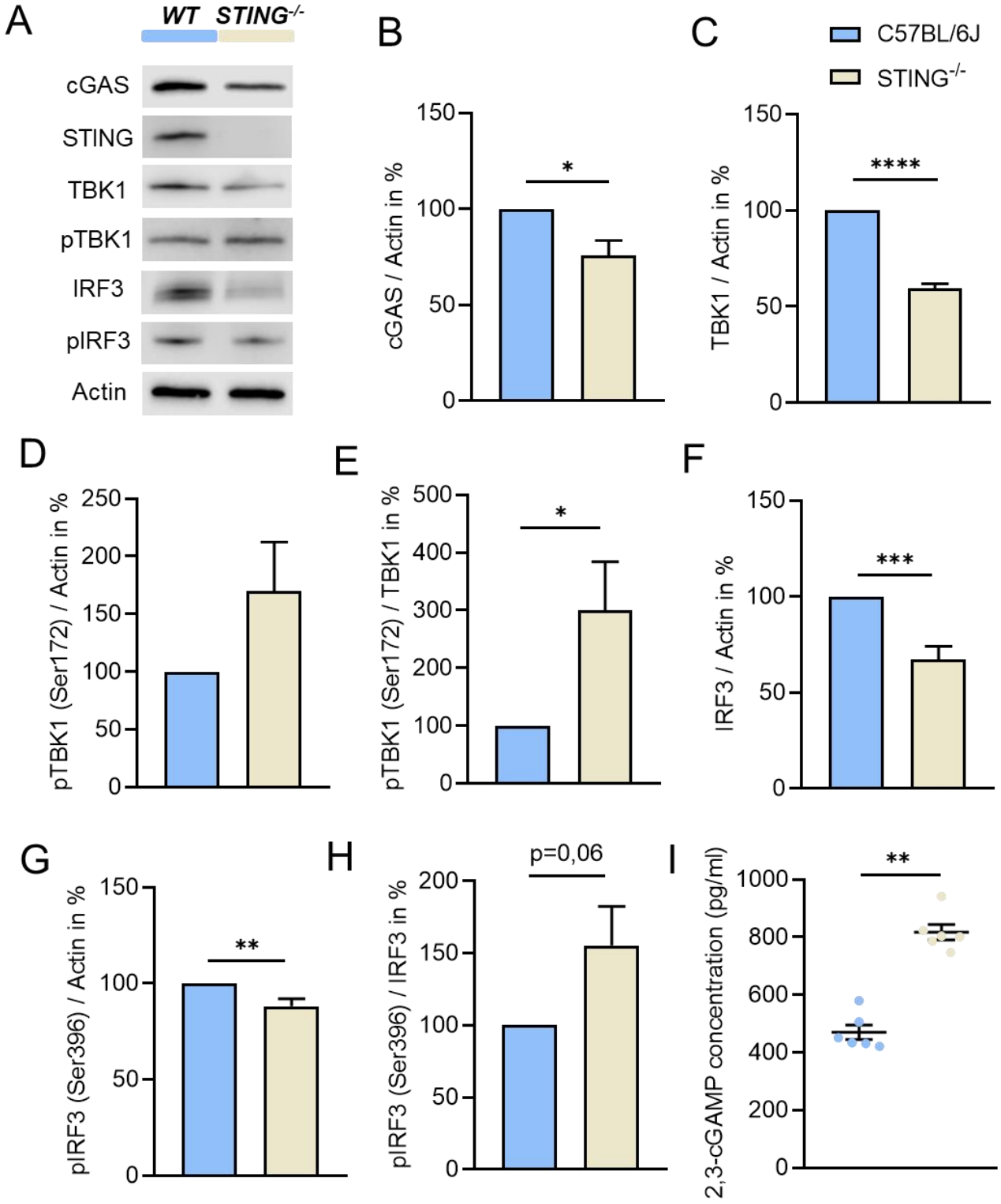

Figure 27: Quantitative analysis of cGAS, TBK1, IRF3 and 2,3-cGAMP level in the cerebellar cortex of STING$^{-/-}$ mice.

Representative blots of selected proteins belonging to the cGAS-STING pathway and Actin as an internal control from cerebral cortices of 24-week-old STING$^{-/-}$ and C57BL/6J WT mice (A). Graphs depicting a statistically significant protein reduction in all elements of the cGAS-STING pathway except pTBK1 in STING$^{-/-}$ cortex brain in comparison with WT ones (B-H). The concentration of 2,3-cGAMP assessed by ELISA indicates an increase in this molecule in STING$^{-/-}$ groups (I). Data are presented as mean ± SEM. The statistical analysis was performed by unpaired t-test followed by Tukey post hoc multiple comparison test (*P < 0.05, **P < 0.01, ***P < 0.001, ****P < 0.0001, n=3 in each group from six independent experiments) (B,I).

Additionally, to the analysis of the cGAS-STING pathway proteins, autophagy related components were analysed. Previous studies, especially in vitro, have shown that autophagy is strongly influenced by removal of cGAS and/or STING. However, this has never been demonstrated in the brain. Therefore, protein levels of p62, LC3 I and LC3 II were determined by WB in order to understand whether autophagic flux is modified in STING-/- mice. First, the cerebral cortices of STING-/- mice showed much lower protein level of p62 than the cerebral cortices of WT mice (Figure 28A, B). At the same time, LC3 I was shown to have a higher protein concentration in STING-/- mice compared to the WT and LC3 II showed no differences between the two groups. The ratio of LC3 II to LC3 I was significantly lower in STING-/- mice than in WT mice (Figure 28C-E). These results indicate a clear impairment of the autophagic flux. Continuing the analysis of the autophagic situation in the analysed tissues, Beclin1 and its phosphorylated form (Ser30), ULK1 and finally pULK1 (Ser555) were examined. Beclin1 and pBeclin1 showed no obvious variation between the two groups examined (Figure 28F, G), whereas for ULK1 a higher protein concentration was found in STING-/- mice compared to the WT (Figure 28H, I). However, the level of pULK1 increased only by trend and not significantly.

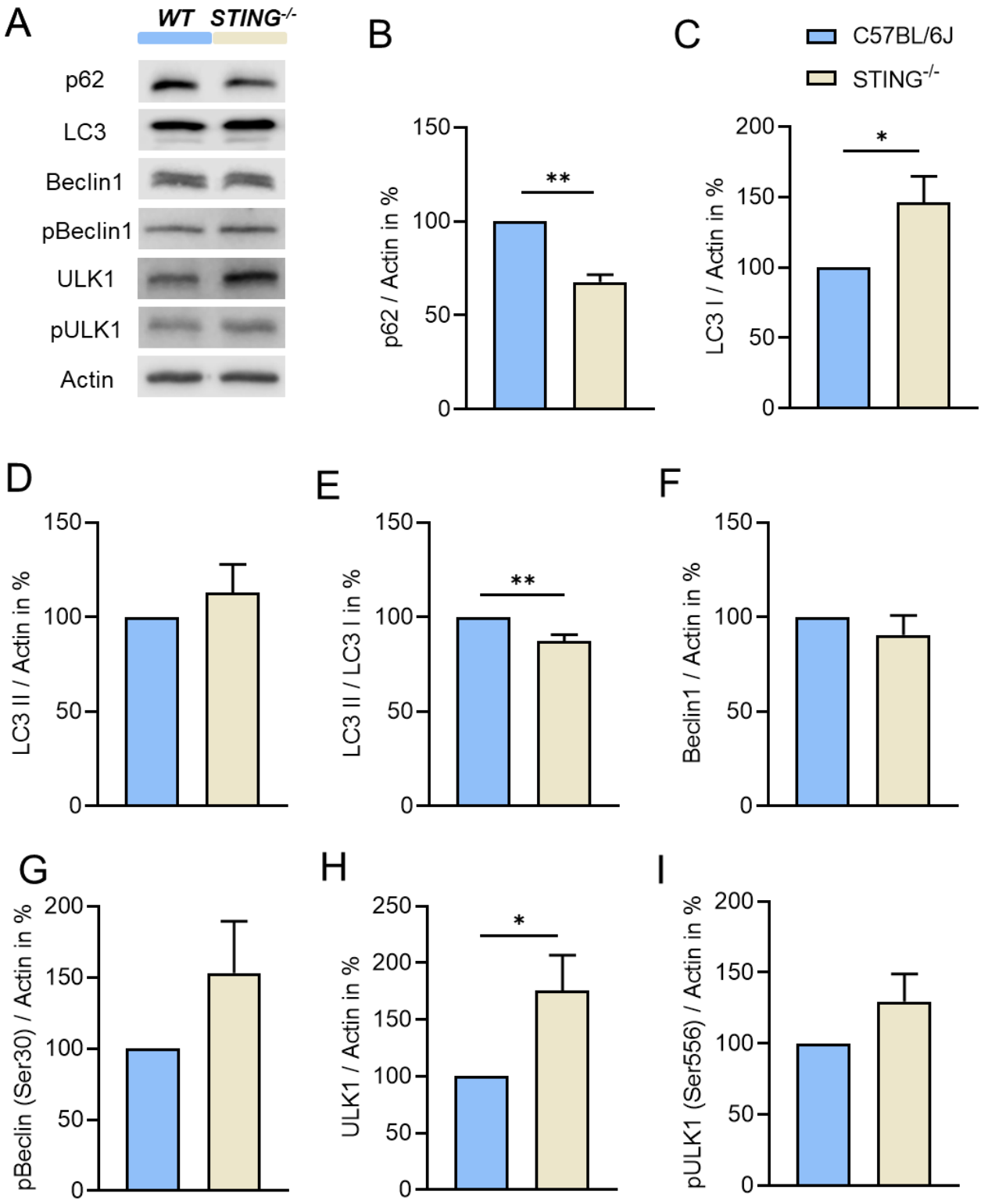

Figure 28. STING$^{-/-}$ mice show clear impairment of autophagic fluxes in the brain.
Representative blots of autophagy related proteins and Actin as an internal control (A). The marked protein decreases of p62 followed by a lower LC3 II / LC3 I ratio demonstrate that the cerebral cortices of STING$^{-/-}$ mice have a much lower amount of autophagosomes than WT mice (C-E). Beclin1 demonstrate any protein change via WB between STING$^{-/-}$ and WT cortices (F-G). Furthermore, the protein amount of ULK1 shows a statistically significant increase in the STING$^{-/-}$ group compared to WT (H-I). Data are presented as mean ± SEM. The statistical analysis was

performed by unpaired t-test by Tukey post hoc multiple comparison test (*P < 0.05, **P < 0.01, n=3 in each group from six independent experiments) (B, C).

Finally, using selected marker proteins for WBs, neurons, microglia, astrocytes, synapses, and the mitochondrial situation were quantitatively analyzed in the cortex of STING$^{-/-}$ mice brains (Figure 29). For NeuN (neuronal marker), GFAP (astrocytic marker) and IBA1 (microglial marker) no statistical differences between STING$^{-/-}$ and WT mice could be detected. Also, WB analysis at the synaptic level showed small, but no significant trends of Homer1 (post-synaptic marker) and Synaptophysin1 (pre-synaptic marker). A clear but not significant increase of TOM20 was seen in the STING$^{-/-}$ groups compared to WT mice. These results will be analysed in more detail in the future using immunofluorescence imaging for NeuN, GFAP and MAP2 and with specific synaptic and mitochondrial function analyses.

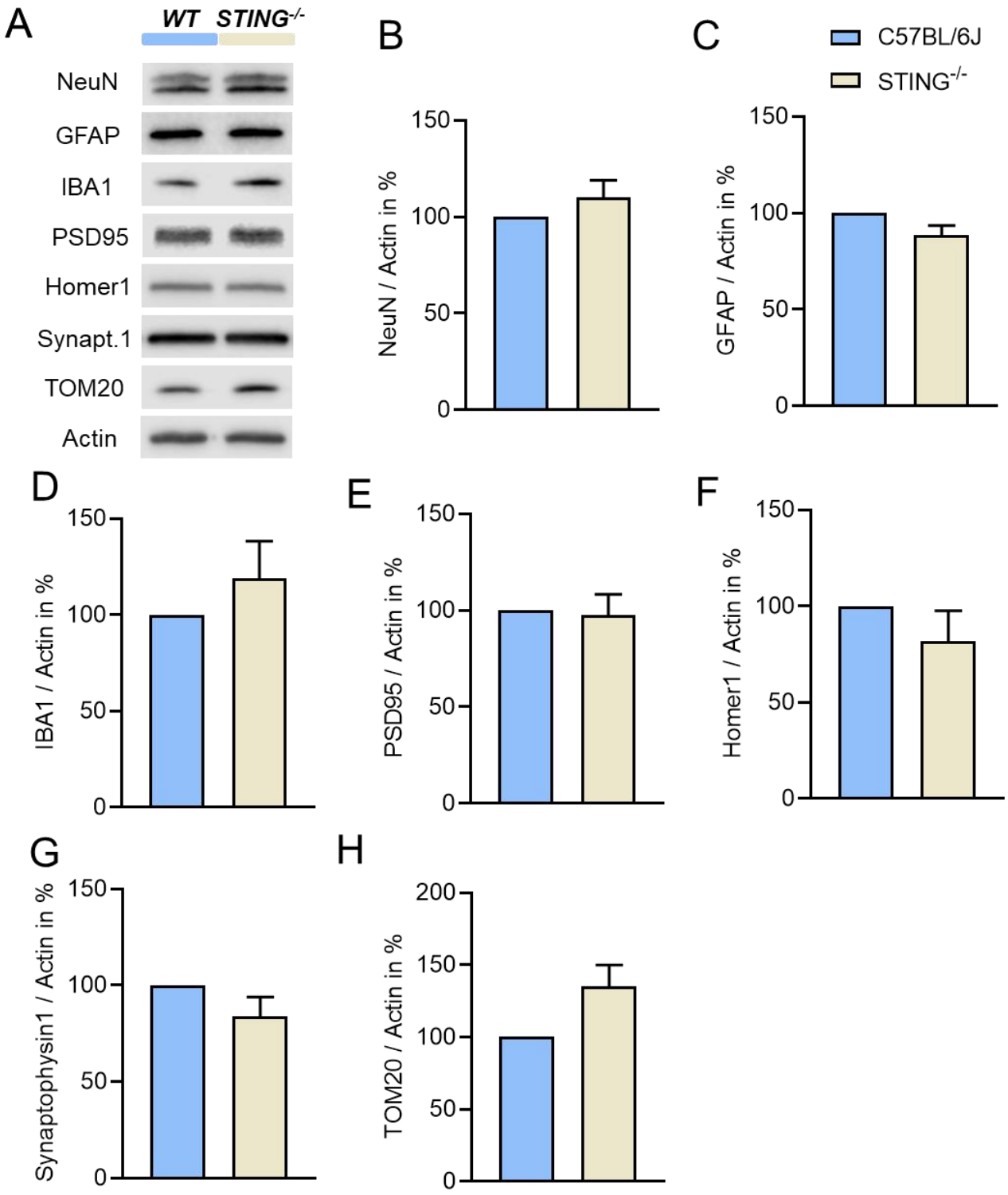

Figure 29: Quantitative protein analysis of cellular, synaptic, and mitochondrial markers in the brains of STING$^{-/-}$ mice.

Representative WB images of the examined markers like NeuN for neurons, GFAP for astrocytes, IBA1 for microglia, PSD95 and Homer1 for postsynaptic density, Synaptophysin1 for presynapsis area and TOM20 for mitochondria (A). Data are presented as mean ± SEM. The statistical analysis was performed by unpaired t-test followed by Tukey post hoc multiple comparison test (n=3 in each group from three or six independent experiments) (B).

Terminally, the relative expression level of ISG 54, IFNα and IFNβ as final products of the cGAS-STING pathway were analysed by quantitative RT-PCR (Figure 30). While ISG 54 did not show any differences clear trends were found for IFNα and IFNβ. Indeed, both the relative expression of IFNα and IFNβ is shown to be lower in 8-week-old STING$^{-/-}$ mice, although not statistically significant, compared to WT mice of the same age.

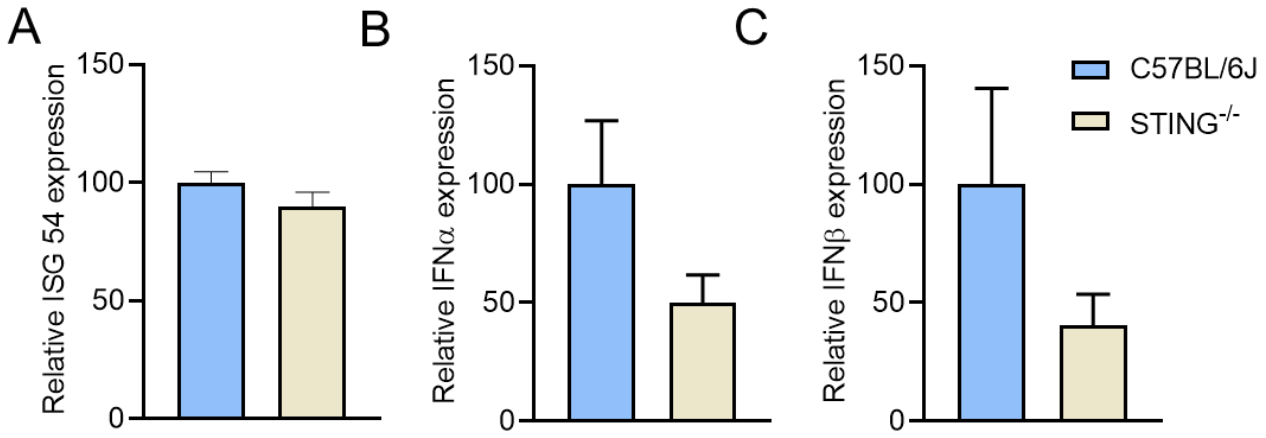

Figure 30: The cerebral cortices of STING$^{-/-}$ mice show a tendency towards a reduced IFNα and IFNβ release.
Quantitative analysis of relative ISG 54 (A), IFNα (B) and IFNβ (C) transcript level obtained by qRT-PCR. The housekeeping gene used for normalisation was GAPDH. Data are presented as mean ± SEM. The statistical analysis was performed by unpaired t-test followed by Tukey post hoc multiple comparison test (n=3 in each group from three independent experiments) (A, B, C).

There is currently a large gap of information about the role of STING at the neuronal level. The possibility of discovering the role of STING in neuronal cells could open the door for potential treatments of various brain diseases. Following the evaluation of specific differences in the cerebral cortex between WT and STING$^{-/-}$ mice, the focus was on the physiological and cellular differences that specifically characterize DIV 21 STING$^{-/-}$ neurons *in vitro* compared to WT neurons at the same age.

First, using Sholl analysis the morphology of STING$^{-/-}$ neurons was determined and compared with WT neurons. As can be seen from the images presented in figure 31, the morphological analysis of the STING$^{-/-}$ neurons revealed no morphological differences between 0 and 100 µm from the soma. However, at a distance between 100 and 200 µm from the soma, the Sholl analysis showed a significant decrease in the number of dendrites of STING$^{-/-}$ neurons compared to neurons from the WT. In addition, a maximum dendritic length analysis was performed, which demonstrated that the dendrites of WT neurons were statistically longer than those of STING$^{-/-}$ neurons.

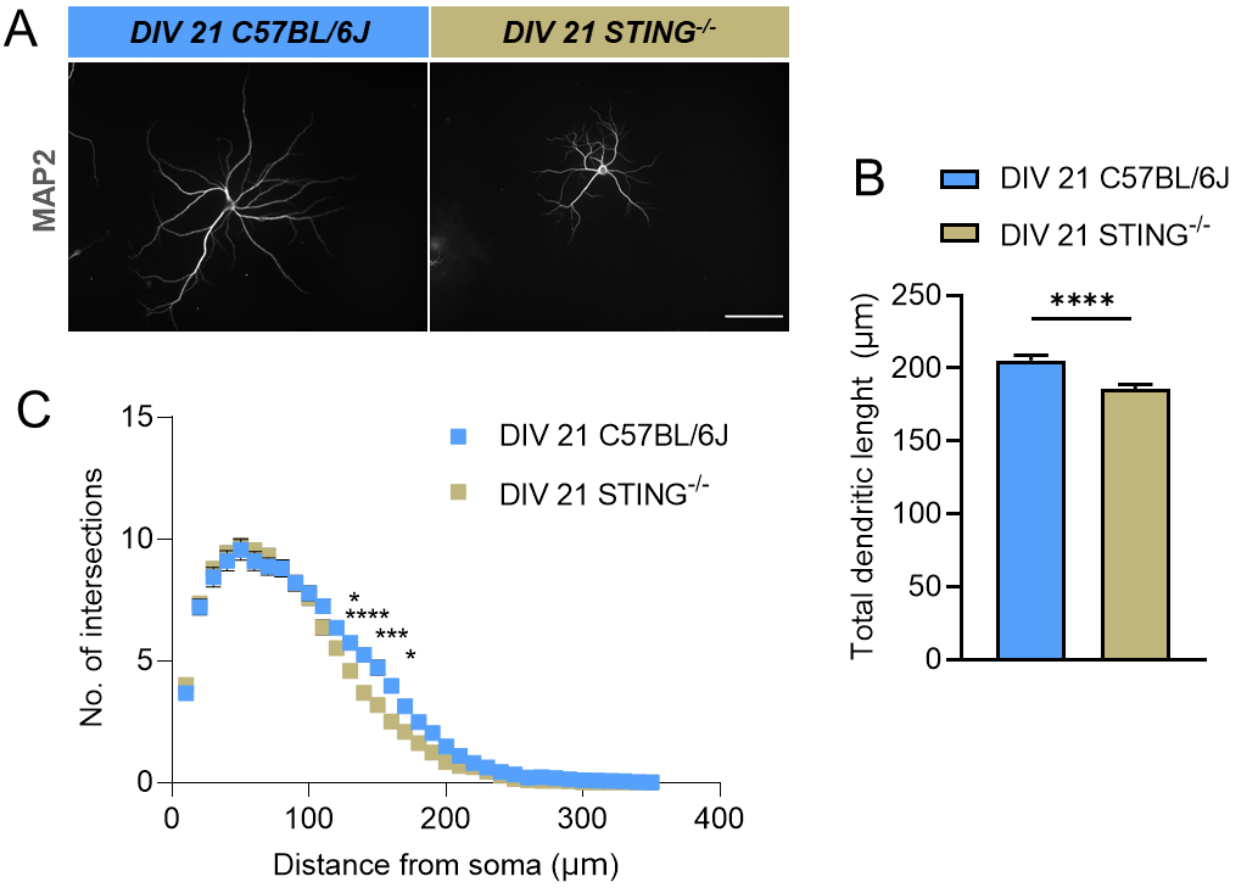

Figure 31: Reduction of dendritic arborisation and dendritic length of STING$^{-/-}$ neurons *in vitro*.
Primary cortical cultures from mice were stained with MAP2 in order to evaluate changes of the morphology between STING$^{-/-}$ and C57BL/6J neurons. Scale bar: 50 µm (A). Sholl analysis data that demonstrate a significant reduction of the total dendritic length and a loss of dendritic arborization of STING$^{-/-}$ neurons in comparison with neurons from C57BL/6J mice. Data are presented as mean ± SEM. The statistical analysis was performed by two-way ANOVA and unpaired t-test followed by Tukey post hoc multiple comparison test (*P < 0.05, ***P < 0.001, ****P < 0.0001, n=125-200 in each group from five independent experiments) (B, C).

Next, the potential impairment of autophagy, as already demonstrated *in vivo* for the cerebral cortexes of STING$^{-/-}$ mice compared to WT mice, was evaluated. For these analyses, immunostaining with antibodies raised against MAP2 and p62 was performed. In addition, cells were treated with 50 µM chloroquine for 4 h. This pharmacological treatment blocks one of the final steps of autophagy, namely the fusion process between lysosomes and autophagosomes (Mauthe et al. 2018). In this way, the neurons continue to produce autophagosomes that are not recycled by the cell, so that all of them produced by the neurons during the 4 h of treatment with chloroquine will be accumulate. As demonstrated

in figure 32, WT neurons were able to accumulate more autophagosomes, labelled with p62, than STING$^{-/-}$ neurons. This result demonstrated a clear impairment of autophagy on STING$^{-/-}$ neurons *in vitro*.

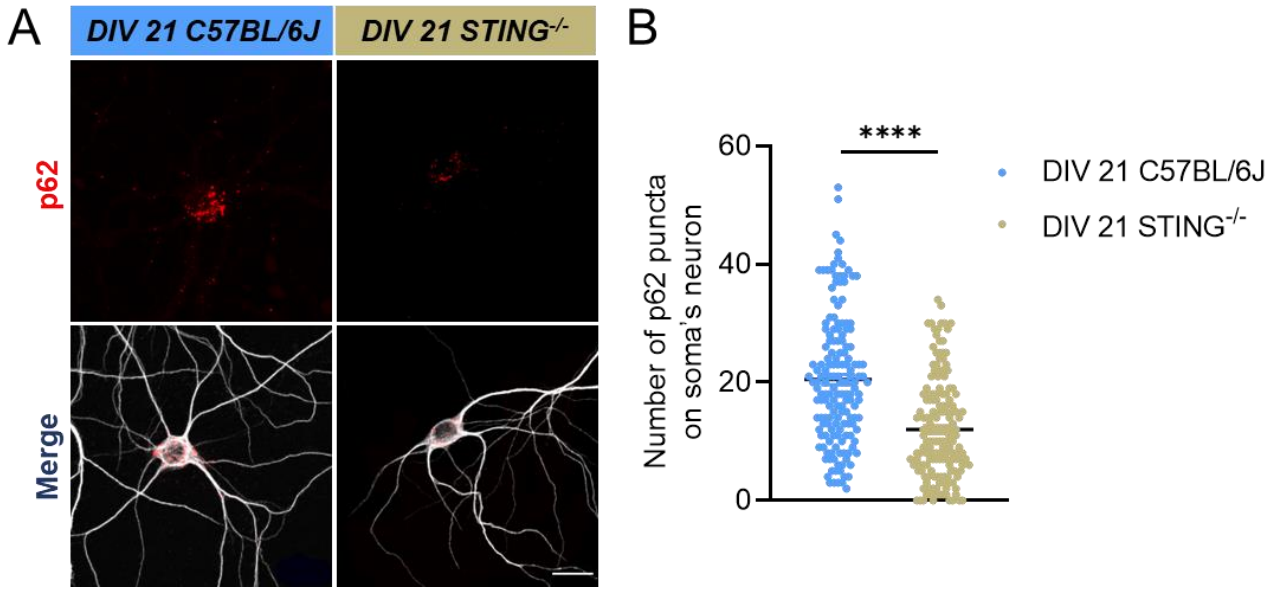

Figure 32: Chloroquine treated STING$^{-/-}$ neurons accumulate significantly less autophagosomes than C57BL/6J neurons *in vitro*.
Representative images of a staining with p62 and MAP2 after treatment with 50 μM chloroquine for 4h. Scale bar: 50 μm (A). Quantitative analysis of p62 dots on the neuronal soma. Data are presented as mean ± SEM. The statistical analysis was performed by unpaired t-test followed by Tukey post hoc multiple comparison test (****P < 0.0001, 160 cell analysed in each group from four independent experiments) (B).

After evaluating differences in autophagy of STING$^{-/-}$ neurons, the question arisses whether protein synthesis in the absence of STING is also impaired. In fact, the balance between autophagy and protein synthesis is very delicate and crucial for proper cellular homeostasis, especially in neurons, which are postmitotic cells and cannot proliferate but need constant and regular homeostasis to maintain proper vital functions (Aranda-Anzaldo 2012). Therefore, FUNCAT was used to determine differences within proteins homeostasis between STING$^{-/-}$ and WT neurons. The results indicated a clear increase in the TAMRA signal at both the dendritic level and the neuronal soma of STING$^{-/-}$ neurons compared to WT neurons (Figure 33).

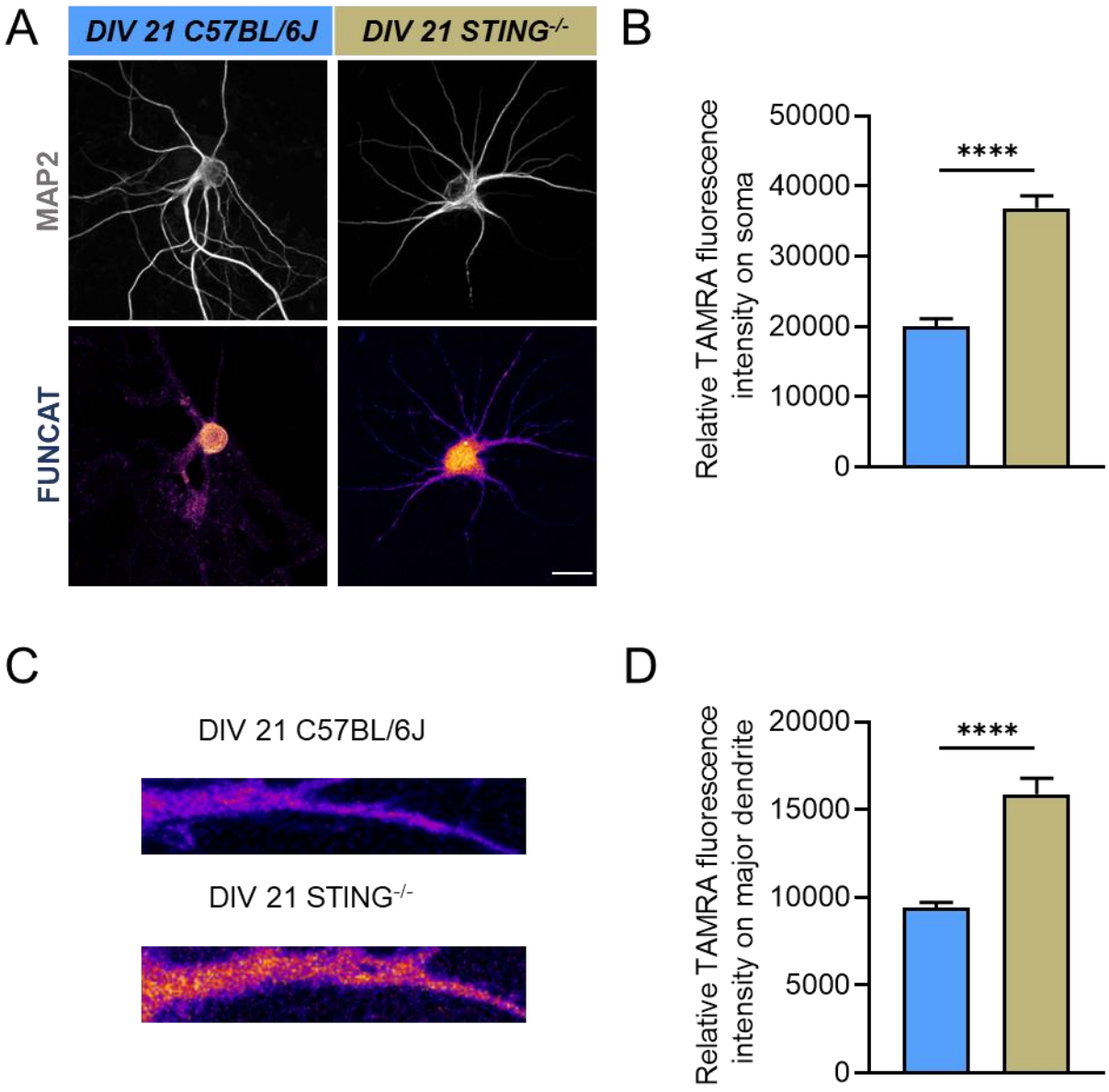

Figure 33: Increase of the TAMRA signal in primary neurons of STING$^{-/-}$ in comparison with WT.

Representative images of a staining with TAMRA and MAP2. Scale bar of 50 μm (A) and higher magnification pictures of major dendrites of WT and STING$^{-/-}$ neurons (C). Evaluation of the intensity of FUNCAT signal on soma and major dendrites of STING$^{-/-}$ and WT neurons (B and D). Data are presented as mean ± SEM. The statistical analysis was performed by unpaired t-test followed by Tukey post hoc multiple comparison test (****P < 0.0001, 160 cell analysed in each group from four independent experiments) (B and D).

Taking into account that both autophagy and protein synthesis are key events in maintaining synaptic homeostasis, in further *in vitro* experiments the effects of STING deficiency on synapes development and maintanance were analysed. WT and STING$^{-/-}$ neurons were stained with MAP2 and the pre-synaptic marker Synaptophysin1, and the amount of Synaptophysin1 puncta as well as the surounding pre-synaptic area at the level

of the major dendrite determined. The obtained results showed that STING$^{-/-}$ neurons at DIV 21 had less Synaptophysin1 puncta than WT neurons (Figure 34).

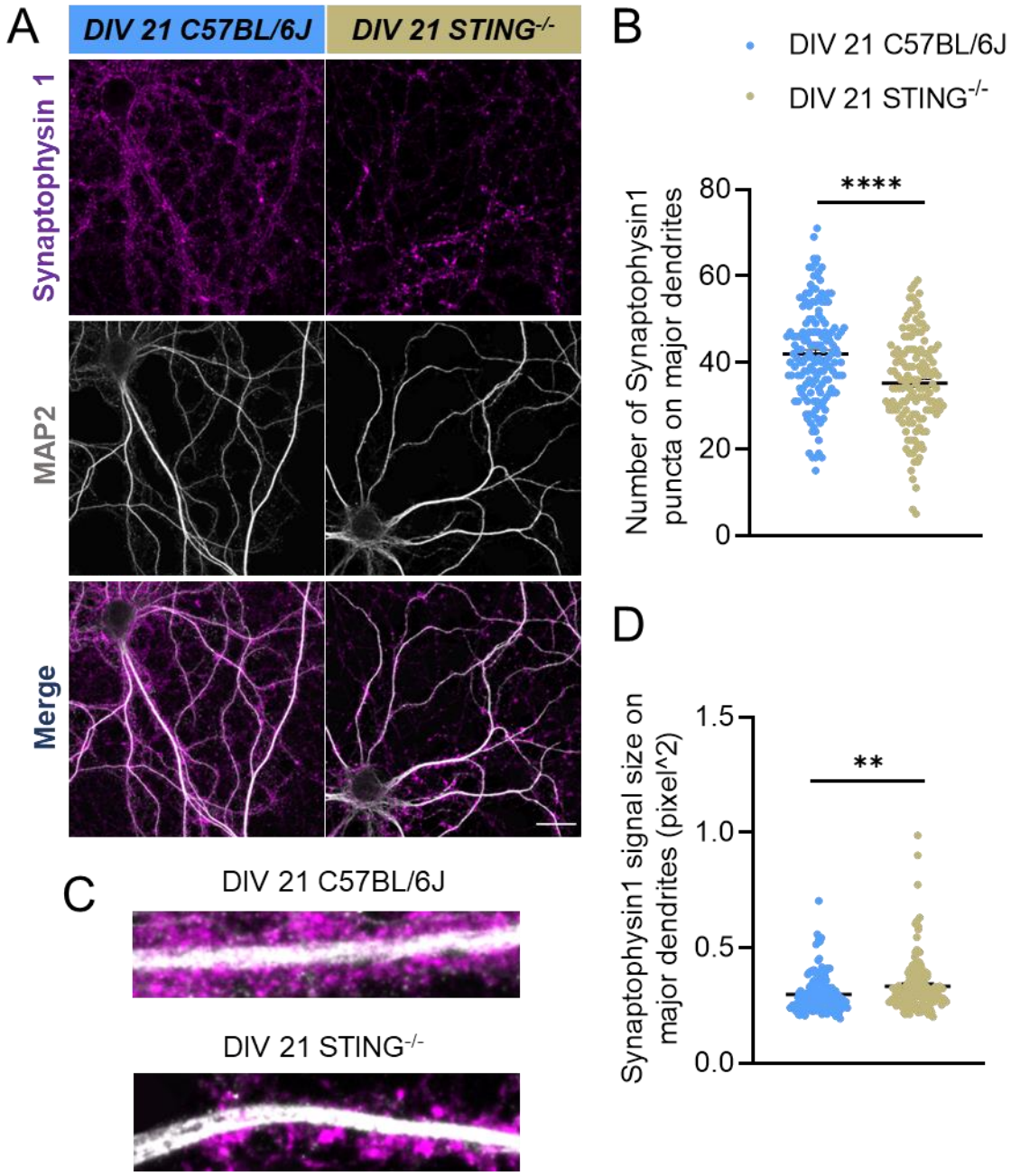

Figure 34. Loss of pre-synapses in STING$^{-/-}$ neurons.
Representative images of a co-staining with Synaptophysin1 and MAP2. Scale bar: 50 μm (A). Analyses were carried out on the major dendrites and show clearly fewer but bigger pre-synaptic puncta in STING$^{-/-}$ neurons respect WT ones (B, D). Data are presented as mean ± SEM. The statistical analysis was performed by unpaired t-test followed by Tukey post hoc multiple comparison test (**P < 0.01, ****P < 0.0001 150-155 cells were analysed in each group from five independent experiments) (B, D).

Similar to the analysis of the presynaptic situation, I focused next to the evaluation of putative postsynaptic changes on neurons in the absence of STING. For the analysis the postsynaptic protein marker Shank3 was used and the number, size and intensity of Shank3 puncta analyzed (Figure 35). The results obtained showed no significant changes in all aspects analysed between WT and STING$^{-/-}$ neurons.

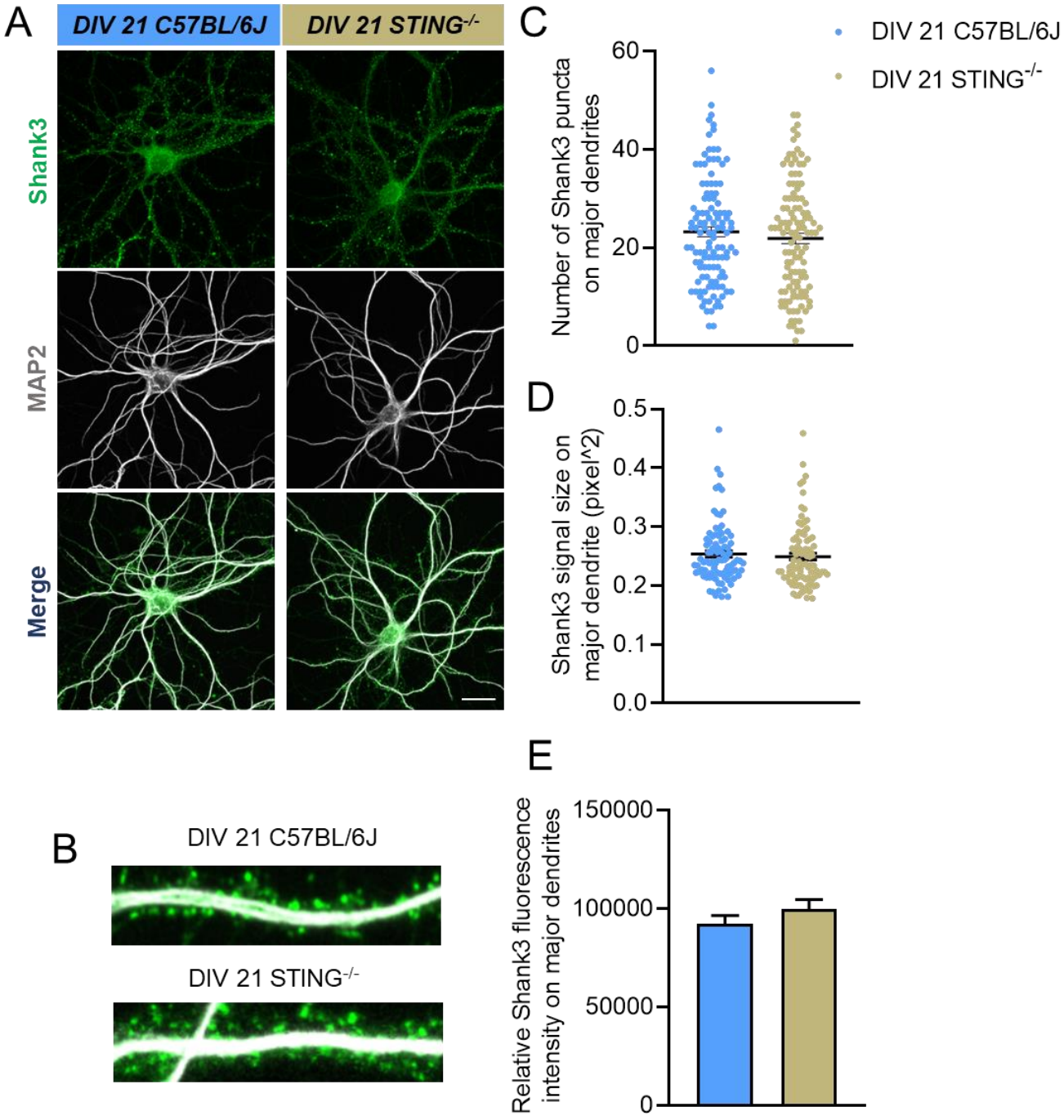

Figure 35. STING$^{-/-}$ neurons show no differences at the postsynaptic level in comparison with C57BL/6J neurons *in vitro*.

Representative images of a co-staining with Shank3 and MAP2 on primary cortical neurons at DIV 21. Scale bar: 50 μm (A, B). The graphs illustrate the similarity of the Shank3 signal at the dendritic level between WT and STING$^{-/-}$ neurons (C-E). Data are presented as mean ± SEM. The statistical analysis was performed by unpaired t-test followed by Tukey post hoc multiple comparison test (*P < 0.05). 150-155 cells were analysed in each group from five independent experiments (C, D, and E).

Finally, the number of active synapses, i.e. the number of colocalizing puncta of Shank3 and Synaptophysin1, were analyzed. Thereby, a significant decrease of active synapses was shown in STING$^{-/-}$ neurons compared to WT (Figure 36). This result was most probably related to a reduction in Synaptophysin positive presynapses observed in primary neurons of STING$^{-/-}$ mice rather than to changes in Shank3 and thus the postsynaptic area.

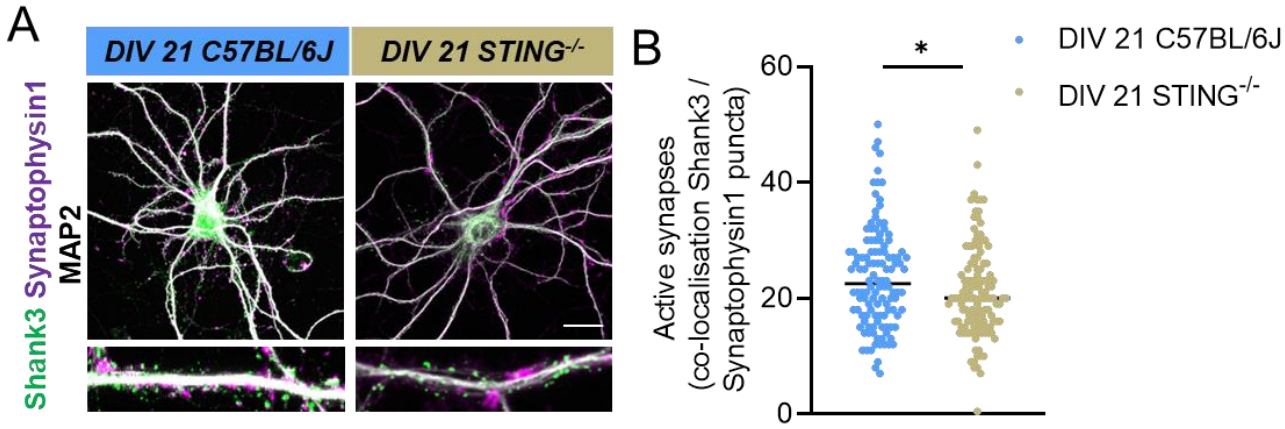

Figure 36. STING$^{-/-}$ neurons show a reduction in the number of active synapses respect C57BL/6J neurons *in vitro*.
Images of WT and STING$^{-/-}$ neurons at DIV 21, stained with MAP2 in white, Synaptophysin1 in purple and Shank3 in green. Scale bar: 50 μm (A). The decrease in colocalization puncta number between the pre- and post-synaptic marker in STING lacking neurons compared to WT indicates a reduction in active synapses. Data are presented as mean ± SEM. The statistical analysis was performed by unpaired t-test followed by Tukey post hoc multiple comparison test. 150-155 cells were analysed in each group from five independent experiments (B).

5 Discussion

5.1 How do neural cells respond to ageing *in vitro*?

With the birth of modern medicine, which began with the discovery of penicillin, and with the improved economic and health conditions that first the West and now also developing countries can afford, life expectancy and human longevity have increased over the last century (Gaynes 2017). Thus, ageing has become a central theme in politics, economics but also in science. In recent years, science has made big steps in explaining and describing what happens at the cellular level during senescence. The study of the ageing of tissues and organs has also accelerated markedly in recent years. For example, we now know what factors induce premature senescence in humans, and science has understood and described the causes that can delay ageing. However, there are still important gaps that scientists must try to address, such as a more specific analysis of the events that lead the brain to age or what triggers neurodegenerative diseases and consequently how to treat age-related diseases. Even today, many lessons learned about the brain ageing are derived from studies on post-mortem brains. The real processes of cerebral and especially neuronal ageing are for the most part still unknown. Therefore, in the first part of my doctoral thesis the focus was the development of an ageing model *in vitro,* using a cortical co-culture system with neurons and astrocytes.

As mentioned above, three timepoints were considered: DIV 21, 40 and 60. The selected ages represent the difference between adult, adult-old and very old neurons. The limit was set at DIV 60 because of the increasing loss of neurons and the racy proliferation of astrocytes that occurs after this date. The first experiment performed was to assess whether the *in vitro* model of ageing contains really 'aged' cells. To answer this question, a staining was carried out using beta-galactosidase in order to assess the number of aged cells present on the coverslips. We chose beta-galactosidase because it has been shown in many applications to be one of the main markers of ageing in different cell types (Alessio et al. 2021; Mera-Rodríguez et al. 2021). The results showed that with increasing age *in vitro* the number of senescent cells increased steadily (Figure 6). These findings are in line with what has already been obtained and demonstrated by Moreno-Blas and colleagues, who showed *in vitro* that in co-cultures of neurons and glia cells the amount of beta-galactosidase-positive cells increase age-dependently (Moreno-Blas et al. 2019). Subsequently, we analysed the morphology of neurons to assess anatomical changes that

could represent neuronal related ageing changes that have also been described *in vivo* (Hall et al. 2021). For the analysis the Sholl analysis was used, and the results showed a significant reduction in the number of dendritic intersections around the soma at DIV 60 compared to DIV 40 and 21 (Figure 7). In addition, the older neurons were also found to be smaller by assessing the total dendritic length. These results are also comparable to already described *in vivo* data on human and mammalian brains (Tsai et al. 2018; Hall et al. 2021). It has been shown that during ageing, the principal age-related neuronal structural alterations involve dendrites reduction in length and number (Dickstein et al. 2007; Bano et al. 2011; Müller-Thomsen et al. 2020). Additionally, in the past years a couple of research groups have shown that during ageing, and also in conjunction with neurodegenerative diseases, such as PD and AD, neurons in different brain areas show less dendritic arborization (Müller-Thomsen et al. 2020). This phenomenon has also been demonstrated in the cerebral cortex. In 2003 Duan and colleagues showed that the cortical neurons of old macaque monkeys had far fewer dendrites than those of young monkeys (Duan et al. 2003). The same concept was evaluated in studies of post-mortem human brains (Uylings and Brabander 2002; Dickstein et al. 2013). From our data and the cited research, we conclude that our *in vitro* model for neuronal ageing mirrors various morphological phenomena already shown *in vivo and* can therefore be used for the evaluation of further age-related aspects *in vitro*. In addition, several researchers describe a substantial axonal loss during ageing *in vivo*, which was also evident in our *in vitro* ageing system (Bloss et al. 2011). In fact, we realized that the loss of Tau1, a specific axonal marker, is significant at DIV 60 compared to DIV 40 and 21 (Figure 8). One aspect that differs between *in vitro* and *in vivo* brain ageing is the clear neuronal loss. Indeed, loss of neuronal cells is present but not prominent in normal aging, and the regions affected by a neuronal loss are restricted (no more than 10%) (Bloss et al. 2011; Dickstein et al. 2013). In our ageing model system, the loss of neuronal complexity and neuronal death assessed with the amount of MAP2 protein is about 30%. In addition, alongside MAP2 reduction, there is a strong astrocytic proliferation (Figure 8). Astrocytes represent the largest group of glial cells and are responsible for a variety of essential functions in the CNS (Sofroniew and Vinters 2010). The number of astrocytes increased especially in the DIV 60 group and this finding was assessed via evaluation of the protein concentration of GFAP, the main astrocyte marker. These results are in line with what has already been demonstrated *in vivo*. In fact, already 1987, Hansen and colleagues found that in the cortex of humans the number of astrocytes increased with age (Hansen et al. 1987). This

is not a constant event for every brain region. In the retina of rodents, a decrease in the number of glial cells has been shown, whereas in other brain areas such as the hippocampus, no differences in the number of astrocytes have been demonstrated (Mansour et al. 2008; Matias et al. 2019). However, our cells used *in vitro* derive from the cortex of mice and the observed increase in the number of astrocytes is in line with the existing literature (Verkerke et al. 2021). Furthermore, the protein increase of GFAP can be traced back to the presence at DIV 60 of more active or reactive astrocytic cells, because it has been shown that reactive astrocytes increase with age and these cells show a higher GFAP protein level than non-active astrocytes (Palmer and Ousman 2018). Therefore, after assessing the amount of neuronal and astroglial proteins and realizing a drastic drop in the level of MAP2 and TAU1, we focused on putative reason for the drastic loss of neurons. Therefore, subsequent experiments focused mainly on cell death and apoptosis. As can be seen from figure 9, during ageing *in vitro* we found an increase in the signal from the TUNEL assay, which indicated an increased presence of fragmented DNA and thus dead cells. Since we could not perform a co-staining performing the TUNEL assay and MAP2 staining caused by the relative lack of the TUNEL signal stability, we performed an immunofluorescence staining with cleaved caspase3 and MAP2 (Figure 9). In this way it was possible to estimate in a cell-specific manner a statistical increase in the signal intensity of cleaved caspase 3 on neurons at DIV 60 compared to neurons at DIV 21. This result indicates a clear increase in the apoptotic process with increasing age *in vitro*. This phenomenon can also be observed *in vivo*. Indeed, there are many reports describing increased neuronal death driven by apoptosis in degenerative diseases such as AD and PD (Okouchi et al. 2007; Wu et al. 2019). Furthermore, it has been shown that even during healthy ageing there is a loss of neurons in areas such as the cortex and hippocampus (Okouchi et al. 2007; Mattson and Magnus 2006). Based on this data, we aimed to understand, what causes neurons *in vitro* to age and die. Thereby we focused on the characterisation of various parameters that can affect neuron viability. We evaluated the quantity of the mitochondrial marker protein TOM20 at the different ages of our cortical cultures. The results indicate a clear decrease in the amount of TOM20 protein at DIV 60 in comparison to DIV 21 and 40. This decrease of mitochondria was associated with a remarkable increase of DNA in the soma of the neurons (Figure 10). The decrease in TOM20 can lead cells to an impairment of mitochondrial function (Cassina et al. 2020). Mitochondria are the main producers of ROS at the cellular level (Babizhayev and Yegorov 2016) and their malfunction leads to induce toxicity derived from increasing free radical

levels (Balaban et al. 2005). The main tool of cells in defence against this type of toxicity is glutathione, which has the ability to prevent damage of important cellular components caused by ROS, such as free radicals (Janikiewicz et al. 2018). The enzyme that catalyses the conjugation of the reduced form of glutathione to xenobiotic substrates for the purpose of detoxification is GST (Tchaikovskaya et al. 2005). In our cultures the protein concentration of GST is extremely higher at DIV 60 than at DIV 40 and 21. This indicates a strong demand of the cells for ROS detoxification, probably due to mitochondrial damage.

The cytosolic increase of DNA can mainly be caused by two reasons: DNA derived from pathogens, such as viral or bacterial DNA, or own DNA, i.e. DNA derived from the cell itself (Randow et al. 2013). In our cell cultures, it is possible to eliminate bacterial or viral DNA from this list. This means that the DNA identified at the cytosolic level in the soma of neurons was predominantly neural or astrocytic DNA. This DNA can be formed in several ways including release of mtDNA into the cytosol as a result of mitochondrial damage, or the damage of nuclear DNA, causing the release of micronuclei or DNA absorbed by phagocytosis. However, the clean-up of cytosolic DNA in damaged neurons is a task performed primarily by glial cells such as microglia and astrocytes (Jäkel and Dimou 2017). This means that the cytosolic DNA present in the soma of neurons *in vitro,* seems to be caused by nuclear instability or mitochondrial damage. The results described so far, with increased apoptotic phenomena and decreased TOM20 level indicate that at DIV 60 most probably both phenomena occur in neuronal cells. In fact, we observed an increase in cytosolic dsDNA in neurons at DIV 60 compared to neurons at DIV 21 and 40 (Figure 10). The increasing presence of dsDNA a in neurons at DIV 60 may be linked to an impairment of related catabolic processes. One of the most important catabolic processes is autophagy (Djajadikerta et al. 2020). Therefore, we decided to analyse the autophagic flux at the neuronal level. First, WBs were made analysing the main autophagic markers, namely p62 and LC3 with its different isoforms (Figure 11). The results showed that the ratio between LC3 II and LC3 I was statistically increased at DIV 60 compared to DIV 21. These data alone were not enough to provide a comprehensive picture of autophagy, especially because p62 WB showed only a trend, but no significant differences. For more specific results, we analysed the intensity of the p62 signal in neurons using IF stainings, leading to a significant result between older and younger neurons. In older cultures, the increase of p62 in neurons and the significant increase of the LC3 II / LC3 I ratio compared to younger cultures seem to indicate autophagic impairment in neurons at DIV 60 in comparison with DIV 21 and 40. In order to substantiate these findings, further tests were

carried out to estimate the presence of lysosomes in neurons. In fact, when autophagy is blocked, there are accumulations of autophagosomes represented by p62 and LC3 II and accumulations of lysosomes that are unable to fuse with each other to form autolysosomes (Evans and Holzbaur 2019). Using Lysotracker, that specifically detects lysosomes, we were able to estimate in neurons a clearly higher accumulation of lysosomes at DIV 60 compared to DIV 40 and DIV 21 (Figure 12). Curiously, although they did not show any differences in previous experiments, the neurons at DIV 40 showed more lysosomes than to the neurons at DIV 21, demonstrating that already at DIV 40 the neurons exhibited a tendency towards aging. Taken together, the presented results revealed a clear impairment of the catabolic machinery at the level of the autophagosome and lysosome axis. These data are in line with existing literature (Gavilán et al. 2015). Indeed, many studies have shown that autophagy is involved in cellular senescence. For example, Pyo and collaborators showed that overexpression of ATG5 increased the lifespan in mice (Pyo et al. 2013). At the same time, good lysosomal functioning also appears to be crucial. In that context Zhang and Cuervo demonstrated that restoration of chaperone-mediated autophagy (CMA) at the lysosomal level in ageing liver improves cellular maintenance and hepatic function (Zhang and Cuervo 2008). More specifically, *in vitro* studies on neurons showed that in senescent cortical neural cells the lysosome-autophagosome fusion was impaired, which resulted in inhibited autophagic flux (Moreno-Blas et al. 2019). Furthermore, considering that lysosomes originate by budding off from the membrane of the cis- and trans-Golgi complex, we decided to evaluate the change of the cis Golgi size during ageing *in vitro*. In this experiment, we were able to show that at DIV 60 the neurons had a much smaller size of the Golgi than at DIV 40 and 21 (Figure 13). These results lead to the hypothesis that in senescent cells the autophagic and lysosomal initiation phases functions normally and the impairment occurs at the level of fusion between autophagosomes and lysosomes.

Finally, following the comprehensive analysis of metabolic processes, we focused our attention on protein synthesis. In fact, an impairment of autophagy generally leads the cell to a subsequent impairment in protein synthesis (Hipp et al. 2019). To evaluate this, we performed FUNCAT on neurons at the three different ages DIV 21, 40 and 60 (Dieterich et al. 2010). This experiment showed that associated with autophagic and lysosomal impairment, the neurons specifically and not the glial cells (results not shown) tended to produce less protein at DIV 60 than at DIV 40 and 21 (Figure 14). A more detailed specific analysis of neuronal areas showed that at the soma level significance was only reached

between DIV 60 and DIV 40, while analysing the signal intensities from the dendrites it was clear that already at DIV 40 the neurons tended to produce less protein compared to the younger group. Therefore, neurons at DIV 60 showed a senescence phenotype characterised by impairment of newly protein synthesis and slowed degradation of old organelles and proteins. During ageing, a deterioration of neuronal autophagy induces cognitive impairment *in vivo* that is linked to impaired synaptic function. Restoring autophagy especially in aged mice using compounds such as spermidine improves cognitive performance (Xu et al. 2020a). Proteostasis is crucial for proper functioning of cognitive functions in the brain. Simultaneously, protein synthesis plays a key role in proper cerebellar and neuronal function. Ingvar et al. found age-related protein synthesis declines in Sprague-Dawley rats in the hippocampal dentate gyrus region, the nucleus accumbens, and the locus coeruleus, regions that mediate and modulate learning and memory (Ingvar et al. 1985). These data have also been confirmed by other studies that have shown a decreased rate of protein synthesis in the dentate gyrus, including reduced synaptic terminals in this area in aged rats (Geinisman et al. 1992).

In conclusion, all these data point to a massive loss of proteostasis at the neuronal level during ageing *in vitro* with many similarities to what has been demonstrated *in vivo,* such as morphological changes, autophagic impairment, mitochondrial dysfunction, reduced protein synthesis, but also with obvious limitations such as excessive neuronal death not found in normal aged rodent and human brains.

5.2 How does brain ageing impact the cGAS-STING pathway?

Our *in vitro* ageing model shows clear variations over time. So far, changes at the level of proteostasis have been described, but how do our cultures change during ageing *in vitro* at the level of innate immunity, and moreover, are components, originally involved in innate immunity, be able to influence the ageing of neurons? To answer these questions, we first had to evaluate the presence of proteins involved in innate immunity at the neuronal level. Starting from an remarkable finding observed on the *in vitro* assays described above, namely the age dependent increase of dsDNA at the cytosolic level, we focused on the pathway mainly involved in detecting cytosolic DNA, leading to the induction of autophagy or inflammatory response, called the cGAS-STING pathway (Xiao and Fitzgerald 2013). This signalling has mainly been described on tumour or immune defence cells. In the CNS, for example, it has been described predominantly on microglia (Reinert et al. 2016; Reinert

et al. 2021). However, to date, the cGAS-STING pathway has been only rarely described at the neuronal level in one publication concerning traumatic brain injury (Abdullah et al. 2018). Thus, the knowledge of the role of this pathway on neuronal function and ageing is very limited. For this reason, the first experiment we carried out was to analyse the presence of proteins related to this signalling pathway cell type-specifically on neurons. The antibodies that were most effective in IF were STING and IRF3. As can be seen from figure 15, a co-staining between STING and MAP2 and IRF3 and MAP2 could be demonstrated, indicative for the presence of the cGAS-STING pathway also in neurons. Starting from these results, we tried to understand if the cGAS-STING pathway can be induced in our neural cell cultures. Therefore, we treated the cell cultures with IFN-γ for 24 h and performed WB and IF. As can be seen from figure 17, cGAS, STING, TBK1, IRF3 and ULK1 are significantly upregulated following this treatment. At the same time, treatment with IFN-γ did not activate the pathway as evidenced by the lack of phosphorylation of TBK1 and IRF3. To evaluate more specifically whether neurons were also susceptible to 24-hour IFN-γ treatment, we performed an IF co-staining for MAP2 and STING (figure 17). The results showed a significant upregulation of STING cell type specifically for neurons. Thus, with these observations we started an evaluation of the specific protein concentration of various proteins of the cGAS-STING pathway during ageing *in vitro*. While no significant changes were evaluated for STING and TBK1, cGAS and IRF3 showed interesting variations. cGAS showed a significant decrease at DIV 60 in comparison with DIV 21. Furthermore, the ratio pIRF3 (Ser396) / IRF3 showed a clear decrease during ageing *in vitro*. These data indicate a clear decrease in the activity of the cGAS-STING pathway at DIV 60 in comparison with DIV 21 and 40 (Figure 16). In addition, these results are perfectly in line with what we have seen before using neural cultures. In fact, as could be demonstrated in previous experiments accumulates the amount of dsDNA at the cytosolic level *in vitro* with increasing age. The increase in cytosolic dsDNA can be caused by mitochondrial dysfunction or DNA damage, but also by a impaired process of DNA removal, which is carried out exclusively by the cGAS-STING pathway (Xiao and Fitzgerald 2013).

Based on this, we decided to shift our attention to brain ageing *in vivo* and tried to evaluate which role the cGAS-STING pathway might play in this process. For this purpose, we used the cerebral cortexes of 8-, 24- and 108-week-old mice. The cortex area was chosen because the neural cultures used *in vitro* were prepared from embryonic cortex, and the cerebral cortex is one of the areas most affected by ageing in mammals (Jobson et al.

2021). Therefore, for the first experiments performed protein extracts from cerebral cortex homogenates were used and the protein quantity of the main proteins involved in the cGAS-STING pathway were estimated by WB's. The results show a significant protein increase of cGAS during ageing, associated, however, with a marked decrease in the protein concentration of STING in the 108-week groups compared to the 8-week groups (Figure 19). In addition, we performed an ELISA to evaluate the levels of 2,3-cGAMP in cortex tissue in order to achieve information about the putative activity of cGAS (Cai and Imler 2021). Curiously, the protein increase of cGAS in the 108-week-old animals was not followed by an increase in its activity. In fact, the 2,3-cGAMP concentration detected in the cortex at different ages decreases with time and at 108 weeks it was significantly lower than in animals of 8 and 24 weeks (Figure 19). These results are contrary to what might have been expected, because a couple of reports are showing that inflammatory processes increase in the elderly age and with neurodegenerative disease (Lee et al. 2000; Enciu et al. 2013). For this reason, it was expectable to observe an increase in the production of 2,3-cGAMP, which induces the activation of the cGAS-STING pathway. To complete the picture, we analysed next TBK1 and its phosphorylated version, which showed no difference during age, and IRF3, which showed a decrease in 108-week-old mice compared to 8-week-old mice. Another parameter that can be used to evaluate the activation of the cGAS-STING pathway is the phosphorylation of IRF3 on serine 396, which indicates the activated form of the protein. Quantitative WB analysis reviled a marked increase of pIRF3 in the 108-week group compared to the 24- and 8-week groups. This result stands in contrast to the decreased concentration of 2,3-cGAMP and points towards an activation of the cGAS-STING pathway (Figure 19). Therefore, in order to estimate whether pIRF3 participates on the induction of inflammation in the cortices of our elderly animals, we evaluated by RT-qPCR the expression of IFN-α and IFN-β as well as the expression of ISG 54, which is the main site of inflammation mediated by IRF3 (Figure 21). However, all results showed a lack of IRF3 mediated activation of inflammation in the cortices of aged mice. The absence of clear induced inflammatory processes in the brains of aged mice during healthy ageing is an event that has already been particularly discussed in literature (Simen et al. 2011; Greenwood and Brown 2021). Indeed, it is possible to find both, researches that report the induction of inflammation in the brain caused by ageing and publications that demonstrate the absence of inflammation during ageing (Enciu et al. 2013; Gabuzda and Yankner 2013). Probably the difference is related to the presence of neurodegenerative diseases (Cerbai et al. 2012). Indeed, it could be

shown that in the case of AD and PD a clear inflammatory situation is developed, but a 'healthy ageing' without the presence of apparent diseases seems to be free of inflammatory processes (Lee et al. 2000). There is also a cell-specific difference to consider between neurons, astrocytes and microglia, which might have different functions, and which are not distinguishable through WB or PCR of an homogenised cortex (Cerbai et al. 2012). Hypothetical, given the intense interconnection between the cGAS-STING pathway and autophagy, it could be that phosphorylation of IRF3 may induce changes at the autophagy level. Therefore, we analysed the main proteins of the cGAS-STING pathway linked to autophagy induction using WB, namely ULK1 and Beclin1, in cortex tissue and found that there is an increase of phosphorylated Beclin1 at Ser30 during ageing (Figure 20). This specific phosphorylation on Beclin1 is carried out by ULK1, which can be induced by inhibition of the mTOR pathway and activation of the cGAS-STING pathway (Deleyto-Seldas and Efeyan 2021). These data are still insufficient to specifically describe what happens during brain ageing at the level of the cGAS-STING pathway and autophagy, but they are nevertheless a good starting point and data that are currently not reported. Next, we focused on the specific role that STING might play during ageing of the brain. Therefore, we performed immunohistochemistry staining of STING to analyse its presence on the essential cell types present in the CNS (Figure 22). As expected and already demonstrated in the literature, STING is mainly expressed in microglia (Reinert et al. 2016). Consequently, I decided to evaluate how microglia and STING vary with increasing age in the mouse brains. We focused mainly on three areas: SCX, CA1 and DG. These brain areas are particularly susceptible to age-related functional and morphological changes (Bloss et al. 2011). In these tissues, was evaluated the number of IBA1 and STING positive cells and the intensity of their signals to describe any region-specific changes. Thus, our results indicate that in SCX the signal intensity of IBA1 and STING was higher in the 8-week-old mice than in the 24- and 108-week-old groups, suggesting that this event is more development-related than a neurodegenerative factor. Instead, in CA1 we have described an increase in the number of positive STING cells in the group of elderly mice compared to adults and young one and the number of IBA1 positive cells tends to increase with age but is not significant. Finally, in the DG the most evident result is the statistically significant increase of the number of microglia that is not followed by an increase in positive STING cells.

These results indicate important differences in the immune response to ageing in the various brain areas. My data are in line with the huge amount of literature that indicates

how different brain areas react differently to ageing. Further experiments are needed to understand the role of STING and microglia in the aging of specific brain areas.

5.3 STING deficiency leads to alterations in the homeostasis of the entire brain and neurons *in vitro*

Given the changes that the cGAS-STING pathway seems to have during ageing and given the evident presence of this pathway also in the brain, especially in neurons, we decided to investigate how the deficiency of STING and thus the lack of the cGAS-STING pathway could affect cerebral and neuronal homeostasis. To this end, first the cortex of 24-week-old mice and in a second set of experiments WT and STING$^{-/-}$ neurons *in vitro* were analysed to assess their morphological and functional differences.

The first analysis performed was a general evaluation of the protein concentration of the cGAS-STING pathway players and their alterations in the absence of STING. Indeed, STING$^{-/-}$ mice showed a significant reduction of cGAS in comparison with WT mice, followed by a significant increase of the cortical concentration of 2,3-cGAMP in STING$^{-/-}$ mice compared to the WT ones (Figure 27). This difference between synthesizing protein (cGAS) and product (2,3-cGAMP) is probably related to a decrease in type I IFN expression and the lack of STING, which is the only known receptor of 2,3-cGAMP to date. Further analysis of the protein quantity of the other proteins involved in the cGAS-STING pathway signalling showed that *in vivo*, the protein concentration of TBK1 was significantly decreased in STING$^{-/-}$ compared to the WT, while curiously, and for a reason still unknown but possibly connected to the autophagic situation, the cortexes of 24-week-old STING$^{-/-}$ mice showed an increase in the concentration of pTBK1 compared to WT mice (Figure 27). As for IRF3 and pIRF3, the protein concentration of these proteins is significantly reduced, most probably due to the absence of STING and the lack of the cGAS-STING pathway induction. In addition, the decrease of the activated form of IRF3, i.e., pIRF3, with a consequent decrease in the amount of this protein in the brain cell nucleus, induced a decrease in the gene expression of type I IFNs. Modulation of the cGAS-STING pathway leads as also described in the introduction mainly to changes in autophagy and in the expression of inflammation-related genes including IFN alpha, beta, interleukins like IL-6 or even chemokines such as CXCL9, CXCL10 and CCL5 (Guo et al. 2020; Yu et al. 2022). As was to be expected, in my results the absence of STING reduced the expression of type I IFN although for a low biological number the difference was not significant. The role

of IFNs in brain physiology and function has been widely studied. For example, IFN-beta deficient mice showed an increase of neuronal apoptosis and reduced neurite network formation (Ejlerskov et al. 2015). Furthermore, Wikman and colleagues demonstrated that neurons express IFNAR on both pre and postsynaptic membranes (Vikman et al. 2001). It was also shown that IFNs modulate neuronal excitability (Prieto-Gomez et al. 1983). Finally, IFNAR ablation led to an impairment of the memory formation, which was associated with a reduced dendritic spine density (Hosseini et al. 2020). Thus, there is a lot of evidence demonstrating the importance of IFNs in neuronal function and it is likely that a reduction of IFNs in the brains of STING KO mice induces effects as yet unknown.

Next, because of the close interaction between the cGAS-STING pathway and autophagy demonstrated in the literature on tumour and HEK cells, we analysed the changes in the autophagic flux in the cerebral cortex of STING$^{-/-}$ mice compared to that of WT mice (Prabakaran et al. 2018). The results showed that STING$^{-/-}$ mice had a statistically lower protein concentration of p62 in the cerebral cortex compared to WT mice (Figure 28). Furthermore, the protein amount of LC3 I was significantly higher in STING$^{-/-}$ mice compared to WT mice. This finding was associated with an unchanged protein concentration of LC3 II between both genotypes of animals. Thus, the LC3 II/ LC3 I ratio was significantly lower in STING$^{-/-}$ mice compared to the WT. These data indicated that STING$^{-/-}$ mice showed an autophagic impairment in the cerebral cortex due to the decrease of p62, the main autophagosome marker, and the increase of LC3 I (with no change for LC3 II), which is considered the inactivated and not yet present form of LC3 in the autophagosome. Therefore, the results obtained on protein analysis of the autophagic proteins LC3 and p62 showed a clear autophagic impairment in STING$^{-/-}$ mice. These results are similar to those demonstrated by Prakandaska and colleagues who showed that STING$^{-/-}$ -HEK 293T cells showed impaired autophagy with reduced p62 levels compared to control cells, but for the first time they are demonstrated by us for the cerebral cortex (Prabakaran et al. 2018). Furthermore, although Beclin1 showed no differences between the two different genotypes of the analysed mice, the protein concentration of ULK1 was higher in STING$^{-/-}$ mice than in WT mice (Figure 28). The overexpression of ULK1 can have substantial effects on the functionality of cells. Jung and colleagues demonstrated that overexpression of ULK1 in HEK 293T cells dramatically reduced cell proliferation rate and that can be translated in a reduction of glial cell production during ageing (Mukhopadhyay et al. 2015). Hypothesising, increasing concentrations of ULK1 in STING$^{-/-}$ mice might be linked to a lower autophagic rate with a

lower utilisation of the autophagic initiation machinery as well. In order to gain further insight into the various cellular compartments present in the CNS of STING$^{-/-}$ mice, we analysed different neuronal, astrocytic, microglial and more specifically mitochondrial and synaptic markers using quantitative WBs. However, the results of proteins such as TOM20, Homer1, PSD95, GFAP, NeuN, and IBA1 did not exhibit significant changes between the cortex of STING$^{-/-}$ and WT mice.

Previously, we described a clear autophagic impairment in the cortexes of STING$^{-/-}$ mice, but using protein extracts derived from homogenates, it was not possible to distinguish on which cell type this occurred. Knowing that microglia are the main cell type in which proteins of the cGAS-STING pathway are, expressed we can speculate that the signal obtained through WB came predominantly from microglia (Reinert et al. 2016).

To determine, whether this autophagic impairment might also be present at the neuronal level, we analysed the accumulation of p62 *in vitro* at DIV 21 in WT and STING$^{-/-}$ neurons, treated with 50 µM chloroquine for 4 h (Figure 32). The results showed a significant increase in p62 positive puncta in WT neurons compared to STING$^{-/-}$ neurons, indicating a clear deficit in autophagy also at the neuronal level caused by STING deficiency. As described above, these results are in line with those demonstrated in the literature on HEK 293T or Hela cells, but for the first time these autophagy deficits in STING$^{-/-}$ cells are demonstrated on primary cultures of neurons (Prabakaran et al. 2018; Gui et al. 2019). Referring to the literature that impairments of autophagy can lead to conformational and functional changes in the neuron, we decided to investigate the neuronal morphology of STING$^{-/-}$ neurons. Indeed, Sholl analyses performed on DIV 21 neurons of STING$^{-/-}$ and WT cells revealed a significant decrease in the number of dendrites around the soma in STING$^{-/-}$ neurons (Figure 31). Furthermore, the evaluation of total dendritic length showed that STING$^{-/-}$ neurons had shorter dendrites than WT neurons. As shown in the first part of the thesis, autophagic impairment and lack of adequate type I IFN production could be the main cause of this neuronal morphological deficit in STING$^{-/-}$ neurons. Further, more specific experiments should be carried out in the future to demonstrate the correlation between both events.

Autophagy related catabolism and the synthesis of new proteins are highly correlated mechanisms (Deleyto-Seldas and Efeyan 2021). The main molecular signalling that induces the synthesis of new proteins is the mTOR pathway that has an inhibitory function on the autophagic process. Following the observation that autophagy is impaired in

neurons *in vitro*, we decided to investigate the impact of STING deficiency on protein synthesis. For this reason, we performed FUNCAT on neurons from both genotypes *in vitro* at DIV 21. Interestingly, this analysis showed that the intensity of the FUNCAT signal was stronger in STING$^{-/-}$ neurons compared to WT neurons, both at the dendritic level as well as on the soma (Figure 33). This finding can be explained by the observation that STING$^{-/-}$ neurons having slowed autophagy takes longer to degrade even newly synthesised proteins. Therefore, further experiments should be performed using FUNCAT and an autophagy inhibitor, such as chloroquine, to unravel how autophagy affects the amount of newly synthesised proteins. To date, there are no data in literature correlating STING deficiency with a change in protein synthesis. Finally, we analysed whether the deficiency of STING induces changes at the synaptic level in neurons *in vitro*. Therefore, we performed staining on neurons *in vitro* at DIV 21 using the presynaptic marker Synaptophysin1 (Figure 34) and the postsynaptic marker Shank3 (Figure 35). Analysis of the dendritic number of puncta and their size revealed that the biggest differences between WT and STING$^{-/-}$ neurons occur at the presynaptic level. In our experiments, no postsynaptic variations in the number and size of Shank3 puncta were found comparing WT and STING$^{-/-}$ neurons. In the Synaptophysin1 analysis, STING$^{-/-}$ neurons had significant less presynaptic puncta than WT neurons. In addition, STING deficient neurons showed an increase in the Synaptophysin 1 signal area compared to WT neurons. These results are also associated with a general decrease in active synapses, defined as co-localized pre- and postsynapses (Figure 36), in STING$^{-/-}$ neurons in comparison with WT, mainly due to the difference at the presynaptic level.

Summing up, these data indicate that STING and consequently the cGAS-STING pathway, although until now poorly studied, seems to be an important element for proper neuronal function.

6 Future perspectives and closing remarks

To date, brain ageing remains a subject with many unexplored areas. In recent years, more and more researchers have focused on the molecular basis that drives cells to age, but there is still a long way to go. In this PhD thesis, an *in vitro* model of ageing has been presented that can help to understand specific molecular features that are responsible for brain ageing. Of course, this *in vitro* model cannot faithfully reproduce what happens during brain ageing *in vivo*, but according to the results we showed, it is the attempt to reproduce, how do neurons age in a situation where there is no inflammation or neurodegenerative disease, where are only steady state conditions. In addition, this model can also be used to study individual pathways and their functioning during ageing such as autophagy and neuronal apoptosis. Indeed, analysing ageing *in vitro* led us to investigate the cGAS-STING pathway and its role during brain ageing. Since its discovery in 2013, the cGAS-STING pathway has gained increasing interest for its important role in tumours and senescent cells (Xiao and Fitzgerald 2013; Sun et al. 2013). For this reason, we aimed to investigate which role this pathway might play during brain ageing. Finally, because of the establishment of primary cultures of STING$^{-/-}$ neural cells, we were able to realise that STING and thus most probably the entire cGAS-STING pathway, although not particularly expressed on neurons (being predominantly present in immune cells, such as microglia in the CNS), nevertheless has an important role in neurons too. Indeed, the deficiency of STING drives neurons to substantial functional and morphological changes, such as the impairment of autophagy and presynaptic changes. Thus, these data demonstrate that the cGAS-STING pathway has an important function at the neuronal level. This finding opens new putative scenarios for the use of agonists or antagonists of the cGAS-STING pathway to improve therapies for neurodegenerative diseases or to ameliorate brain ageing situations due to the important involvement of this signalling in the correct autophagic functioning and the production of type I IFNs. Of course, our results are still incomplete and further studies need to be done to investigate how to wisely use an activation or inhibition of the cGAS-STING pathway in the brain for therapeutic interventions. In this doctoral thesis, the aim was to demonstrate that the cGAS-STING pathway can be considered not only regarding tumours or viral and bacterial infections, but also for its role in cerebral and more specifically neuronal homeostasis. Furthermore, further studies need to be done on the role of the cGAS-STING pathway in brain ageing. We were able to show

that the functioning of the pathway is impaired during brain ageing *in vitro and in vivo*. The limitations of our data are that we were not able to indicate which factor is unambiguously responsible for the cerebral imbalance of the cGAS-STING pathway during brain ageing. Furthermore, we still have to find out in more detail what induces an impairment of the cGAS-STING pathway in the brain in addition to the reduction of IFNs production, impairment of the autophagic process and the alteration of presynapses.

In general, the experiments described in this thesis delineate more accurately what are the main characteristics of aging neurons. They also open the door to a new role that the cGAS-STING pathway has been shown to play in neuronal aging. These concepts could serve as a starting point for new approaches to healthy brain aging and possible future anti-aging treatments or neurodegenerative pathologies concerning the cGAS-STING pathway.

7 Bibliography

Abdullah, Amar; Zhang, Moses; Frugier, Tony; Bedoui, Sammy; Taylor, Juliet M.; Crack, Peter J. (2018): STING-mediated type-I interferons contribute to the neuroinflammatory process and detrimental effects following traumatic brain injury. In *J Neuroinflammation* 15 (1), p. 323. DOI: 10.1186/s12974-018-1354-7.

Aguado, Julio; Chaggar, Harman K.; Gómez-Inclán, Cecilia; Shaker, Mohammed R.; Leeson, Hannah C.; Mackay-Sim, Alan; Wolvetang, Ernst J. (2021): Inhibition of the cGAS-STING pathway ameliorates the premature senescence hallmarks of Ataxia-Telangiectasia brain organoids. In *Aging Cell* 20 (9), e13468. DOI: 10.1111/acel.13468.

Ahmad, Waqar; Ijaz, Bushra; Shabbiri, Khadija; Ahmed, Fayyaz; Rehman, Sidra (2017): Oxidative toxicity in diabetes and Alzheimer's disease: mechanisms behind ROS/ RNS generation. In *J Biomed Sci* 24 (1), p. 76. DOI: 10.1186/s12929-017-0379-z.

Alessio, Nicola; Aprile, Domenico; Cappabianca, Salvatore; Peluso, Gianfranco; Di Bernardo, Giovanni; Galderisi, Umberto (2021): Different Stages of Quiescence, Senescence, and Cell Stress Identified by Molecular Algorithm Based on the Expression of Ki67, RPS6, and Beta-Galactosidase Activity. In *International Journal of Molecular Sciences* 22 (6), p. 3102. DOI: 10.3390/ijms22063102.

Aranda-Anzaldo, Armando (2012): The post-mitotic state in neurons correlates with a stable nuclear higher-order structure. In *Communicative & Integrative Biology* 5 (2), pp. 134–139. DOI: 10.4161/cib.18761.

Arshadi, Cameron; Günther, Ulrik; Eddison, Mark; Harrington, Kyle I. S.; Ferreira, Tiago A. (2021): SNT: a unifying toolbox for quantification of neuronal anatomy. In *Nature methods* 18 (4), pp. 374–377. DOI: 10.1038/s41592-021-01105-7.

Babizhayev, Mark A.; Yegorov, Yegor E. (2016): Reactive Oxygen Species and the Aging Eye: Specific Role of Metabolically Active Mitochondria in Maintaining Lens Function and in the Initiation of the Oxidation-Induced Maturity Onset Cataract--A Novel Platform of Mitochondria-Targeted Antioxidants With Broad Therapeutic Potential for Redox Regulation and Detoxification of Oxidants in Eye Diseases. In *American journal of therapeutics* 23 (1), e98-117. DOI: 10.1097/MJT.0b013e3181ea31ff.

Balaban, Robert S.; Nemoto, Shino; Finkel, Toren (2005): Mitochondria, oxidants, and aging. In *Cell* 120 (4), pp. 483–495. DOI: 10.1016/j.cell.2005.02.001.

Ballabio, Andrea; Bonifacino, Juan S. (2020): Lysosomes as dynamic regulators of cell and organismal homeostasis. In *Nat Rev Mol Cell Biol* 21 (2), pp. 101–118. DOI: 10.1038/s41580-019-0185-4.

Banker, G.; Goslin, K. (1988): Developments in neuronal cell culture. In *Nature* 336 (6195), pp. 185–186. DOI: 10.1038/336185a0.

Bano, Daniele; Agostini, Massimiliano; Melino, Gerry; Nicotera, Pierluigi (2011): Ageing, neuronal connectivity and brain disorders: an unsolved ripple effect. In *Mol Neurobiol* 43 (2), pp. 124–130. DOI: 10.1007/s12035-011-8164-6.

Barber, Glen N. (2011): Cytoplasmic DNA innate immune pathways. In *Immunological Reviews* 243 (1), pp. 99–108. DOI: 10.1111/j.1600-065X.2011.01051.x.

Bazopoulou, Daphne; Knoefler, Daniela; Zheng, Yongxin; Ulrich, Kathrin; Oleson, Bryndon J.; Xie, Lihan et al. (2019): Developmental ROS individualizes organismal stress resistance and lifespan. In *Nature* 576 (7786), pp. 301–305. DOI: 10.1038/s41586-019-1814-y.

Bengtsson, Tommy; Scott, Kirk (2010): The Ageing Population. In : Population Ageing - A Threat to the Welfare State?: Springer, Berlin, Heidelberg, pp. 7–22. Available online at https://link.springer.com/chapter/10.1007/978-3-642-12612-3_2.

Bjørkøy, Geir; Lamark, Trond; Pankiv, Serhiy; Øvervatn, Aud; Brech, Andreas; Johansen, Terje (2009): Chapter 12 Monitoring Autophagic Degradation of p62/SQSTM1. In *Methods in Enzymology* 452, pp. 181–197. DOI: 10.1016/S0076-6879(08)03612-4.

Bloss, Erik B.; Janssen, William G.; Ohm, Daniel T.; Yuk, Frank J.; Wadsworth, Shannon; Saardi, Karl M. et al. (2011): Evidence for reduced experience-dependent dendritic spine plasticity in the aging prefrontal cortex. In *J. Neurosci.* 31 (21), pp. 7831–7839. DOI: 10.1523/JNEUROSCI.0839-11.2011.

Bokov, Alex; Chaudhuri, Asish; Richardson, Arlan (2004): The role of oxidative damage and stress in aging. In *Mechanisms of Ageing and Development* 125 (10-11), pp. 811–826. DOI: 10.1016/j.mad.2004.07.009.

Bruce Alberts; Alexander Johnson; Julian Lewis; Martin Raff; Keith Roberts; Peter Walter (2002): Transport from the Trans Golgi Network to Lysosomes. In Bruce Alberts, Alexander Johnson, Julian Lewis, Martin Raff, Keith Roberts, Peter Walter (Eds.):

Molecular Biology of the Cell. 4th edition: Garland Science. Available online at https://www.ncbi.nlm.nih.gov/books/NBK26844/.

Cai, Hua; Imler, Jean-Luc (2021): cGAS-STING: insight on the evolution of a primordial antiviral signaling cassette. In *Faculty reviews* 10, p. 54. DOI: 10.12703/r/10-54.

Cao, Qing-Hua; Liu, Fang; Yang, Zu-Li; Fu, Xin-Hui; Yang, Zi-Huan; Liu, Quentin et al. (2016): Prognostic value of autophagy related proteins ULK1, Beclin 1, ATG3, ATG5, ATG7, ATG9, ATG10, ATG12, LC3B and p62/SQSTM1 in gastric cancer. In *American Journal of Translational Research* 8 (9), pp. 3831–3847.

Carrel, Alexis (1911): On the permanent life of tissue outside of the organism.

Cassina, Laura; Chiaravalli, Marco; Boletta, Alessandra (2020): Increased mitochondrial fragmentation in polycystic kidney disease acts as a modifier of disease progression. In *The FASEB Journal* 34 (5), pp. 6493–6507. DOI: 10.1096/fj.201901739RR.

Cerbai, Francesca; Lana, Daniele; Nosi, Daniele; Petkova-Kirova, Polina; Zecchi, Sandra; Brothers, Holly M. et al. (2012): The neuron-astrocyte-microglia triad in normal brain ageing and in a model of neuroinflammation in the rat hippocampus. In *PLOS ONE* 7 (9), e45250. DOI: 10.1371/journal.pone.0045250.

Chen, Qi; Sun, Lijun; Chen, Zhijian J. (2016): Regulation and function of the cGAS-STING pathway of cytosolic DNA sensing. In *Nat Immunol* 17 (10), pp. 1142–1149. DOI: 10.1038/ni.3558.

Choi, Insup; Zhang, Yuanxi; Seegobin, Steven P.; Pruvost, Mathilde; Wang, Qian; Purtell, Kerry et al. (2020): Microglia clear neuron-released α-synuclein via selective autophagy and prevent neurodegeneration. In *Nat Commun* 11 (1), p. 1386. DOI: 10.1038/s41467-020-15119-w.

Clegg, Andrew; Young, John; Iliffe, Steve; Rikkert, Marcel Olde; Rockwood, Kenneth (2013): Frailty in elderly people. In *The Lancet* 381 (9868), pp. 752–762. DOI: 10.1016/S0140-6736(12)62167-9.

Corral-Debrinski, M.; Horton, T.; Lott, M. T.; Shoffner, J. M.; Beal, M. F.; Wallace, D. C. (1992): Mitochondrial DNA deletions in human brain: regional variability and increase with advanced age. In *Nat Genet* 2 (4), pp. 324–329. DOI: 10.1038/ng1292-324.

da Costa, Anaelle; Metais, Thibaud; Mouthon, Franck; Kerkovich, Danielle; Charvériat, Mathieu (2021): Evaluating and modulating TFEB in the control of autophagy: toward new

treatments in CNS disorders. In *Fundamental & clinical pharmacology* 35 (3), pp. 539–551. DOI: 10.1111/fcp.12634.

Darzynkiewicz, Zbigniew; Galkowski, Dariusz; Zhao, Hong (2008): Analysis of apoptosis by cytometry using TUNEL assay. In *Methods* 44 (3), pp. 250–254. DOI: 10.1016/j.ymeth.2007.11.008.

Decout, Alexiane; Katz, Jason D.; Venkatraman, Shankar; Ablasser, Andrea (2021): The cGAS-STING pathway as a therapeutic target in inflammatory diseases. In *Nat Rev Immunol* 21 (9), pp. 548–569. DOI: 10.1038/s41577-021-00524-z.

Decressac, Mickael; Mattsson, Bengt; Weikop, Pia; Lundblad, Martin; Jakobsson, Johan; Björklund, Anders (2013): TFEB-mediated autophagy rescues midbrain dopamine neurons from α-synuclein toxicity. In *Proceedings of the National Academy of Sciences of the United States of America* 110 (19), E1817-26. DOI: 10.1073/pnas.1305623110.

Dehay, Benjamin; Bové, Jordi; Rodríguez-Muela, Natalia; Perier, Celine; Recasens, Ariadna; Boya, Patricia; Vila, Miquel (2010): Pathogenic lysosomal depletion in Parkinson's disease. In *J. Neurosci.* 30 (37), pp. 12535–12544. DOI: 10.1523/JNEUROSCI.1920-10.2010.

Deleyto-Seldas, Nerea; Efeyan, Alejo (2021): The mTOR-Autophagy Axis and the Control of Metabolism. In *Front. Cell Dev. Biol.* 9, p. 655731. DOI: 10.3389/fcell.2021.655731.

Di Micco, Raffaella; Krizhanovsky, Valery; Baker, Darren; Di d'Adda Fagagna, Fabrizio (2021): Cellular senescence in ageing: from mechanisms to therapeutic opportunities. In *Nat Rev Mol Cell Biol* 22 (2), pp. 75–95. DOI: 10.1038/s41580-020-00314-w.

Dias, Vera; Junn, Eunsung; Mouradian, M. Maral (2013): The role of oxidative stress in Parkinson's disease. In *Journal of Parkinson's disease* 3 (4), pp. 461–491. DOI: 10.3233/JPD-130230.

Dickstein, D. L.; Weaver, C. M.; Luebke, J. I.; Hof, P. R. (2013): Dendritic spine changes associated with normal aging. In *Neuroscience* 251, pp. 21–32. DOI: 10.1016/j.neuroscience.2012.09.077.

Dickstein, Dara L.; Kabaso, Doron; Rocher, Anne B.; Luebke, Jennifer I.; Wearne, Susan L.; Hof, Patrick R. (2007): Changes in the structural complexity of the aged brain. In *Aging Cell* 6 (3), pp. 275–284. DOI: 10.1111/j.1474-9726.2007.00289.x.

Dieterich, Daniela C.; Hodas, Jennifer J. L.; Gouzer, Géraldine; Shadrin, Ilya Y.; Ngo, John T.; Triller, Antoine et al. (2010): In situ visualization and dynamics of newly synthesized proteins in rat hippocampal neurons. In *Nat Neurosci* 13 (7), pp. 897–905. DOI: 10.1038/nn.2580.

Dillon, Serena E.; Tsivos, Demitra; Knight, Michael; McCann, Bryony; Pennington, Catherine; Shiel, Anna I. et al. (2017): The impact of ageing reveals distinct roles for human dentate gyrus and CA3 in pattern separation and object recognition memory. In *Sci Rep* 7 (1), p. 14069. DOI: 10.1038/s41598-017-13853-8.

Ding, Rui; Li, Haiyan; Liu, Yaqi; Ou, Weiyang; Zhang, Xifang; Chai, Huihui et al. (2022): Activating cGAS-STING axis contributes to neuroinflammation in CVST mouse model and induces inflammasome activation and microglia pyroptosis. In *J Neuroinflammation* 19 (1), p. 137. DOI: 10.1186/s12974-022-02511-0.

Djajadikerta, Alvin; Keshri, Swati; Pavel, Mariana; Prestil, Ryan; Ryan, Laura; Rubinsztein, David C. (2020): Autophagy Induction as a Therapeutic Strategy for Neurodegenerative Diseases. In *Journal of molecular biology* 432 (8), pp. 2799–2821. DOI: 10.1016/j.jmb.2019.12.035.

Dobbs, Nicole; Burnaevskiy, Nikolay; Chen, Didi; Gonugunta, Vijay K.; Alto, Neal M.; Yan, Nan (2015): STING Activation by Translocation from the ER Is Associated with Infection and Autoinflammatory Disease. In *Cell host & microbe* 18 (2), pp. 157–168. DOI: 10.1016/j.chom.2015.07.001.

Duan, Huiling; Wearne, Susan L.; Rocher, Anne B.; Macedo, Aisha; Morrison, John H.; Hof, Patrick R. (2003): Age-related dendritic and spine changes in corticocortically projecting neurons in macaque monkeys. In *Cereb Cortex* 13 (9), pp. 950–961. DOI: 10.1093/cercor/13.9.950.

Duan, Na; Zhang, Yanpeng; Tan, Shuwen; Sun, Jianyu; Ye, Mao; Gao, Hui et al. (2022): Therapeutic targeting of STING-TBK1-IRF3 signalling ameliorates chronic stress induced depression-like behaviours by modulating neuroinflammation and microglia phagocytosis. In *Neurobiology of Disease* 169, p. 105739. DOI: 10.1016/j.nbd.2022.105739.

Ejlerskov, Patrick; Hultberg, Jeanette Göransdotter; Wang, JunYang; Carlsson, Robert; Ambjørn, Malene; Kuss, Martin et al. (2015): Lack of Neuronal IFN-β-IFNAR Causes Lewy Body- and Parkinson's Disease-like Dementia. In *Cell* 163 (2), pp. 324–339. DOI: 10.1016/j.cell.2015.08.069.

Enciu, Ana-Maria; Gherghiceanu, Mihaela; Popescu, Bogdan O. (2013): Triggers and effectors of oxidative stress at blood-brain barrier level: relevance for brain ageing and neurodegeneration. In *Oxidative Medicine and Cellular Longevity* 2013, p. 297512. DOI: 10.1155/2013/297512.

Engelender, Simone (2008): Ubiquitination of alpha-synuclein and autophagy in Parkinson's disease. In *Autophagy* 4 (3), pp. 372–374. DOI: 10.4161/auto.5604.

Evans, Chantell S.; Holzbaur, Erika L. F. (2019): Autophagy and mitophagy in ALS. In *Neurobiology of Disease* 122, pp. 35–40. DOI: 10.1016/j.nbd.2018.07.005.

Evans, Tracey; Button, Robert; Anichtchik, Oleg; Luo, Shouqing (2019): Visualization and Measurement of Multiple Components of the Autophagy Flux. In *Methods in molecular biology (Clifton, N.J.)* 1854, pp. 1–12. DOI: 10.1007/7651_2018_168.

Ferro, Austin; Sheeler, Carrie; Cvetanovic, Marija (2019): Microglial Self-Recognition STINGs in A-T Neurodegeneration. In *Trends in neurosciences* 42 (11), pp. 753–755. DOI: 10.1016/j.tins.2019.09.005.

Fischer, Tara D.; Wang, Chunxin; Padman, Benjamin S.; Lazarou, Michael; Youle, Richard J. (2020): STING induces LC3B lipidation onto single-membrane vesicles via the V-ATPase and ATG16L1-WD40 domain. In *The Journal of cell biology* 219 (12). DOI: 10.1083/jcb.202009128.

Frenk, Stephen; Houseley, Jonathan (2018): Gene expression hallmarks of cellular ageing. In *Biogerontology* 19 (6), pp. 547–566. DOI: 10.1007/s10522-018-9750-z.

Gavilán, Elena; Pintado, Cristina; Gavilan, Maria P.; Daza, Paula; Sánchez-Aguayo, Inmaculada; Castaño, Angélica; Ruano, Diego (2015): Age-related dysfunctions of the autophagy lysosomal pathway in hippocampal pyramidal neurons under proteasome stress. In *Neurobiology of Aging* 36 (5), pp. 1953–1963. DOI: 10.1016/j.neurobiolaging.2015.02.025.

Gaynes, Robert (2017): The Discovery of Penicillin—New Insights After More Than 75 Years of Clinical Use. In *Emerg. Infect. Dis.* 23 (5), pp. 849–853. DOI: 10.3201/eid2305.161556.

Ge, Liang; Melville, David; Zhang, Min; Schekman, Randy (2013): The ER–Golgi intermediate compartment is a key membrane source for the LC3 lipidation step of autophagosome biogenesis. In *eLife* 2. DOI: 10.7554/eLife.00947.

Geinisman, Y.; deToledo-Morrell, L.; Morrell, F.; Persina, I. S.; Rossi, M. (1992): Age-related loss of axospinous synapses formed by two afferent systems in the rat dentate gyrus as revealed by the unbiased stereological dissector technique. In *Hippocampus* 2 (4), pp. 437–444. DOI: 10.1002/hipo.450020411.

Glick, Danielle; Barth, Sandra; Macleod, Kay F. (2010): Autophagy: cellular and molecular mechanisms. In *The Journal of pathology* 221 (1), pp. 3–12. DOI: 10.1002/path.2697.

Glück, Selene; Ablasser, Andrea (2019): Innate immunosensing of DNA in cellular senescence. In *Current Opinion in Immunology* 56, pp. 31–36. DOI: 10.1016/j.coi.2018.09.013.

Glück, Selene; Guey, Baptiste; Gulen, Muhammet Fatih; Wolter, Katharina; Kang, Tae-Won; Schmacke, Niklas Arndt et al. (2017): Innate immune sensing of cytosolic chromatin fragments through cGAS promotes senescence. In *Nat Cell Biol* 19 (9), pp. 1061–1070. DOI: 10.1038/ncb3586.

Gonugunta, Vijay K.; Sakai, Tomomi; Pokatayev, Vladislav; Yang, Kun; Wu, Jianjun; Dobbs, Nicole; Yan, Nan (2017): Trafficking-Mediated STING Degradation Requires Sorting to Acidified Endolysosomes and Can Be Targeted to Enhance Anti-tumor Response. In *Cell Reports* 21 (11), pp. 3234–3242. DOI: 10.1016/j.celrep.2017.11.061.

Greenwood, Eleanor K.; Brown, David R. (2021): Senescent Microglia: The Key to the Ageing Brain? In *International Journal of Molecular Sciences* 22 (9). DOI: 10.3390/ijms22094402.

Gui, Xiang; Yang, Hui; Li, Tuo; Tan, Xiaojun; Shi, Peiqing; Li, Minghao et al. (2019): Autophagy induction via STING trafficking is a primordial function of the cGAS pathway. In *Nature* 567 (7747), pp. 262–266. DOI: 10.1038/s41586-019-1006-9.

Guo, Fang; Liu, Xinyao; Cai, Huaibin; Le, Weidong (2018): Autophagy in neurodegenerative diseases: pathogenesis and therapy. In *Brain pathology (Zurich, Switzerland)* 28 (1), pp. 3–13. DOI: 10.1111/bpa.12545.

Guo, Yue; Gu, Ruiping; Gan, Dekang; Hu, Fangyuan; Li, Gang; Xu, Gezhi (2020): Mitochondrial DNA drives noncanonical inflammation activation via cGAS-STING signaling pathway in retinal microvascular endothelial cells. In *Cell Commun Signal* 18 (1), p. 172. DOI: 10.1186/s12964-020-00637-3.

Haag, Simone M.; Gulen, Muhammet F.; Reymond, Luc; Gibelin, Antoine; Abrami, Laurence; Decout, Alexiane et al. (2018): Targeting STING with covalent small-molecule inhibitors. In *Nature* 559 (7713), pp. 269–273. DOI: 10.1038/s41586-018-0287-8.

Hall, Chloe M.; Moeendarbary, Emad; Sheridan, Graham K. (2021): Mechanobiology of the brain in ageing and Alzheimer's disease. In *European Journal of Neuroscience* 53 (12), pp. 3851–3878. DOI: 10.1111/ejn.14766.

Hansen, L. A.; Armstrong, D. M.; Terry, R. D. (1987): An immunohistochemical quantification of fibrous astrocytes in the aging human cerebral cortex. In *Neurobiology of Aging* 8 (1), pp. 1–6. DOI: 10.1016/0197-4580(87)90051-0.

Hayflick, L.; Moorhead, P. S. (1961): The serial cultivation of human diploid cell strains. In *Experimental Cell Research* 25 (3), pp. 585–621. DOI: 10.1016/0014-4827(61)90192-6.

Heckmann, Bradlee L.; Teubner, Brett J. W.; Boada-Romero, Emilio; Tummers, Bart; Guy, Clifford; Fitzgerald, Patrick et al. (2020): Noncanonical function of an autophagy protein prevents spontaneous Alzheimer's disease. In *Science advances* 6 (33), eabb9036. DOI: 10.1126/sciadv.abb9036.

Hinkle, Jared T.; Patel, Jaimin; Panicker, Nikhil; Karuppagounder, Senthilkumar S.; Biswas, Devanik; Belingon, Bonn et al. (2022): STING mediates neurodegeneration and neuroinflammation in nigrostriatal α-synucleinopathy. In *Proceedings of the National Academy of Sciences of the United States of America* 119 (15), e2118819119. DOI: 10.1073/pnas.2118819119.

Hipp, Mark S.; Kasturi, Prasad; Hartl, F. Ulrich (2019): The proteostasis network and its decline in ageing. In *Nat Rev Mol Cell Biol* 20 (7), pp. 421–435. DOI: 10.1038/s41580-019-0101-y.

Holt, I. J.; Harding, A. E.; Morgan-Hughes, J. A. (1988): Deletions of muscle mitochondrial DNA in patients with mitochondrial myopathies. In *Nature* 331 (6158), pp. 717–719. DOI: 10.1038/331717a0.

Hong, Yang; Liu, Yunjiang; Zhang, Geng; Wu, Honghai; Hou, Yanning (2018): Progesterone suppresses Aβ42-induced neuroinflammation by enhancing autophagy in astrocytes. In *International immunopharmacology* 54, pp. 336–343. DOI: 10.1016/j.intimp.2017.11.044.

Hosseini, Shirin; Michaelsen-Preusse, Kristin; Grigoryan, Gayane; Chhatbar, Chintan; Kalinke, Ulrich; Korte, Martin (2020): Type I Interferon Receptor Signaling in Astrocytes Regulates Hippocampal Synaptic Plasticity and Cognitive Function of the Healthy CNS. In *Cell Reports* 31 (7), p. 107666. DOI: 10.1016/j.celrep.2020.107666.

Hou, Xu; Watzlawik, Jens O.; Fiesel, Fabienne C.; Springer, Wolfdieter (2020): Autophagy in Parkinson's Disease. In *Journal of molecular biology* 432 (8), pp. 2651–2672. DOI: 10.1016/j.jmb.2020.01.037.

Hou, Yujun; Wei, Yong; Lautrup, Sofie; Yang, Beimeng; Wang, Yue; Cordonnier, Stephanie et al. (2021): NAD+ supplementation reduces neuroinflammation and cell senescence in a transgenic mouse model of Alzheimer's disease via cGAS-STING. In *Proceedings of the National Academy of Sciences of the United States of America* 118 (37). DOI: 10.1073/pnas.2011226118.

Houlden, Henry; Singleton, Andrew B. (2012): The genetics and neuropathology of Parkinson's disease. In *Acta Neuropathol* 124 (3), pp. 325–338. DOI: 10.1007/s00401-012-1013-5.

Ingvar, M. C.; Maeder, P.; Sokoloff, L.; Smith, C. B. (1985): Effects of ageing on local rates of cerebral protein synthesis in Sprague-Dawley rats. In *Brain : a journal of neurology* 108 (Pt 1), pp. 155–170. DOI: 10.1093/brain/108.1.155.

Jäkel, Sarah; Dimou, Leda (2017): Glial Cells and Their Function in the Adult Brain: A Journey through the History of Their Ablation. In *Front. Cell. Neurosci.* 11, p. 24. DOI: 10.3389/fncel.2017.00024.

Janikiewicz, Justyna; Szymański, Jędrzej; Malinska, Dominika; Patalas-Krawczyk, Paulina; Michalska, Bernadeta; Duszyński, Jerzy et al. (2018): Mitochondria-associated membranes in aging and senescence: structure, function, and dynamics. In *Cell Death Dis* 9 (3), p. 332. DOI: 10.1038/s41419-017-0105-5.

Jauhari, Abhishek; Baranov, Sergei V.; Suofu, Yalikun; Kim, Jinho; Singh, Tanisha; Yablonska, Svitlana et al. (2020): Melatonin inhibits cytosolic mitochondrial DNA-induced neuroinflammatory signaling in accelerated aging and neurodegeneration. In *J Clin Invest* 130 (6), pp. 3124–3136. DOI: 10.1172/JCI135026.

Jin, Meihua; Shiwaku, Hiroki; Tanaka, Hikari; Obita, Takayuki; Ohuchi, Sakurako; Yoshioka, Yuki et al. (2021): Tau activates microglia via the PQBP1-cGAS-STING

pathway to promote brain inflammation. In *Nat Commun* 12 (1), p. 6565. DOI: 10.1038/s41467-021-26851-2.

Jobson, Dan D.; Hase, Yoshiki; Clarkson, Andrew N.; Kalaria, Rajesh N. (2021): The role of the medial prefrontal cortex in cognition, ageing and dementia. In *Brain Commun* 3 (3), fcab125. DOI: 10.1093/braincomms/fcab125.

Juhász, Gábor; Erdi, Balázs; Sass, Miklós; Neufeld, Thomas P. (2007): Atg7-dependent autophagy promotes neuronal health, stress tolerance, and longevity but is dispensable for metamorphosis in Drosophila. In *Genes & development* 21 (23), pp. 3061–3066. DOI: 10.1101/gad.1600707.

Jung, Chang Hwa; Ro, Seung-Hyun; Cao, Jing; Otto, Neil Michael; Kim, Do-Hyung (2010): mTOR regulation of autophagy. In *FEBS letters* 584 (7), pp. 1287–1295. DOI: 10.1016/j.febslet.2010.01.017.

Kaech, Stefanie; Banker, Gary (2006): Culturing hippocampal neurons. In *Nat Protoc* 1 (5), pp. 2406–2415. DOI: 10.1038/nprot.2006.356.

Kemp, Michael G.; Lindsey-Boltz, Laura A.; Sancar, Aziz (2015): UV Light Potentiates STING (Stimulator of Interferon Genes)-dependent Innate Immune Signaling through Deregulation of ULK1 (Unc51-like Kinase 1). In *The Journal of biological chemistry* 290 (19), pp. 12184–12194. DOI: 10.1074/jbc.M115.649301.

Khacho, Mireille; Harris, Richard; Slack, Ruth S. (2019): Mitochondria as central regulators of neural stem cell fate and cognitive function. In *Nat Rev Neurosci* 20 (1), pp. 34–48. DOI: 10.1038/s41583-018-0091-3.

Klionsky, Daniel J.; Eskelinen, Eeva-Liisa; Deretic, Vojo (2014): Autophagosomes, phagosomes, autolysosomes, phagolysosomes, autophagolysosomes… wait, I'm confused. In *Autophagy* 10 (4), pp. 549–551. DOI: 10.4161/auto.28448.

Konno, Hiroyasu; Konno, Keiko; Barber, Glen N. (2013): Cyclic dinucleotides trigger ULK1 (ATG1) phosphorylation of STING to prevent sustained innate immune signaling. In *Cell* 155 (3), pp. 688–698. DOI: 10.1016/j.cell.2013.09.049.

Korolchuk, Viktor I.; Menzies, Fiona M.; Rubinsztein, David C. (2010): Mechanisms of cross-talk between the ubiquitin-proteasome and autophagy-lysosome systems. In *FEBS letters* 584 (7), pp. 1393–1398. DOI: 10.1016/j.febslet.2009.12.047.

Krivega, Maria; Stiefel, Clara M.; Karbassi, Sahar; Andersen, Line L.; Chunduri, Narendra K.; Donnelly, Neysan et al. (2021): Genotoxic stress in constitutive trisomies induces autophagy and the innate immune response via the cGAS-STING pathway. In *Commun Biol* 4 (1), p. 831. DOI: 10.1038/s42003-021-02278-9.

Kuma, Akiko; Matsui, Makoto; Mizushima, Noboru (2007): LC3, an autophagosome marker, can be incorporated into protein aggregates independent of autophagy: caution in the interpretation of LC3 localization. In *Autophagy* 3 (4), pp. 323–328. DOI: 10.4161/auto.4012.

Kumar, Alok; Kalita, J.; Sinha, Rohit A.; Singh, Gajendra; B, Anjum; Shukla, Mukti et al. (2020): Impaired Autophagy Flux is Associated with Proinflammatory Microglia Activation Following Japanese Encephalitis Virus Infection. In *Neurochem Res* 45 (9), pp. 2184–2195. DOI: 10.1007/s11064-020-03080-5.

LAEMMLI, U. K. (1970): Cleavage of structural proteins during the assembly of the head of bacteriophage T4. In *Nature* 227 (5259), pp. 680–685. DOI: 10.1038/227680a0.

Larkin, Bridget; Ilyukha, Vladimir; Sorokin, Maxim; Buzdin, Anton; Vannier, Edouard; Poltorak, Alexander (2017): Cutting Edge: Activation of STING in T Cells Induces Type I IFN Responses and Cell Death. In *Journal of immunology (Baltimore, Md. : 1950)* 199 (2), pp. 397–402. DOI: 10.4049/jimmunol.1601999.

Le Ber, Isabelle; Septenville, Anne de; Millecamps, Stéphanie; Camuzat, Agnès; Caroppo, Paola; Couratier, Philippe et al. (2015): TBK1 mutation frequencies in French frontotemporal dementia and amyotrophic lateral sclerosis cohorts. In *Neurobiology of Aging* 36 (11), 3116.e5-3116.e8. DOI: 10.1016/j.neurobiolaging.2015.08.009.

Lee, Bo Yun; Han, Jung A.; Im, Jun Sub; Morrone, Amelia; Johung, Kimberly; Goodwin, Edward C. et al. (2006): Senescence-associated beta-galactosidase is lysosomal beta-galactosidase. In *Aging Cell* 5 (2), pp. 187–195. DOI: 10.1111/j.1474-9726.2006.00199.x.

Lee, C. K.; Weindruch, R.; Prolla, T. A. (2000): Gene-expression profile of the ageing brain in mice. In *Nat Genet* 25 (3), pp. 294–297. DOI: 10.1038/77046.

Lee, Ju-Hyun; Rao, Mala V.; Yang, Dun-Sheng; Stavrides, Philip; Im, Eunju; Pensalfini, Anna et al. (2019): Transgenic expression of a ratiometric autophagy probe specifically in neurons enables the interrogation of brain autophagy in vivo. In *Autophagy* 15 (3), pp. 543–557. DOI: 10.1080/15548627.2018.1528812.

Lesuisse, Christian; Martin, Lee J. (2002): Long-term culture of mouse cortical neurons as a model for neuronal development, aging, and death. In *Journal of Neurobiology* 51 (1), pp. 9–23. DOI: 10.1002/neu.10037.

Li, Tuo; Chen, Zhijian J. (2018): The cGAS-cGAMP-STING pathway connects DNA damage to inflammation, senescence, and cancer. In *J Exp Med* 215 (5), pp. 1287–1299. DOI: 10.1084/jem.20180139.

Liang, Qiming; Seo, Gil Ju; Choi, Youn Jung; Kwak, Mi-Jeong; Ge, Jianning; Rodgers, Mary A. et al. (2014): Crosstalk between the cGAS DNA sensor and Beclin-1 autophagy protein shapes innate antimicrobial immune responses. In *Cell host & microbe* 15 (2), pp. 228–238. DOI: 10.1016/j.chom.2014.01.009.

Liguori, Ilaria; Russo, Gennaro; Curcio, Francesco; Bulli, Giulia; Aran, Luisa; Della-Morte, David et al. (2018): Oxidative stress, aging, and diseases. In *Clinical Interventions in Aging* 13, pp. 757–772. DOI: 10.2147/CIA.S158513.

Lipinski, Marta M.; Zheng, Bin; Lu, Tao; Yan, Zhenyu; Py, Bénédicte F.; Ng, Aylwin et al. (2010): Genome-wide analysis reveals mechanisms modulating autophagy in normal brain aging and in Alzheimer's disease. In *Proceedings of the National Academy of Sciences of the United States of America* 107 (32), pp. 14164–14169. DOI: 10.1073/pnas.1009485107.

Lippai, Mónika; Szatmári, Zsuzsanna (2017): Autophagy-from molecular mechanisms to clinical relevance. In *Cell Biol Toxicol* 33 (2), pp. 145–168. DOI: 10.1007/s10565-016-9374-5.

Liu, Dong; Wu, Hao; Wang, Chenguang; Li, Yanjun; Tian, Huabin; Siraj, Sami et al. (2019): STING directly activates autophagy to tune the innate immune response. In *Cell Death Differ* 26 (9), pp. 1735–1749. DOI: 10.1038/s41418-018-0251-z.

Liu, Nanxin; Pang, Xiaoxiao; Zhang, Hua; Ji, Ping (2021a): The cGAS-STING Pathway in Bacterial Infection and Bacterial Immunity. In *Front. Immunol.* 12, p. 814709. DOI: 10.3389/fimmu.2021.814709.

Liu, Nanxin; Pang, Xiaoxiao; Zhang, Hua; Ji, Ping (2021b): The cGAS-STING Pathway in Bacterial Infection and Bacterial Immunity. In *Front. Immunol.* 12, p. 814709. DOI: 10.3389/fimmu.2021.814709.

Liu, Yuan; Gordesky-Gold, Beth; Leney-Greene, Michael; Weinbren, Nathan L.; Tudor, Matthew; Cherry, Sara (2018): Inflammation-Induced, STING-Dependent Autophagy

Restricts Zika Virus Infection in the Drosophila Brain. In *Cell host & microbe* 24 (1), 57-68.e3. DOI: 10.1016/j.chom.2018.05.022.

Livak, K. J.; Schmittgen, T. D. (2001): Analysis of relative gene expression data using real-time quantitative PCR and the 2(-Delta Delta C(T)) Method. In *Methods* 25 (4), pp. 402–408. DOI: 10.1006/meth.2001.1262.

Loo, Deryk T. (2002): TUNEL assay. An overview of techniques. In *Methods in molecular biology (Clifton, N.J.)* 203, pp. 21–30. DOI: 10.1385/1-59259-179-5:21.

Loo, Tze Mun; Miyata, Kenichi; Tanaka, Yoko; Takahashi, Akiko (2020): Cellular senescence and senescence-associated secretory phenotype via the cGAS-STING signaling pathway in cancer. In *Cancer Science* 111 (2), pp. 304–311. DOI: 10.1111/cas.14266.

Loving, Bailey A.; Tang, Maoping; Neal, Mikaela C.; Gorkhali, Sachi; Murphy, Robert; Eckel, Robert H.; Bruce, Kimberley D. (2021): Lipoprotein Lipase Regulates Microglial Lipid Droplet Accumulation. In *Cells* 10 (2). DOI: 10.3390/cells10020198.

Lynch-Day, Melinda A.; Mao, Kai; Wang, Ke; Zhao, Mantong; Klionsky, Daniel J. (2012): The role of autophagy in Parkinson's disease. In *Cold Spring Harbor Perspectives in Medicine* 2 (4), a009357. DOI: 10.1101/cshperspect.a009357.

Mansour, Hussein; Chamberlain, Coral G.; Weible, Michael W.; Hughes, Suzanne; Chu, Yi; Chan-Ling, Tailoi (2008): Aging-related changes in astrocytes in the rat retina: imbalance between cell proliferation and cell death reduces astrocyte availability. In *Aging Cell* 7 (4), pp. 526–540. DOI: 10.1111/j.1474-9726.2008.00402.x.

Marí, Montserrat; Morales, Albert; Colell, Anna; García-Ruiz, Carmen; Fernández-Checa, José C. (2009): Mitochondrial glutathione, a key survival antioxidant. In *Antioxidants & redox signaling* 11 (11), pp. 2685–2700. DOI: 10.1089/ARS.2009.2695.

Mathur, Vidhu; Burai, Ritwik; Vest, Ryan T.; Bonanno, Liana N.; Lehallier, Benoit; Zardeneta, Macy E. et al. (2017): Activation of the STING-Dependent Type I Interferon Response Reduces Microglial Reactivity and Neuroinflammation. In *Neuron* 96 (6), 1290-1302.e6. DOI: 10.1016/j.neuron.2017.11.032.

Matias, Isadora; Morgado, Juliana; Gomes, Flávia Carvalho Alcantara (2019): Astrocyte Heterogeneity: Impact to Brain Aging and Disease. In *Front. Aging Neurosci.* 11, p. 59. DOI: 10.3389/fnagi.2019.00059.

Mattson, Mark P.; Magnus, Tim (2006): Ageing and neuronal vulnerability. In *Nat Rev Neurosci* 7 (4), pp. 278–294. DOI: 10.1038/nrn1886.

Mauthe, Mario; Orhon, Idil; Rocchi, Cecilia; Zhou, Xingdong; Luhr, Morten; Hijlkema, Kerst-Jan et al. (2018): Chloroquine inhibits autophagic flux by decreasing autophagosome-lysosome fusion. In *Autophagy* 14 (8), pp. 1435–1455. DOI: 10.1080/15548627.2018.1474314.

Mazumder, Suparna; Plesca, Dragos; Almasan, Alexandru (2008): Caspase-3 Activation is a Critical Determinant of Genotoxic Stress-Induced Apoptosis. In : Apoptosis and Cancer: Humana Press, pp. 13–21.

Mera-Rodríguez, José Antonio de; Álvarez-Hernán, Guadalupe; Gañán, Yolanda; Martín-Partido, Gervasio; Rodríguez-León, Joaquín; Francisco-Morcillo, Javier (2021): Is Senescence-Associated β-Galactosidase a Reliable in vivo Marker of Cellular Senescence During Embryonic Development? In *Front. Cell Dev. Biol.* 9, p. 623175. DOI: 10.3389/fcell.2021.623175.

Mercer, Carol A.; Kaliappan, Alagammai; Dennis, Patrick B. (2009): A novel, human Atg13 binding protein, Atg101, interacts with ULK1 and is essential for macroautophagy. In *Autophagy* 5 (5), pp. 649–662. DOI: 10.4161/auto.5.5.8249.

Miwa, S.; Brand, M. D. (2003): Mitochondrial matrix reactive oxygen species production is very sensitive to mild uncoupling. In *Biochem Soc Trans* 31 (Pt 6), pp. 1300–1301. DOI: 10.1042/bst0311300.

Mizushima, Noboru (2007): Autophagy: process and function. In *Genes & development* 21 (22), pp. 2861–2873. DOI: 10.1101/gad.1599207.

Moreno-Blas, Daniel; Gorostieta-Salas, Elisa; Pommer-Alba, Alexander; Muciño-Hernández, Gabriel; Gerónimo-Olvera, Cristian; Maciel-Barón, Luis Angel et al. (2019): Cortical neurons develop a senescence-like phenotype promoted by dysfunctional autophagy. In *Aging* 11 (16), pp. 6175–6198. DOI: 10.18632/aging.102181.

Motwani, Mona; Pesiridis, Scott; Fitzgerald, Katherine A. (2019): DNA sensing by the cGAS-STING pathway in health and disease. In *Nat Rev Genet* 20 (11), pp. 657–674. DOI: 10.1038/s41576-019-0151-1.

Mputhia, Zoe; Hone, Eugene; Tripathi, Timir; Sargeant, Tim; Martins, Ralph; Bharadwaj, Prashant (2019): Autophagy Modulation as a Treatment of Amyloid Diseases. In *Molecules (Basel, Switzerland)* 24 (18). DOI: 10.3390/molecules24183372.

Mukai, Kojiro; Konno, Hiroyasu; Akiba, Tatsuya; Uemura, Takefumi; Waguri, Satoshi; Kobayashi, Toshihide et al. (2016): Activation of STING requires palmitoylation at the Golgi. In *Nat Commun* 7 (1), p. 11932. DOI: 10.1038/ncomms11932.

Mukhopadhyay, Subhadip; Das, Durgesh Nandini; Panda, Prashanta Kumar; Sinha, Niharika; Naik, Prajna Paramita; Bissoyi, Akalabya et al. (2015): Autophagy protein Ulk1 promotes mitochondrial apoptosis through reactive oxygen species. In *Free radical biology & medicine* 89, pp. 311–321. DOI: 10.1016/j.freeradbiomed.2015.07.159.

Muller, Florian L.; Lustgarten, Michael S.; Jang, Youngmok; Richardson, Arlan; van Remmen, Holly (2007): Trends in oxidative aging theories. In *Free radical biology & medicine* 43 (4), pp. 477–503. DOI: 10.1016/j.freeradbiomed.2007.03.034.

Müller-Thomsen, Lennart; Borgmann, Diba; Morcinek, Kerstin; Schröder, Sophia; Dengler, Brigitte; Moser, Natasha et al. (2020): Consequences of hyperphosphorylated tau on the morphology and excitability of hippocampal neurons in aged tau transgenic mice. In *Neurobiology of Aging* 93, pp. 109–123. DOI: 10.1016/j.neurobiolaging.2020.03.007.

Nakamura, N.; Rabouille, C.; Watson, R.; Nilsson, T.; Hui, N.; Slusarewicz, P. et al. (1995): Characterization of a cis-Golgi matrix protein, GM130. In *J Cell Biol* 131 (6 Pt 2), pp. 1715–1726. DOI: 10.1083/jcb.131.6.1715.

Naoi, Makoto; Wu, Yuqiu; Shamoto-Nagai, Masayo; Maruyama, Wakako (2019): Mitochondria in Neuroprotection by Phytochemicals: Bioactive Polyphenols Modulate Mitochondrial Apoptosis System, Function and Structure. In *International Journal of Molecular Sciences* 20 (10). DOI: 10.3390/ijms20102451.

Nazmi, Arshed; Field, Robert H.; Griffin, Eadaoin W.; Haugh, Orla; Hennessy, Edel; Cox, Donal et al. (2019): Chronic neurodegeneration induces type I interferon synthesis via STING, shaping microglial phenotype and accelerating disease progression. In *Glia* 67 (7), pp. 1254–1276. DOI: 10.1002/glia.23592.

Ng, Kok Yew; Gui, Meei Mei (2020): COVID-19: Development of a robust mathematical model and simulation package with consideration for ageing population and time delay for control action and resusceptibility. In *Physica D: Nonlinear Phenomena* 411, p. 132599. DOI: 10.1016/j.physd.2020.132599.

Nichols, Emma; Steinmetz, Jaimie D.; Vollset, Stein Emil; Fukutaki, Kai; Chalek, Julian;

Abd-Allah, Foad et al. (2022): Estimation of the global prevalence of dementia in 2019 and forecasted prevalence in 2050: an analysis for the Global Burden of Disease Study 2019. In *The Lancet Public Health* 7 (2), e105-e125. DOI: 10.1016/S2468-2667(21)00249-8.

Ning, Xiaohan; Wang, Yutao; Jing, Miao; Sha, Mengyin; Lv, Mengze; Gao, Pengfei et al. (2019): Apoptotic Caspases Suppress Type I Interferon Production via the Cleavage of cGAS, MAVS, and IRF3. In *Molecular Cell* 74 (1), 19-31.e7. DOI: 10.1016/j.molcel.2019.02.013.

Oakes, James A.; Davies, Maria C.; Collins, Mark O. (2017): TBK1: a new player in ALS linking autophagy and neuroinflammation. In *Mol Brain* 10 (1), p. 5. DOI: 10.1186/s13041-017-0287-x.

O'Connell, Douglas; Liang, Chengyu (2016): Autophagy interaction with herpes simplex virus type-1 infection. In *Autophagy* 12 (3), pp. 451–459. DOI: 10.1080/15548627.2016.1139262.

Ogawa, Emari; Mukai, Kojiro; Saito, Kota; Arai, Hiroyuki; Taguchi, Tomohiko (2018): The binding of TBK1 to STING requires exocytic membrane traffic from the ER. In *Biochemical and Biophysical Research Communications* 503 (1), pp. 138–145. DOI: 10.1016/j.bbrc.2018.05.199.

Okouchi, Masahiro; Ekshyyan, Oleksandr; Maracine, Magdalena; Aw, Tak Yee (2007): Neuronal apoptosis in neurodegeneration. In *Antioxidants & redox signaling* 9 (8), pp. 1059–1096. DOI: 10.1089/ars.2007.1511.

Overhoff, Melina; Bruyckere, Elodie de; Kononenko, Natalia L. (2021): Mechanisms of neuronal survival safeguarded by endocytosis and autophagy. In *Journal of neurochemistry* 157 (2), pp. 263–296. DOI: 10.1111/jnc.15194.

Palmer, Alexandra L.; Ousman, Shalina S. (2018): Astrocytes and Aging. In *Front. Aging Neurosci.* 10, p. 337. DOI: 10.3389/fnagi.2018.00337.

Passos, João F.; Zglinicki, Thomas von (2005): Mitochondria, telomeres and cell senescence. In *Experimental gerontology* 40 (6), pp. 466–472. DOI: 10.1016/j.exger.2005.04.006.

Pickford, Fiona; Masliah, Eliezer; Britschgi, Markus; Lucin, Kurt; Narasimhan, Ramya; Jaeger, Philipp A. et al. (2008): The autophagy-related protein beclin 1 shows reduced

expression in early Alzheimer disease and regulates amyloid beta accumulation in mice. In *The Journal of clinical investigation* 118 (6), pp. 2190–2199. DOI: 10.1172/JCI33585.

Pike, Christian J.; Walencewicz, Andrea J.; Glabe, Charles G.; Cotman, Carl W. (1991): In vitro aging of ß-amyloid protein causes peptide aggregation and neurotoxicity. In *Brain Research* 563 (1-2), pp. 311–314. DOI: 10.1016/0006-8993(91)91553-D.

Pikó, Lajos; Hougham, Andrina J.; Bulpitt, Ken J. (1988): Studies of sequence heterogeneity of mitochondrial DNA from rat and mouse tissues: Evidence for an increased frequency of deletions/additions with aging. In *Mechanisms of Ageing and Development* 43 (3), pp. 279–293. DOI: 10.1016/0047-6374(88)90037-1.

Pilli, Manohar; Arko-Mensah, John; Ponpuak, Marisa; Roberts, Esteban; Master, Sharon; Mandell, Michael A. et al. (2012): TBK-1 promotes autophagy-mediated antimicrobial defense by controlling autophagosome maturation. In *Immunity* 37 (2), pp. 223–234. DOI: 10.1016/j.immuni.2012.04.015.

Population Ageing - A Threat to the Welfare State? (2010): Springer, Berlin, Heidelberg.

Prabakaran, Thaneas; Bodda, Chiranjeevi; Krapp, Christian; Zhang, Bao-Cun; Christensen, Maria H.; Sun, Chenglong et al. (2018): Attenuation of cGAS-STING signaling is mediated by a p62/SQSTM1-dependent autophagy pathway activated by TBK1. In *The EMBO journal* 37 (8). DOI: 10.15252/embj.201797858.

Prieto-Gomez, B.; Reyes-Vazquez, C.; Dafny, N. (1983): Differential effects of interferon on ventromedial hypothalamus and dorsal hippocampus. In *Journal of neuroscience research* 10 (3), pp. 273–278. DOI: 10.1002/jnr.490100305.

Putt, Karson S.; Chen, Grace W.; Pearson, Jennifer M.; Sandhorst, Joseph S.; Hoagland, Martin S.; Kwon, Jung-Taek et al. (2006): Small-molecule activation of procaspase-3 to caspase-3 as a personalized anticancer strategy. In *Nat Chem Biol* 2 (10), pp. 543–550. DOI: 10.1038/nchembio814.

Pyo, Jong-Ok; Yoo, Seung-Min; Ahn, Hye-Hyun; Nah, Jihoon; Hong, Se-Hoon; Kam, Tae-In et al. (2013): Overexpression of Atg5 in mice activates autophagy and extends lifespan. In *Nat Commun* 4 (1), p. 2300. DOI: 10.1038/ncomms3300.

Radkiewicz, Cecilia; Järkvik Krönmark, Jessica; Adami, Hans-Olov; Edgren, Gustaf (2022): Declining Cancer Incidence in the Elderly: Decreasing Diagnostic Intensity or Biology? In *Cancer epidemiology, biomarkers & prevention : a publication of the American*

Association for Cancer Research, cosponsored by the American Society of Preventive Oncology 31 (1), pp. 280–286. DOI: 10.1158/1055-9965.EPI-21-0797.

Rahman, Md Ataur; Rahman, Md Saidur; Rahman, M. D. Hasanur; Rasheduzzaman, Mohammad; Mamun-Or-Rashid, Anm; Uddin, Md Jamal et al. (2020): Modulatory Effects of Autophagy on APP Processing as a Potential Treatment Target for Alzheimer's Disease. In *Biomedicines* 9 (1). DOI: 10.3390/biomedicines9010005.

Randow, Felix; MacMicking, John D.; James, Leo C. (2013): Cellular self-defense: how cell-autonomous immunity protects against pathogens. In *Science (New York, N.Y.)* 340 (6133), pp. 701–706. DOI: 10.1126/science.1233028.

Reinert, Line S.; Lopušná, Katarína; Winther, Henriette; Sun, Chenglong; Thomsen, Martin K.; Nandakumar, Ramya et al. (2016): Sensing of HSV-1 by the cGAS-STING pathway in microglia orchestrates antiviral defence in the CNS. In *Nat Commun* 7 (1), p. 13348. DOI: 10.1038/ncomms13348.

Reinert, Line S.; Rashidi, Ahmad S.; Tran, Diana N.; Katzilieris-Petras, Georgios; Hvidt, Astrid K.; Gohr, Mette et al. (2021): Brain immune cells undergo cGAS/STING-dependent apoptosis during herpes simplex virus type 1 infection to limit type I IFN production. In *J Clin Invest* 131 (1). DOI: 10.1172/JCI136824.

Ribas, Vicent; García-Ruiz, Carmen; Fernández-Checa, José C. (2014): Glutathione and mitochondria. In *Front. Pharmacol.* 5, p. 151. DOI: 10.3389/fphar.2014.00151.

Richter, Torsten; Proctor, Carole (2007): The role of intracellular peroxide levels on the development and maintenance of telomere-dependent senescence. In *Experimental gerontology* 42 (11), pp. 1043–1052. DOI: 10.1016/j.exger.2007.08.004.

Rossiello, Francesca; Jurk, Diana; Passos, João F.; Di d'Adda Fagagna, Fabrizio (2022): Telomere dysfunction in ageing and age-related diseases. In *Nat Cell Biol* 24 (2), pp. 135–147. DOI: 10.1038/s41556-022-00842-x.

Rusmini, Paola; Cortese, Katia; Crippa, Valeria; Cristofani, Riccardo; Cicardi, Maria Elena; Ferrari, Veronica et al. (2019): Trehalose induces autophagy via lysosomal-mediated TFEB activation in models of motoneuron degeneration. In *Autophagy* 15 (4), pp. 631–651. DOI: 10.1080/15548627.2018.1535292.

Russell, Ryan C.; Tian, Ye; Yuan, Haixin; Park, Hyun Woo; Chang, Yu-Yun; Kim, Joungmok et al. (2013): ULK1 induces autophagy by phosphorylating Beclin-1 and activating VPS34 lipid kinase. In *Nat Cell Biol* 15 (7), pp. 741–750. DOI: 10.1038/ncb2757.

Sabatini, David D.; Adesnik, Milton (2013): Christian de Duve: Explorer of the cell who discovered new organelles by using a centrifuge. In *Proceedings of the National Academy of Sciences of the United States of America* 110 (33), pp. 13234–13235. DOI: 10.1073/pnas.1312084110.

Sandri, Marco (2013): Protein breakdown in muscle wasting: role of autophagy-lysosome and ubiquitin-proteasome. In *The International Journal of Biochemistry & Cell Biology* 45 (10), pp. 2121–2129. DOI: 10.1016/j.biocel.2013.04.023.

Sasaki, Toru; Unno, Keiko; Tahara, Shoichi; Kaneko, Takao (2010): Age-related increase of reactive oxygen generation in the brains of mammals and birds: is reactive oxygen a signaling molecule to determine the aging process and life span? In *Geriatrics & gerontology international* 10 Suppl 1, S10-24. DOI: 10.1111/j.1447-0594.2010.00601.x.

Sato, Shigeto; Uchihara, Toshiki; Fukuda, Takahiro; Noda, Sachiko; Kondo, Hiromi; Saiki, Shinji et al. (2018): Loss of autophagy in dopaminergic neurons causes Lewy pathology and motor dysfunction in aged mice. In *Sci Rep* 8 (1), p. 2813. DOI: 10.1038/s41598-018-21325-w.

Satoo, Kenji; Noda, Nobuo N.; Kumeta, Hiroyuki; Fujioka, Yuko; Mizushima, Noboru; Ohsumi, Yoshinori; Inagaki, Fuyuhiko (2009): The structure of Atg4B-LC3 complex reveals the mechanism of LC3 processing and delipidation during autophagy. In *The EMBO journal* 28 (9), pp. 1341–1350. DOI: 10.1038/emboj.2009.80.

Savelieff, Masha G.; Nam, Geewoo; Kang, Juhye; Lee, Hyuck Jin; Lee, Misun; Lim, Mi Hee (2019): Development of Multifunctional Molecules as Potential Therapeutic Candidates for Alzheimer's Disease, Parkinson's Disease, and Amyotrophic Lateral Sclerosis in the Last Decade. In *Chemical Reviews* 119 (2), pp. 1221–1322. DOI: 10.1021/acs.chemrev.8b00138.

Schaaf, Marco B.; Houbaert, Diede; Meçe, Odeta; Agostinis, Patrizia (2019): Autophagy in endothelial cells and tumor angiogenesis. In *Cell Death Differ* 26 (4), pp. 665–679. DOI: 10.1038/s41418-019-0287-8.

Schumacher, Björn; Pothof, Joris; Vijg, Jan; Hoeijmakers, Jan H. J. (2021): The central role of DNA damage in the ageing process. In *Nature* 592 (7856), pp. 695–703. DOI: 10.1038/s41586-021-03307-7.

Seltzer, Benjamin; Vasterling, Jennifer J.; Mathias, Charles W.; Brennan, Angela (2001): Clinical and Neuropsychological Correlates of Impaired Awareness of Deficits in Alzheimer Disease and Parkinson Disease: A Comparative Study. In *Cognitive and Behavioral Neurology* 14 (2), p. 122. DOI: aspx.

Shao, Yufang; Gao, Zhonghua; Feldman, Taya; Jiang, Xuejun (2007): Stimulation of ATG12-ATG5 conjugation by ribonucleic acid. In *Autophagy* 3 (1), pp. 10–16. DOI: 10.4161/auto.3270.

Shay, J. W.; Wright, W. E. (2000): Hayflick, his limit, and cellular ageing. In *Nature reviews. Molecular cell biology* 1 (1), pp. 72–76. DOI: 10.1038/35036093.

Shibata, Mamoru; Lu, Tao; Furuya, Tsuyoshi; Degterev, Alexei; Mizushima, Noboru; Yoshimori, Tamotsu et al. (2006): Regulation of intracellular accumulation of mutant Huntingtin by Beclin 1. In *The Journal of biological chemistry* 281 (20), pp. 14474–14485. DOI: 10.1074/jbc.M600364200.

Shields, Hazel J.; Traa, Annika; van Raamsdonk, Jeremy M. (2021): Beneficial and Detrimental Effects of Reactive Oxygen Species on Lifespan: A Comprehensive Review of Comparative and Experimental Studies. In *Front. Cell Dev. Biol.* 9, p. 628157. DOI: 10.3389/fcell.2021.628157.

Shigenaga, M. K.; Hagen, T. M.; Ames, B. N. (1994): Oxidative damage and mitochondrial decay in aging. In *Proc. Natl. Acad. Sci. U.S.A.* 91 (23), pp. 10771–10778. DOI: 10.1073/pnas.91.23.10771.

Shimizu, Shigeomi; Arakawa, Satoko; Nishida, Yuya (2010): Autophagy takes an alternative pathway. In *Autophagy* 6 (2), pp. 290–291. DOI: 10.4161/auto.6.2.11127.

Simen, Arthur A.; Bordner, Kelly A.; Martin, Mark P.; Moy, Lawrence A.; Barry, Lisa C. (2011): Cognitive dysfunction with aging and the role of inflammation. In *Therapeutic advances in chronic disease* 2 (3), pp. 175–195. DOI: 10.1177/2040622311399145.

Sofroniew, Michael V.; Vinters, Harry V. (2010): Astrocytes: biology and pathology. In *Acta Neuropathol* 119 (1), pp. 7–35. DOI: 10.1007/s00401-009-0619-8.

Song, Xuan; Ma, Fulin; Herrup, Karl (2019): Accumulation of Cytoplasmic DNA Due to ATM Deficiency Activates the Microglial Viral Response System with Neurotoxic Consequences. In *J. Neurosci.* 39 (32), pp. 6378–6394. DOI: 10.1523/JNEUROSCI.0774-19.2019.

Starkov, Anatoly A.; Fiskum, Gary (2003): Regulation of brain mitochondrial H2O2 production by membrane potential and NAD(P)H redox state. In *Journal of neurochemistry* 86 (5), pp. 1101–1107. DOI: 10.1046/j.1471-4159.2003.01908.x.

Stefanatos, Rhoda; Sanz, Alberto (2018): The role of mitochondrial ROS in the aging brain. In *FEBS letters* 592 (5), pp. 743–758. DOI: 10.1002/1873-3468.12902.

Strohm, Laura; Behrends, Christian (2020): Glia-specific autophagy dysfunction in ALS. In *Seminars in cell & developmental biology* 99, pp. 172–182. DOI: 10.1016/j.semcdb.2019.05.024.

Sun, Lijun; Wu, Jiaxi; Du, Fenghe; Chen, Xiang; Chen, Zhijian J. (2013): Cyclic GMP-AMP synthase is a cytosolic DNA sensor that activates the type I interferon pathway. In *Science (New York, N.Y.)* 339 (6121), pp. 786–791. DOI: 10.1126/science.1232458.

Taguchi, Tomohiko; Mukai, Kojiro; Takaya, Eiko; Shindo, Ruri (2021): STING Operation at the ER/Golgi Interface. In *Frontiers in immunology* 12, p. 646304. DOI: 10.3389/fimmu.2021.646304.

Takeshige, K.; Baba, M.; Tsuboi, S.; Noda, T.; Ohsumi, Y. (1992): Autophagy in yeast demonstrated with proteinase-deficient mutants and conditions for its induction. In *J Cell Biol* 119 (2), pp. 301–311. DOI: 10.1083/jcb.119.2.301.

Tanida, Isei; Ueno, Takashi; Kominami, Eiki (2004): LC3 conjugation system in mammalian autophagy. In *The International Journal of Biochemistry & Cell Biology* 36 (12), pp. 2503–2518. DOI: 10.1016/j.biocel.2004.05.009.

Tanida, Isei; Ueno, Takashi; Kominami, Eiki (2008): LC3 and Autophagy. In *Methods in molecular biology (Clifton, N.J.)* 445, pp. 77–88. DOI: 10.1007/978-1-59745-157-4_4.

Tchaikovskaya, Tatyana; Fraifeld, Vadim; Urphanishvili, Tinatin; Andorfer, John H.; Davies, Peter; Listowsky, Irving (2005): Glutathione S-transferase hGSTM3 and ageing-associated neurodegeneration: relationship to Alzheimer's disease. In *Mechanisms of Ageing and Development* 126 (2), pp. 309–315. DOI: 10.1016/j.mad.2004.08.029.

Tinker, Anthea (2002): The social implications of an ageing population. In *Mechanisms of Ageing and Development* 123 (7), pp. 729–735. DOI: 10.1016/S0047-6374(01)00418-3.

Torres Acosta, Manuel A.; Singer, Benjamin D. (2020): Pathogenesis of COVID-19-induced ARDS: implications for an ageing population. In *European Respiratory Journal* 56 (3). DOI: 10.1183/13993003.02049-2020.

Trifunovic, A.; Larsson, N-G (2008): Mitochondrial dysfunction as a cause of ageing. In *Journal of internal medicine* 263 (2), pp. 167–178. DOI: 10.1111/j.1365-2796.2007.01905.x.

Tsai, Sheng-Feng; Ku, Nai-Wen; Wang, Tzu-Feng; Yang, Yan-Hsiang; Shih, Yao-Hsiang; Wu, Shih-Ying et al. (2018): Long-Term Moderate Exercise Rescues Age-Related Decline in Hippocampal Neuronal Complexity and Memory. In *GER* 64 (6), pp. 551–561. DOI: 10.1159/000488589.

Tsukada, Miki; Ohsumi, Yoshinori (1993): Isolation and characterization of autophagy-defective mutants of Saccharomyces cerevisiae. In *FEBS letters* 333 (1-2), pp. 169–174. DOI: 10.1016/0014-5793(93)80398-E.

Turco, Eleonora; Fracchiolla, Dorotea; Martens, Sascha (2020): Recruitment and Activation of the ULK1/Atg1 Kinase Complex in Selective Autophagy. In *Journal of molecular biology* 432 (1), pp. 123–134. DOI: 10.1016/j.jmb.2019.07.027.

Uylings, Harry B. M.; Brabander, J. M. de (2002): Neuronal changes in normal human aging and Alzheimer's disease. In *Brain and Cognition* 49 (3), pp. 268–276. DOI: 10.1006/brcg.2001.1500.

Verkerke, Marloes; Hol, Elly M.; Middeldorp, Jinte (2021): Physiological and Pathological Ageing of Astrocytes in the Human Brain. In *Neurochem Res* 46 (10), pp. 2662–2675. DOI: 10.1007/s11064-021-03256-7.

Vikman, Kristina S.; Owe-Larsson, Björn; Brask, Johan; Kristensson, Krister S.; Hill, Russell H. (2001): Interferon-γ-induced changes in synaptic activity and AMPA receptor clustering in hippocampal cultures. In *Brain Research* 896 (1-2), pp. 18–29. DOI: 10.1016/S0006-8993(00)03238-8.

Vougioukalaki, Maria; Demmers, Joris; Vermeij, Wilbert P.; Baar, Marjolein; Bruens, Serena; Magaraki, Aristea et al. (2022): Different responses to DNA damage determine

ageing differences between organs. In *Aging Cell* 21 (4), e13562. DOI: 10.1111/acel.13562.

Wallings, Rebecca L.; Tansey, Malú G. (2019): LRRK2 regulation of immune-pathways and inflammatory disease. In *Biochem Soc Trans* 47 (6), pp. 1581–1595. DOI: 10.1042/BST20180463.

Waltl, Inken; Kalinke, Ulrich (2022): Beneficial and detrimental functions of microglia during viral encephalitis. In *Trends in neurosciences* 45 (2), pp. 158–170. DOI: 10.1016/j.tins.2021.11.004.

Wang, Shukun; Li, Baoguo; Qiao, Huimin; Lv, Xiaohui; Liang, Qingli; Shi, Zixiao et al. (2014): Autophagy-related gene Atg5 is essential for astrocyte differentiation in the developing mouse cortex. In *EMBO reports* 15 (10), pp. 1053–1061. DOI: 10.15252/embr.201338343.

Wang, Yizhi; Wang, Congchao; Ranefall, Petter; Broussard, Gerard Joey; Wang, Yinxue; Shi, Guilai et al. (2020): SynQuant: an automatic tool to quantify synapses from microscopy images. In *Bioinformatics (Oxford, England)* 36 (5), pp. 1599–1606. DOI: 10.1093/bioinformatics/btz760.

Ward, Diane M.; Cloonan, Suzanne M. (2019): Mitochondrial Iron in Human Health and Disease. In *Annual review of physiology* 81, pp. 453–482. DOI: 10.1146/annurev-physiol-020518-114742.

Weindel, Chi G.; Bell, Samantha L.; Vail, Krystal J.; West, Kelsi O.; Patrick, Kristin L.; Watson, Robert O. (2020): LRRK2 maintains mitochondrial homeostasis and regulates innate immune responses to Mycobacterium tuberculosis. In *eLife* 9. DOI: 10.7554/eLife.51071.

West, A. Phillip; Shadel, Gerald S. (2017): Mitochondrial DNA in innate immune responses and inflammatory pathology. In *Nat Rev Immunol* 17 (6), pp. 363–375. DOI: 10.1038/nri.2017.21.

Winslow, Ashley R.; Chen, Chien-Wen; Corrochano, Silvia; Acevedo-Arozena, Abraham; Gordon, David E.; Peden, Andrew A. et al. (2010): α-Synuclein impairs macroautophagy: implications for Parkinson's disease. In *The Journal of cell biology* 190 (6), pp. 1023–1037. DOI: 10.1083/jcb.201003122.

Winslow, Ashley R.; Rubinsztein, David C. (2011): The Parkinson disease protein α-synuclein inhibits autophagy. In *Autophagy* 7 (4), pp. 429–431. DOI: 10.4161/auto.7.4.14393.

Wong, Yvette C.; Kim, Soojin; Peng, Wesley; Krainc, Dimitri (2019): Regulation and Function of Mitochondria-Lysosome Membrane Contact Sites in Cellular Homeostasis. In *Trends in cell biology* 29 (6), pp. 500–513. DOI: 10.1016/j.tcb.2019.02.004.

Wu, Yuanbo; Chen, Meiqiao; Jiang, Jielong (2019): Mitochondrial dysfunction in neurodegenerative diseases and drug targets via apoptotic signaling. In *Mitochondrion* 49, pp. 35–45. DOI: 10.1016/j.mito.2019.07.003.

Xiao, T. Sam; Fitzgerald, Katherine A. (2013): The cGAS-STING pathway for DNA sensing. In *Molecular Cell* 51 (2), pp. 135–139. DOI: 10.1016/j.molcel.2013.07.004.

Xu, Ting-Ting; Li, Han; Dai, Zhao; Lau, George K.; Li, Ben-Yue; Zhu, Wen-Li et al. (2020a): Spermidine and spermine delay brain aging by inducing autophagy in SAMP8 mice. In *Aging* 12 (7), pp. 6401–6414. DOI: 10.18632/aging.103035.

Xu, Zhenru; Han, Xu; Ou, Daming; Liu, Ting; Li, Zunxiong; Jiang, Guanmin et al. (2020b): Targeting PI3K/AKT/mTOR-mediated autophagy for tumor therapy. In *Appl Microbiol Biotechnol* 104 (2), pp. 575–587. DOI: 10.1007/s00253-019-10257-8.

Yamashiro, Lívia H.; Wilson, Stephen C.; Morrison, Huntly M.; Karalis, Vasiliki; Chung, Jing-Yi J.; Chen, Katherine J. et al. (2020): Interferon-independent STING signaling promotes resistance to HSV-1 in vivo. In *Nat Commun* 11 (1), p. 3382. DOI: 10.1038/s41467-020-17156-x.

Yang, Hui; Wang, Hanze; Ren, Junyao; Chen, Qi; Chen, Zhijian J. (2017): cGAS is essential for cellular senescence. In *Proceedings of the National Academy of Sciences of the United States of America* 114 (23), E4612-E4620. DOI: 10.1073/pnas.1705499114.

Yim, Willa Wen-You; Mizushima, Noboru (2020): Lysosome biology in autophagy. In *Cell Discov* 6 (1), p. 6. DOI: 10.1038/s41421-020-0141-7.

Yu, Yongsheng; Xue, Xiaochun; Tang, Wendong; Su, Li; Zhang, Lei; Zhang, Yuefan (2022): Cytosolic DNA–Mediated STING-Dependent Inflammation Contributes to the Progression of Psoriasis. In *The Journal of investigative dermatology* 142 (3 Pt B), 898-906.e4. DOI: 10.1016/j.jid.2021.08.430.

Yum, Seoyun; Li, Minghao; Fang, Yan; Chen, Zhijian J. (2021): TBK1 recruitment to STING activates both IRF3 and NF-κB that mediate immune defense against tumors and viral infections. In *Proceedings of the National Academy of Sciences of the United States of America* 118 (14). DOI: 10.1073/pnas.2100225118.

Zhang, Bao-Cun; Nandakumar, Ramya; Reinert, Line S.; Huang, Jinrong; Laustsen, Anders; Gao, Zong-liang et al. (2020): STEEP mediates STING ER exit and activation of signaling. In *Nat Immunol* 21 (8), pp. 868–879. DOI: 10.1038/s41590-020-0730-5.

Zhang, Cong; Cuervo, Ana Maria (2008): Restoration of chaperone-mediated autophagy in aging liver improves cellular maintenance and hepatic function. In *Nat Med* 14 (9), pp. 959–965. DOI: 10.1038/nm.1851.

Zhang, Gaohua; Guo, Zhenfang; Cheng, Qianyi; Sanz, Ivan; Hamad, Abdulsattar Abdullah (2021): Multi-level integrated health management model for empty nest elderly people's to strengthen their lives. In *Aggression and Violent Behavior*, p. 101542. DOI: 10.1016/j.avb.2020.101542.

Zhang, Xu; Wu, Jiaxi; Du, Fenghe; Xu, Hui; Sun, Lijun; Chen, Zhe et al. (2014): The cytosolic DNA sensor cGAS forms an oligomeric complex with DNA and undergoes switch-like conformational changes in the activation loop. In *Cell Reports* 6 (3), pp. 421–430. DOI: 10.1016/j.celrep.2014.01.003.

Zhao, Mengmeng; Wang, Fei; Wu, Juehui; Cheng, Yuanna; Cao, Yajuan; Wu, Xiangyang et al. (2021): CGAS is a micronucleophagy receptor for the clearance of micronuclei. In *Autophagy* 17 (12), pp. 3976–3991. DOI: 10.1080/15548627.2021.1899440.

Zheng, Wanglong; Xia, Nengwen; Zhang, Jiajia; Chen, Nanhua; Meurens, François; Liu, Zongping; Zhu, Jianzhong (2021): How the Innate Immune DNA Sensing cGAS-STING Pathway Is Involved in Autophagy. In *International Journal of Molecular Sciences* 22 (24), p. 13232. DOI: 10.3390/ijms222413232.

Zhitomirsky, Benny; Farber, Hodaya; Assaraf, Yehuda G. (2018): LysoTracker and MitoTracker Red are transport substrates of P-glycoprotein: implications for anticancer drug design evading multidrug resistance. In *Journal of cellular and molecular medicine* 22 (4), pp. 2131–2141. DOI: 10.1111/jcmm.13485.

Zhou, Dingxi; Borsa, Mariana; Simon, Anna Katharina (2021): Hallmarks and detection techniques of cellular senescence and cellular ageing in immune cells. In *Aging Cell* 20 (2), e13316. DOI: 10.1111/acel.13316.

Zhu, Zhou; Yang, Chuanbin; Iyaswamy, Ashok; Krishnamoorthi, Senthilkumar; Sreenivasmurthy, Sravan Gopalkrishnashetty; Liu, Jia et al. (2019): Balancing mTOR Signaling and Autophagy in the Treatment of Parkinson's Disease. In *International Journal of Molecular Sciences* 20 (3), p. 728. DOI: 10.3390/ijms20030728.

8 Declaration of Honour

“I hereby declare that I prepared this thesis without the impermissible help of third parties and that none other than the aids indicated have been used; all sources of information are clearly marked, including my own publications.
In particular I have not consciously:

- fabricated data or rejected undesirable results,
- misused statistical methods with the aim of drawing other conclusions than those warranted by the available data,
- plagiarized external data or publications,
- presented the results of other researchers in a distorted way.

I am aware that violations of copyright may lead to injunction and damage claims by the author and also to prosecution by law enforcement authorities.
I hereby agree that the thesis may be electronically reviewed with the aim of identifying plagiarism.

This work has not been submitted as a doctoral thesis in the same or a similar form in Germany, nor in any other country. It has not yet been published as a whole.”

Magdeburg,

Sergio Passarella